

3rd Generation Partnership Project;
Technical Specification Group Radio Access Network;
3GPP TR 38.9XX v1.0.0 (2017.02)
Study on channel model for frequencies from 0.5 to 100 GHz
Technical Report
(Release 14)



The present document has been developed within the 3rd Generation Partnership Project (3GPP™) and may be further elaborated for the purposes of 3GPP. The present document has not been subject to any approval process by the 3GPP Organizational Partners and shall not be implemented. This Report is provided for future development work within 3GPP only. The Organizational Partners accept no liability for any use of this Specification. Specifications and Reports for implementation of the 3GPP™ system should be obtained via the 3GPP Organizational Partners' Publications Offices.

Keywords
New Radio

3GPP

Postal address

3GPP support office address

650 Route des Lucioles – Sophia Antipolis
Valbonne – France
Tel. : +33 4 92 94 42 00 Fax : +33 4 93 65 47 16

Internet

<http://www.3gpp.org>

Copyright Notification

No part may be reproduced except as authorized by written permission.
The copyright and the foregoing restriction extend to reproduction in all media.

© 2016, 3GPP Organizational Partners (ARIB, ATIS, CCSA, ETSI, TSDSI, TTA, TTC).
All rights reserved.

UMTS™ is a Trade Mark of ETSI registered for the benefit of its members
3GPP™ is a Trade Mark of ETSI registered for the benefit of its Members and of the 3GPP Organizational Partners
LTE™ is a Trade Mark of ETSI registered for the benefit of its Members and of the 3GPP Organizational Partners
GSM® and the GSM logo are registered and owned by the GSM Association

Contents

Foreword.....	5
1 Scope.....	6
2 References.....	6
3 Definitions, symbols and abbreviations.....	7
3.1 Definitions.....	7
3.2 Symbols.....	7
3.3 Abbreviations.....	8
4 Introduction.....	9
5 General.....	10
6 Status/Expectation of existing information on high frequencies.....	10
6.1 Channel modelling works outside of 3GPP.....	10
6.2 Scenarios of interest.....	12
6.3 Channel measurement capabilities.....	12
6.4 Modelling objectives.....	13
7 Channel model(s) for 0.5-100 GHz.....	14
7.1 Coordinate system.....	14
7.1.1 Definition.....	14
7.1.2 Local and global coordinate systems.....	14
7.1.3 Transformation from a LCS to a GCS.....	15
7.1.4 Transformation from an LCS to a GCS for downtilt angle only.....	18
7.2 Scenarios.....	19
7.3 Antenna modelling.....	21
7.3.1 Antenna port mapping.....	22
7.3.2 Polarized antenna modelling.....	23
7.4 Pathloss, LOS probability and penetration modelling.....	24
7.4.1 Pathloss.....	24
7.4.2 LOS probability.....	27
7.4.3 O2I penetration loss.....	27
7.4.4 Autocorrelation of shadow fading.....	29
7.5 Fast fading model.....	29
7.6 Additional modelling components.....	43
7.6.1 Oxygen absorption.....	44
7.6.2 Large bandwidth and large antenna array.....	44
7.6.3 Spatial consistency.....	46
7.6.4 Blockage.....	51
7.6.5 Correlation modelling for multi-frequency simulations.....	56
7.6.6 Time-varying Doppler shift.....	58
7.6.7 UT rotation.....	59
7.6.8 Explicit ground reflection model.....	59
7.7 Channel models for link-level evaluations.....	62
7.7.1 Clustered Delay Line (CDL) models.....	62
7.7.2 Tapped Delay Line (TDL) models.....	66
7.7.3 Scaling of delays.....	69
7.7.4 Spatial filter for generating TDL channel model.....	70
7.7.5 Extension for MIMO simulations.....	71
7.7.6 K-factor for LOS channel models.....	73
7.8 Channel model calibration.....	73
7.8.1 Large scale calibration.....	73
7.8.2 Full calibration.....	74
7.8.3 Calibration of additional features.....	75
8 Map-based hybrid channel model (Alternative channel model methodology).....	77
8.1 Coordinate system.....	77

8.2 Scenarios.....77

8.3 Antenna modelling.....77

8.4 Channel generation.....77

Foreword

This Technical Report has been produced by the 3rd Generation Partnership Project (3GPP).

The contents of the present document are subject to continuing work within the TSG and may change following formal TSG approval. Should the TSG modify the contents of the present document, it will be re-released by the TSG with an identifying change of release date and an increase in version number as follows:

Version x.y.z

where:

- x the first digit:
 - 1 presented to TSG for information;
 - 2 presented to TSG for approval;
 - 3 or greater indicates TSG approved document under change control.
- Y the second digit is incremented for all changes of substance, i.e. technical enhancements, corrections, updates, etc.
- z the third digit is incremented when editorial only changes have been incorporated in the document.

1 Scope

The present document captures the findings of the study item, “Study on channel model for frequency spectrum above 6 GHz” [2] and from further findings of the study item, “Study on New Radio Access Technology [X].” The channel models in the present document address the frequency range 0.5-100 GHz. The purpose of this TR is to help TSG RAN WG1 to properly model and evaluate the performance of physical layer techniques using the appropriate channel model(s). Therefore the TR will be kept up-to-date via CRs in the future.

This document relates to the 3GPP evaluation methodology and covers the modelling of the physical layer of both Mobile Equipment and Access Network of 3GPP systems.

This document is intended to capture the channel model(s) for frequencies from 0.5GHz up to 100GHz.

2 References

The following documents contain provisions which, through reference in this text, constitute provisions of the present document.

- References are either specific (identified by date of publication, edition number, version number, etc.) or non-specific.
- For a specific reference, subsequent revisions do not apply.
- For a non-specific reference, the latest version applies. In the case of a reference to a 3GPP document (including a GSM document), a non-specific reference implicitly refers to the latest version of that document *in the same Release as the present document*.

- [1] 3GPP TR 21.905: “Vocabulary for 3GPP Specifications”.
- [2] 3GPP TD RP-151606: “Study on channel model for frequency spectrum above 6 GHz “.
- [3] 3GPP TR 36.873 (V12.2.0): “Study on 3D channel model for LTE”.
- [4] 3GPP RP-151847: “Report of RAN email discussion about >6GHz channel modelling”, Samsung
- [5] 3GPP R1-163408: “Additional Considerations on Building Penetration Loss Modeling for 5G System Performance Evaluation,” Straight Path Communications
- [6] METIS channel model, METIS 2020,ICT-317667-METIS/D1.4, Feb, 2015
- [7] A S. Glassner, An introduction to ray tracing. Elsevier, 1989
- [8] J. W. McKown, R. L. Hamilton. “Ray tracing as a design tool for radio networks,” Network, IEEE, 1991(6): 27-30.
- [9] T. Kurner, D. J. Cichon, W.Wiesbeck, “Concepts and results for 3D digital terrain-based wave propagation models: An overview,” IEEE J.Select. Areas Commun., vol. 11, pp. 1002–1012, 1993.
- [10] M. Born, E. Wolf, Principles of optics: electromagnetic theory of propagation, interference and diffraction of light. CUP Archive, 2000
- [11] H. Friis, “A note on a simple transmission formula,” proc. IRE, vol. 34, no. 5, pp. 254–256, 1946
- [12] R. G. Kouyoumjian and P. H. Pathak, “A uniform geometrical theory of diffraction for an edge in a perfectly conducting surface,” Proc. IEEE, vol. 62, pp. 1448–1461, Nov. 1974.
- [13] P. Pathak, W. Burnside, and R. Marhefka, “A Uniform GTD Analysis of the Diffraction of Electromagnetic Waves by a Smooth Convex Surface,” IEEE Transactions on Antennas and Propagation, vol. 28, no. 5, pp. 631–642, 1980
- [14] IST-WINNER II Deliverable 1.1.2 v.1.2, “WINNER II Channel Models”, IST-WINNER2, Tech. Rep., 2007 (<http://www.ist-winner.org/deliverables.html>).

- [15] 3GPP TR36.101: “User Equipment (UE) radio transmission and reception”
- [16] 3GPP TR36.104: “Base Station (BS) radio transmission and reception”
- [17] H. Asplund et al., “A simplified approach to applying the 3GPP spatial channel model”, in Proc. Of PIMRC 2006
- [18] ITU-R Rec. P.1816: “The prediction of the time and the spatial profile for broadband land mobile services using UHF and SHF bands”
- [19] ITU-R Rec. P.2040-1, “Effects of building materials and structures on radiowave propagation above about 100 MHz”, International Telecommunication Union Radiocommunication Sector ITU-R, 07/2015.
- [20] ITU-R Rec. P.527-3, “Electrical characteristics of the surface of the earth”, International Telecommunication Union Radiocommunication Sector ITU-R, 03/1992
- [21] E. C. Jordan, K. G. Balmain, “Electromagnetic Waves and Radiating Systems”, Prentice-Hall Inc., 1968

3 Definitions, symbols and abbreviations

3.1 Definitions

For the purposes of the present document, the terms and definitions given in TR 21.905 [1] and the following apply. A term defined in the present document takes precedence over the definition of the same term, if any, in TR 21.905 [1].

3.2 Symbols

For the purposes of the present document, the following symbols apply:

A	antenna radiation power pattern
A_{\max}	maximum attenuation
d_{2D}	2D distance between Tx and Rx
d_{3D}	3D distance between Tx and Rx
d_H	antenna element spacing in horizontal direction
d_V	antenna element spacing in vertical direction
f	frequency
f_c	center frequency / carrier frequency
$F_{rx,u,\theta}$	Receive antenna element u field pattern in the direction of the spherical basis vector $\hat{\theta}$
$F_{rx,u,\phi}$	Receive antenna element u field pattern in the direction of the spherical basis vector $\hat{\phi}$
$F_{tx,s,\theta}$	Transmit antenna element s field pattern in the direction of the spherical basis vector $\hat{\theta}$
$F_{tx,s,\phi}$	Transmit antenna element s field pattern in the direction of the spherical basis vector $\hat{\phi}$
h_{BS}	antenna height for BS
h_{UT}	antenna height for UT
$\hat{r}_{rx,n,m}$	spherical unit vector of cluster n , ray m , for receiver
$\hat{r}_{tx,n,m}$	spherical unit vector of cluster n , ray m , for transmitter
α	bearing angle
β	downtilt angle
γ	slant angle
λ	wavelength
κ	cross-polarization power ratio in linear scale
μ_{lgASA}	mean value of 10-base logarithm of azimuth angle spread of arrival

μ_{lgASD}	mean value of 10-base logarithm of azimuth angle spread of departure
μ_{lgDS}	mean value of 10-base logarithm of delay spread
μ_{lgZSA}	mean value of 10-base logarithm of zenith angle spread of arrival
μ_{lgZSD}	mean value of 10-base logarithm of zenith angle spread of departure
SLA_v	side-lobe attenuation in vertical direction
σ_{lgASA}	standard deviation of 10-base logarithm of azimuth angle spread of arrival
σ_{lgASD}	standard deviation of 10-base logarithm of azimuth angle spread of departure
σ_{lgDS}	standard deviation value of 10-base logarithm of delay spread
σ_{lgZSA}	standard deviation of 10-base logarithm of zenith angle spread of arrival
σ_{lgZSD}	standard deviation of 10-base logarithm of zenith angle spread of departure
σ_{SF}	standard deviation of SF
ϕ	azimuth angle
θ	zenith angle
$\hat{\phi}$	spherical basis vector (unit vector) for GCS
$\hat{\phi}'$	spherical basis vector (unit vector) for LCS
ϕ_{3dB}	horizontal 3 dB beamwidth of an antenna
$\hat{\theta}$	spherical basis vector (unit vector), orthogonal to $\hat{\phi}$, for GCS
$\hat{\theta}'$	spherical basis vector (unit vector), orthogonal to $\hat{\phi}'$, for LCS
θ_{etilt}	electrical steering angle in vertical direction
θ_{3dB}	vertical 3 dB beamwidth of an antenna
ψ	Angular displacement between two pairs of unit vectors

3.3 Abbreviations

For the purposes of the present document, the abbreviations given in TR 21.905 [1] and the following apply. An abbreviation defined in the present document takes precedence over the definition of the same abbreviation, if any, in TR 21.905 [1].

2D	two-dimensional
3D	three-dimensional
AOA	Azimuth angle Of Arrival
AOD	Azimuth angle Of Departure
AS	Angular Spread
ASA	Azimuth angle Spread of Arrival
ASD	Azimuth angle Spread of Departure
BF	Beamforming
BS	Base Station
BP	Breakpoint
BW	Beamwidth
CDF	Cumulative Distribution Function
CDL	Clustered Delay Line
CRS	Common Reference Signal
D2D	Device-to-Device
DFT	Discrete Fourier Transform
DS	Delay Spread
GCS	Global Coordinate System
IID	Independent and identically distributed
InH	Indoor Hotspot
IRR	Infrared Reflecting
ISD	Intersite Distance
K	Ricean K factor
LCS	Local Coordinate System
LOS	Line Of Sight

MIMO	Multiple-Input-Multiple-Output
MPC	Multipath Component
NLOS	Non-LOS
O2I	Outdoor-to-Indoor
O2O	Outdoor-to-Outdoor
OFDM	Orthogonal Frequency-Division Multiplexing
PAS	Power angular spectrum
PL	Path Loss
PRB	Physical Resource Block
RCS	Radar cross-section
Rma	Rural Macro
RMS	Root Mean Square
RSRP	Reference Signal Received Power
Rx	Receiver
SCM	Spatial Channel Model
SINR	Signal-to-Interference-plus-Noise Ratio
SIR	Signal-to-Interference Ratio
SSCM	Statistical Spatial Channel Model
SF	Shadow Fading
SLA	Sidelobe Attenuation
TDL	Tapped Delay Line
TOA	Time Of Arrival
TRP	Transmission Reception Point
Tx	Transmitter
Uma	Urban Macro
Umi	Urban Micro
UT	User Terminal
UTD	Uniform Theory of Diffraction
V2V	Vehicle-to-Vehicle
XPR	Cross-Polarization Ratio
ZOA	Zenith angle Of Arrival
ZOD	Zenith angle Of Departure
ZSA	Zenith angle Spread of Arrival
ZSD	Zenith angle Spread of Departure

4 Introduction

At 3GPP TSG RAN #69 meeting the Study Item Description on “Study on channel model for frequency spectrum above 6 GHz” was approved [2]. This study item covers the identification of the status/expectation of existing information on high frequencies (e.g. spectrum allocation, scenarios of interest, measurements, etc), and the channel model(s) for frequencies up to 100 GHz. This technical report documents the channel model(s). The new channel model has to a large degree been aligned with earlier channel models for <6 GHz such as the 3D SCM model (3GPP TR 36.873) or IMT-Advanced (ITU-R M.2135). The new model supports comparisons across frequency bands over the range 0.5-100 GHz. The modelling methods defined in this technical report are generally applicable over the range 0.5-100 GHz, unless explicitly mentioned otherwise in this technical report for specific modelling method, involved parameters and/or scenario.

The channel model is applicable for link and system level simulations in the following conditions:

- For system level simulations, supported scenarios are urban microcell street canyon, urban macrocell, indoor office, and rural macrocell.
- Bandwidth is supported up to 10% of the center frequency but no larger than 2GHz.
- Mobility of one end of the link is supported
- For the stochastic model, spatial consistency is supported by correlation of LSPs and SSPs as well as LOS/NLOS state.
- Large array support is based on far field assumption and stationary channel over the size of the array.

5 General

6 Status/Expectation of existing information on high frequencies

6.1 Channel modelling works outside of 3GPP

This section summarizes the Channel Modelling works outside of 3GPP based on the input from companies.

Groups and projects with channel models:

- METIS (Mobile and wireless communications Enablers for the Twenty-twenty Information Society)
- MiWEBA (Millimetre-Wave Evolution for Backhaul and Access)
- ITU-R M
- COST2100
- IEEE 802.11
- NYU WIRELESS: interdisciplinary academic research center
- Fraunhofer HHI has developed the QuaDRiGa channel model, Matlab implementation is available at <http://quadriga-channel-model.de>

Groups and projects which intend to develop channel models:

- 5G mmWave Channel Model Alliance: NIST initiated, North America based
- mmMAGIC (Millimetre-Wave Based Mobile Radio Access Network for Fifth Generation Integrated Communications): Europe based
- IMT-2020 5G promotion association: China based

METIS Channel Models:

- Identified 5G requirements (e.g., wide frequency range, high bandwidth, massive MIMO, 3-D and accurate polarization modelling)
- Performed channel measurements at various bands between 2GHz and 60 GHz
- Provided different channel model methodologies (map-based model, stochastic model or hybrid model). For stochastic model, the proposed channel is focused on outdoor square, Indoor cafeteria and indoor shopping mall scenarios.

MiWEBA Channel Models:

- Addressed various challenges: Shadowing, spatial consistency, environment dynamics, spherical wave modelling, dual mobility Doppler model, ratio between diffuse and specular reflections, polarization
- Proposed Quasi-deterministic channel model
- Performed channel measurements at 60 GHz
- Focused on university campus, street canyon, hotel lobby, backhaul, and D2D scenarios.

ITU-R M Channel Models:

- Addressed the propagation loss and atmospheric loss on mmW

- Introduced enabling antenna array technology and semiconductor technology
- Proposed deployment scenarios, focused on dense urban environment for high data rate service: indoor shopping mall, indoor enterprise, in home, urban hotspot in a square/street, mobility in city.

COST2100 and COST IC1004 Channel Models:

- Geometry-based stochastic channel model that reproduce the stochastic properties of MIMO channels over time, frequency and space. It is a cluster-level model where the statistics of the large scale parameters are always guaranteed in each series of channel instances.

NYU WIRELESS Channel Models:

- Conducted many urban propagation measurements on 28/38/60/73 GHz bands for both outdoor and indoor channels, measurements are continuing.
- Proposed 3 areas for 5G mmWave channel modeling which are small modifications or extensions from 3GPP's current below 6GHz channel models
- 1) LOS/NLOS/blockage modeling (a squared exponential term); 2). Wideband power delay profiles (time clusters and spatial lobes for a simple extension to the existing 3GPP SSCM model); 3). Physics-based path loss model (using the existing 3GPP path loss equations, but simply replacing the “floating” optimization parameter with a deterministic 1 m “close-in” free space reference term in order to provide a standard and stable definition of “path loss exponent” across all different parties, scenarios, and frequencies).

802.11 ad/ay Channel Models:

- Conducted ray-tracing methodology on 60 GHz band indoor channels, including conference room, cubicle, living room scenarios
- Intra cluster parameters were proposed in terms of ray excess delay and ray power distribution
- Human blockage models were proposed in terms of blockage probability and blockage attenuation

5G mmWave Channel Model Alliance:

- Will provide a venue to promote fundamental research into measurement, analysis, identification of physical parameters, and statistical representations of mmWave propagation channels.
- Divided into six collaborative working groups that include a Steering Committee; Modeling Methodology Group; Measurement Methodology Group; and groups that focus on defining and parameterizing Indoor, Outdoor, and Emerging Usage Scenarios.
- Sponsored by Communications Technology Research Laboratory within the NIST.

mmMAGIC:

- Brings together major infrastructure vendors, major European operators, leading research institutes and universities, measurement equipment vendors and one SME.
- Will undertake extensive radio channel measurements in the 6-100 GHz range.
- Will develop and validate advanced channel models that will be used for rigorous validation and feasibility analysis of the proposed concepts and system, as well as for usage in regulatory and standards I.

IMT-2020 5G promotion association

- Jointly established by three ministries of China based on the original IMT-Advanced promotion group
- Members including the main operators, vendors, universities and research institutes in China
- The major platform to promote 5G technology research in China and to facilitate international communication and cooperation

QuaDRiGa (Fraunhofer HHI)

- QuaDRiGa (QUasi Deterministic RadIo channel GenerAtor) was developed at the [Fraunhofer Heinrich Hertz Institute](#) within the [Wireless Communications and Networks Department](#) to enable the modeling of MIMO radio channels for specific network configurations, such as indoor, satellite or heterogeneous configurations.
- Besides being a fully-fledged 3D geometry-based stochastic channel model (well aligned with TR36.873), QuaDRiGa contains a collection of features created in SCMI and WINNER channel models along with novel modeling approaches which provide features to enable quasi-deterministic multi-link tracking of users (receiver)

movements in changing environments. QuaDRiGa supports Massive MIMO modeling enabled through a new multi-bounce scattering approach and spherical wave propagation. It will be continuously extended with features required by 5G and frequencies beyond 6 GHz. The QuaDRiGa model is supported by data from extensive channel measurement campaigns at 10 / 28 / 43 / 60 / 82 GHz performed by the same group.

6.2 Scenarios of interest

Brief description of the key scenarios of interest identified¹:

- (2017) Umi (Street canyon, open area) with O2O and O2I: This is similar to 3D-Umi scenario, where the BSs are mounted below rooftop levels of surrounding buildings. Umi open area is intended to capture real-life scenarios such as a city or station square. The width of the typical open area is in the order of 50 to 100 m.

Example: [Tx height:10m, Rx height: 1.5-2.5 m, ISD: 200m]

- (2) Uma with O2O and O2I: This is similar to 3D-Uma scenario, where the BSs are mounted above rooftop levels of surrounding buildings.

Example: [Tx height:25m, Rx height: 1.5-2.5 m, ISD: 500m]

- (3) Indoor: This scenario is intended to capture various typical indoor deployment scenarios, including office environments, and shopping malls. The typical office environment is comprised of open cubicle areas, walled offices, open areas, corridors etc. The BSs are mounted at a height of 2-3 m either on the ceilings or walls. The shopping malls are often 1-5 stories high and may include an open area (or “atrium”) shared by several floors. The BSs are mounted at a height of approximately 3 m on the walls or ceilings of the corridors and shops.

Example: [Tx height: 2-3m, Rx height: 1.5m, area: 500 square meters]

- (4) Backhaul, including outdoor above roof top backhaul in urban area and street canyon scenario where small cell BSs are placed at lamp posts.

- (5) D2D/V2V. Device-to-device access in open area, street canyon, and indoor scenarios. V2V is a special case where the devices are mobile.

- (6) Other scenarios such as Stadium (open-roof) and Gym (close-roof).

6.3 Channel measurement capabilities

The measurement capability as reported by each company is summarized in the table below.

¹ The scenarios of interest are based on the plenary email discussion and different from the supported scenarios in section 7

Table 6.3-1: Channel measurement capabilities

	6 – 20 GHz	20 – 30 GHz	30 – 60 GHz	>60 GHz
Urban macro	CMCC Nokia/Aalborg	Nokia/Aalborg	NYU	
Urban micro	Aalto University CMCC Ericsson Intel/Fraunhofer HHI Nokia/Aalborg NTT DOCOMO Orange	AT&T Aalto University CMCC Huawei Intel/Fraunhofer HHI Nokia/Aalborg NTT DOCOMO NYU Qualcomm Samsung CATT KT ETRI ITRI/CCU ZTE	AT&T Huawei Intel/Fraunhofer HHI NTT DOCOMO Qualcomm CATT ETRI ITRI/CCU ZTE	AT&T Aalto University Huawei Intel/Fraunhofer HHI NYU
Indoor	Aalto University CMCC Ericsson Huawei Intel/Fraunhofer HHI Nokia/Aalborg NTT DOCOMO Orange	AT&T Alcatel-Lucent Aalto University BUPT CMCC Huawei Intel/Fraunhofer HHI Nokia/Aalborg NTT DOCOMO NYU Qualcomm Samsung CATT KT ETRI ITRI/CCU ZTE	AT&T Ericsson Huawei Intel/Fraunhofer HHI NTT DOCOMO NYU Qualcomm CATT ETRI ITRI/CCU ZTE	AT&T Aalto University Huawei Intel/Fraunhofer HHI NYU
O2I	Ericsson Huawei Intel/Fraunhofer HHI Nokia/Aalborg NTT DOCOMO Orange	AT&T Alcatel-Lucent Ericsson Huawei Intel/Fraunhofer HHI NTT DOCOMO NYU Samsung KT	AT&T Ericsson Huawei Intel/Fraunhofer HHI NTT DOCOMO	AT&T Huawei Intel/Fraunhofer HHI

6.4 Modelling objectives

The requirements for channel modelling are as follows.

- Channel model SI should take into account the outcome of RAN-level discussion in the ‘5G’ requirement study item
- Complexity in terms of Description, Generating channel coefficients, development complexity and Simulation time should be considered.
- Support frequency range up to 100 GHz.
 - The critical path of the SI is 6 – 100 GHz
 - Take care of mmW propagation aspects such as blocking and atmosphere attenuation.

- The model should be consistent in space, time and frequency
- Support large channel bandwidths (up to 10% of carrier frequency)
- Aim for the channel model to cover a range of coupling loss considering current typical cell sizes, e.g. up to km-range macro cells. Note: This is to enable investigation of the relevance of the 5G system using higher frequency bands to existing deployments.
- Accommodate UT mobility
 - Mobile speed up to 500 km/h.
 - Develop a methodology considering that model extensions to D2D and V2V may be developed in future SI.
- Support large antenna arrays

7 Channel model(s) for 0.5-100 GHz

7.1 Coordinate system

7.1.1 Definition

A coordinate system is defined by the x, y, z axes, the spherical angles and the spherical unit vectors as shown in Figure 7.1.1. Figure 7.1.1 defines the zenith angle θ and the azimuth angle ϕ in a Cartesian coordinate system. Note that $\theta = 0$ points to the zenith and $\theta = 90^\circ$ points to the horizon. The field component in the direction of $\hat{\theta}$ is given by F_θ and the field component in the direction of $\hat{\phi}$ is given by F_ϕ .

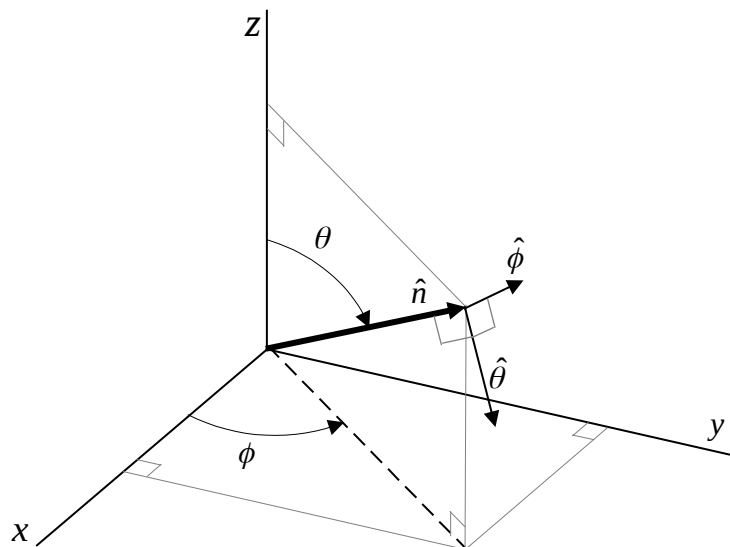


Figure 7.1.1: Definition of spherical angles and spherical unit vectors in a Cartesian coordinate system, where \hat{n} is the given direction, $\hat{\theta}$ and $\hat{\phi}$ are the spherical basis vectors

7.1.2 Local and global coordinate systems

A Global Coordinate System (GCS) is defined for a system comprising multiple BSs and Uts. An array antenna for a BS or a UT can be defined in a Local Coordinate System (LCS). An LCS is used as a reference to define the vector far-field that is pattern and polarization, of each antenna element in an array. It is assumed that the far-field is known in the LCS by formulae. The placement of an array within the GCS is defined by the translation between the GCS and a LCS. The

orientation of the array with respect to the GCS is defined in general by a sequence of rotations (described in clause 7.1.3). Since this orientation is in general different from the GCS orientation, it is necessary to map the vector fields of the array elements from the LCS to the GCS. This mapping depends only on the orientation of the array and is given by the equations in clause 7.1.3.

Note that any arbitrary mechanical orientation of the array can be achieved by rotating the LCS with respect to the GCS.

7.1.3 Transformation from a LCS to a GCS

A GCS with coordinates (x, y, z, θ, ϕ) and unit vectors $(\hat{\theta}, \hat{\phi})$ and an LCS with “primed” coordinates $(x', y', z', \theta', \phi')$ and “primed” unit vectors $(\hat{\theta}', \hat{\phi}')$ are defined with a common origins in Figures 7.1.3-1 and 7.1.3-2.

Figure 7.1.3-1 illustrates the sequence of rotations that relate the GCS (gray) and the LCS (blue). Figure 7.1.3-2 shows the coordinate direction and unit vectors of the GCS (gray) and the LCS (blue). Note that the vector fields of the array antenna elements are defined in the LCS. In Figure 7.1.3-1 we consider an arbitrary 3D-rotation of the LCS with respect to the GCS given by the angles α, β, γ . The set of angles α, β, γ can also be termed as the orientation of the array antenna with respect to the GCS.

Note that the transformation from a LCS to a GCS depends only on the angles α, β, γ . The angle α is called the bearing angle, β is called the downtilt angle and γ is called the slant angle.

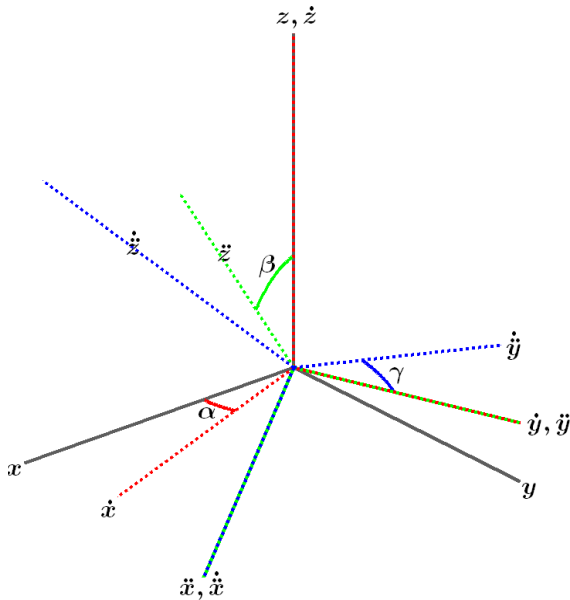


Figure 7.1.3-1: Orienting the LCS (blue) with respect to the GCS (gray) by a sequence of 3 rotations: α, β, γ .

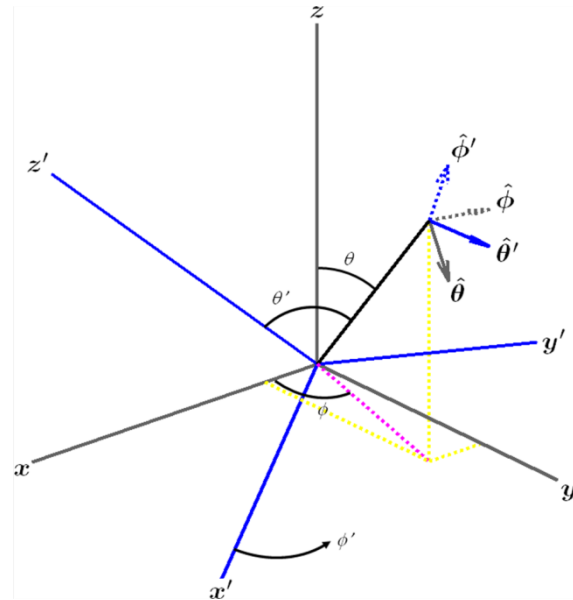


Figure 7.1.3-2: Definition of spherical coordinates and unit vectors in both the GCS and LCS.

Let $A'(\theta', \phi')$ denote an antenna element pattern in the LCS and $A(\theta, \phi)$ denote the same antenna element pattern in the GCS. Then the two are related simply by

$$A(\theta, \phi) = A'(\theta', \phi') \quad (7.1-1)$$

with θ' and ϕ' given by (7.1-7) and (7.1-8).

Let us denote the polarized field components in the LCS by $F_{\theta'}(\theta', \phi')$, $F_{\phi'}(\theta', \phi')$ and in the GCS by $F_{\theta}(\theta, \phi)$, $F_{\phi}(\theta, \phi)$. Then they are related by equation (7.1-11).

Any arbitrary 3-D rotation can be specified by at most 3 elemental rotations, and following the framework of Figure 7.1.3-1, a series of rotations about the z , \dot{y} and \ddot{x} axes are assumed here, in that order. The dotted and double-dotted marks indicate that the rotations are intrinsic, which means that they are the result of one (\cdot) or two ($\ddot{\cdot}$)

intermediate rotations. In other words, the \dot{Y} axis is the original y axis after the first rotation about z, and the \ddot{X} axis is the original x axis after the first rotation about z and the second rotation about \dot{Y} . A first rotation of α about z sets the antenna bearing angle (i.e. the sector pointing direction for a BS antenna element). The second rotation of β about \dot{Y} sets the antenna downtilt angle. Finally, the third rotation of γ about \ddot{X} sets the antenna slant angle. The orientation of the x, y and z axes after all three rotations can be denoted as \ddot{X} , \ddot{Y} and \ddot{Z} . These triple-dotted axes represents the final orientation of the LCS, and for notational purposes denoted as the x' , y' and z' axes (local or “primed” coordinate system).

In order to establish the equations for transformation of the coordinate system and the polarized antenna field patterns between the GCS and the LCS, it is necessary to determine the composite rotation matrix that describes the transformation of point (x, y, z) in the GCS into point (x', y', z') in the LCS. This rotation matrix is computed as the product of three elemental rotation matrices. The matrix to describe rotations about the z, \dot{Y} and \ddot{X} axes by the angles α , β and γ respectively and in that order is defined as

$$R = R_z(\alpha)R_Y(\beta)R_X(\gamma) = \begin{bmatrix} \cos \alpha & -\sin \alpha & 0 \\ \sin \alpha & \cos \alpha & 0 \\ 0 & 0 & 1 \end{bmatrix} \begin{bmatrix} \cos \beta & 0 & \sin \beta \\ 0 & 1 & 0 \\ -\sin \beta & 0 & \cos \beta \end{bmatrix} \begin{bmatrix} 1 & 0 & 0 \\ 0 & \cos \gamma & -\sin \gamma \\ 0 & \sin \gamma & \cos \gamma \end{bmatrix} \quad (7.1-2)$$

The reverse transformation is given by the inverse of R, which is also equal to the transpose of R since it is orthogonal.

$$R^{-1} = R_X(-\gamma)R_Y(-\beta)R_Z(-\alpha) = R^T \quad (7.1-3)$$

The simplified forward and reverse composite rotation matrices are given by

$$R = \begin{bmatrix} \cos \alpha \cos \beta & \cos \alpha \sin \beta \sin \gamma - \sin \alpha \cos \gamma & \cos \alpha \sin \beta \cos \gamma + \sin \alpha \sin \gamma \\ \sin \alpha \cos \beta & \sin \alpha \sin \beta \sin \gamma + \cos \alpha \cos \gamma & \sin \alpha \sin \beta \cos \gamma - \cos \alpha \sin \gamma \\ -\sin \beta & \cos \beta \sin \gamma & \cos \beta \cos \gamma \end{bmatrix} \quad (7.1-4)$$

and

$$R^{-1} = \begin{bmatrix} \cos \alpha \cos \beta & \sin \alpha \cos \beta & -\sin \beta \\ \cos \alpha \sin \beta \sin \gamma - \sin \alpha \cos \gamma & \sin \alpha \sin \beta \sin \gamma + \cos \alpha \cos \gamma & \cos \beta \sin \gamma \\ \cos \alpha \sin \beta \cos \gamma + \sin \alpha \sin \gamma & \sin \alpha \sin \beta \cos \gamma - \cos \alpha \sin \gamma & \cos \beta \cos \gamma \end{bmatrix} \quad (7.1-5)$$

These transformations can be used to derive the angular and polarization relationships between the two coordinate systems.

In order to establish the angular relationships, consider a point (x, y, z) on the unit sphere defined by the spherical coordinates $(\rho=1, \theta, \phi)$, where ρ is the unit radius, θ is the zenith angle measured from the +z-axis, and ϕ is the azimuth angle measured from the +x-axis in the x-y plane. The Cartesian representation of that point is given by

$$\hat{\rho} = \begin{bmatrix} x \\ y \\ z \end{bmatrix} = \begin{bmatrix} \sin\theta \cos\phi \\ \sin\theta \sin\phi \\ \cos\theta \end{bmatrix}$$

(7.1-6)

The zenith angle is computed as $\arccos(\hat{\rho} \cdot \hat{z})$ and the azimuth angle as $\arg(\hat{x} \cdot \hat{\rho} + j \hat{y} \cdot \hat{\rho})$, where \hat{x} , \hat{y} and \hat{z} are the Cartesian unit vectors. If this point represents a location in the GCS defined by θ and ϕ , the corresponding position in the LCS is given by $R^{-1}\hat{\rho}$, from which local angles θ' and ϕ' can be computed. The results are given in equations (7.1-7) and (7.1-8).

$$\theta'(\alpha, \beta, \gamma, \theta, \phi) = \arccos \begin{bmatrix} 0 \\ 0 \\ 1 \end{bmatrix}^T R^{-1} \hat{\rho} = \arccos(\cos\beta \cos\gamma \cos\theta + (\sin\beta \cos\gamma \cos(\phi - \alpha) - \sin\gamma \sin(\phi - \alpha)) \sin\theta)$$

(7.1-7)

$$\phi'(\alpha, \beta, \gamma, \theta, \phi) = \arg \begin{bmatrix} 1 \\ 0 \\ 0 \end{bmatrix}^T R^{-1} \hat{\rho} = \arg \begin{bmatrix} (\cos\beta \sin\theta \cos(\phi - \alpha) - \sin\beta \cos\theta) + j(\cos\beta \sin\gamma \cos\theta + (\sin\beta \sin\gamma \cos(\phi - \alpha) + \cos\gamma \sin(\phi - \alpha)) \sin\theta) \end{bmatrix}$$

(7.1-8)

These formulae relate the spherical angles (θ, ϕ) of the GCS to the spherical angles (θ', ϕ') of the LCS given the rotation operation defined by the angles (α, β, γ) .

Let us denote the polarized field components $F_\theta(\theta, \phi)$, $F_\phi(\theta, \phi)$ in the GCS and $F_{\theta'}(\theta', \phi')$, $F_{\phi'}(\theta', \phi')$ in the LCS. These are related by

$$\begin{bmatrix} F_{\theta}(\theta, \phi) \\ F_{\phi}(\theta, \phi) \end{bmatrix} = \begin{bmatrix} \hat{\theta}(\theta, \phi)^T R \hat{\theta}(\theta, \phi) & \hat{\theta}(\theta, \phi)^T R \hat{\phi}(\theta, \phi) \\ \hat{\phi}(\theta, \phi)^T R \hat{\theta}(\theta, \phi) & \hat{\phi}(\theta, \phi)^T R \hat{\phi}(\theta, \phi) \end{bmatrix} \begin{bmatrix} F_{\theta}(\theta, \phi) \\ F_{\phi}(\theta, \phi) \end{bmatrix} \quad (7.1-9)$$

In this equation, $\hat{\theta}$ and $\hat{\phi}$ represent the spherical unit vectors of the GCS, and $\hat{\theta}'$ and $\hat{\phi}'$ are the representations in the LCS. The forward rotation matrix R transforms the LCS unit vectors into the GCS frame of reference. These pairs of unit vectors are orthogonal and can be represented as shown in Figure 7.1.3-3.

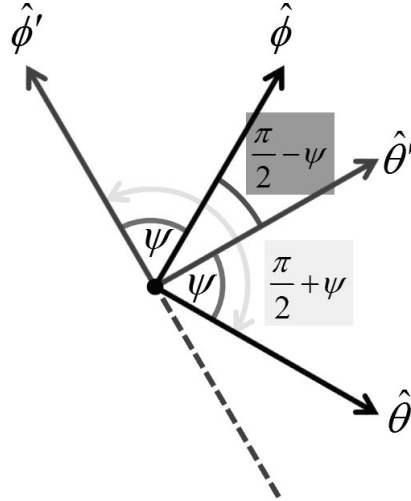


Figure 7.1.3-3: Rotation of the spherical basis vectors by an angle ψ due to the orientation of the LCS with respect to the GCS

Assuming an angular displacement of ψ between the two pairs of unit vectors, the rotation matrix of equation (7.1-9) can be further simplified as:

$$\begin{bmatrix} \hat{\theta}(\theta, \phi)^T R \hat{\theta}(\theta, \phi) & \hat{\theta}(\theta, \phi)^T R \hat{\phi}(\theta, \phi) \\ \hat{\phi}(\theta, \phi)^T R \hat{\theta}(\theta, \phi) & \hat{\phi}(\theta, \phi)^T R \hat{\phi}(\theta, \phi) \end{bmatrix} = \begin{bmatrix} \cos \psi & \cos(\pi/2 + \psi) \\ \cos(\pi/2 - \psi) & \cos \psi \end{bmatrix} = \begin{bmatrix} +\cos \psi & -\sin \psi \\ +\sin \psi & +\cos \psi \end{bmatrix} \quad (7.1-10)$$

and equation (7.1-9) can be written as:

$$\begin{bmatrix} F_{\theta}(\theta, \phi) \\ F_{\phi}(\theta, \phi) \end{bmatrix} = \begin{bmatrix} +\cos \psi & -\sin \psi \\ +\sin \psi & +\cos \psi \end{bmatrix} \begin{bmatrix} F_{\theta}(\theta, \phi) \\ F_{\phi}(\theta, \phi) \end{bmatrix} \quad (7.1-11)$$

The angle ψ can be computed in numerous ways from equation (7.1-10), with one such way approach being

$$\psi = \arg(\hat{\theta}(\theta, \phi)^T R \hat{\theta}(\theta, \phi) + j \hat{\phi}(\theta, \phi)^T R \hat{\theta}(\theta, \phi)) \quad (7.1-12)$$

The dot products are readily computed using the Cartesian representation of the spherical unit vectors. The general expressions for these unit vectors are given by

$$\hat{\theta} = \begin{bmatrix} \cos \theta \cos \phi \\ \cos \theta \sin \phi \\ -\sin \theta \end{bmatrix} \quad (7.1-13)$$

and

$$\hat{\phi} = \begin{bmatrix} -\sin \phi \\ \cos \phi \\ 0 \end{bmatrix} \quad (7.1-14)$$

The angle ψ can be expressed as a function of mechanical orientation (α, β, γ) and spherical position (θ, ϕ) , and is given by

$$\psi = \arg \begin{bmatrix} (\sin \gamma \cos \theta \sin(\phi - \alpha) + \cos \gamma (\cos \beta \sin \theta - \sin \beta \cos \theta \cos(\phi - \alpha))) + j(\sin \gamma \cos(\phi - \alpha) + \sin \beta \cos \gamma \sin(\phi - \alpha)) \\ \end{bmatrix} \quad (7.1-15)$$

It can be shown that $\cos \psi$ and $\sin \psi$ can be expressed as:

$$\cos \psi = \frac{\cos \beta \cos \gamma \sin \theta - (\sin \beta \cos \gamma \cos(\phi - \alpha) - \sin \gamma \sin(\phi - \alpha)) \cos \theta}{\sqrt{1 - (\cos \beta \cos \gamma \cos \theta + (\sin \beta \cos \gamma \cos(\phi - \alpha) - \sin \gamma \sin(\phi - \alpha)) \sin \theta)^2}} \quad (7.1-16)$$

$$\sin \psi = \frac{\sin \beta \cos \gamma \sin(\phi - \alpha) + \sin \gamma \cos(\phi - \alpha)}{\sqrt{1 - (\cos \beta \cos \gamma \cos \theta + (\sin \beta \cos \gamma \cos(\phi - \alpha) - \sin \gamma \sin(\phi - \alpha)) \sin \theta)^2}} \quad (7.1-17)$$

7.1.4 Transformation from an LCS to a GCS for downtilt angle only

In this clause equations are provided for the transformation from LCS to GCS assuming that the orientation of the LCS (with respect to the GCS) is such that the bearing angle $\alpha=0$, the downtilt angle β is non-zero and the slant angle $\gamma=0$. In other words the y' -axis of the LCS is parallel to the y -axis of the GCS. Considering a BS antenna element the x -axis of the GCS is aligned with the pointing direction of the sector. Mechanical downtilt is modelled as a rotation of the LCS around the y -axis. For zero mechanical downtilt the LCS coincides with the GCS.

This transformation relates the spherical angles (θ, ϕ) in the global coordinate system to spherical angles (θ', ϕ') in the local (antenna-fixed) coordinate system and is defined as follows:

$$\theta' = \arccos(\cos \phi \sin \theta \sin \beta + \cos \theta \cos \beta) \quad (7.1-18)$$

$$\phi' = \arg(\cos \phi \sin \theta \cos \beta - \cos \theta \sin \beta + j \sin \phi \sin \theta) \quad (7.1-19)$$

where β is the mechanical tilt angle around the y -axis as defined in Figure 7.1.4. Note that the equations (7.1-7), (7.1-8) reduce to equations (7.1-18), (7.1-19) if both α and γ are zero.

The antenna element pattern $A(\theta, \phi)$ in the GCS is related to the antenna element pattern $A'(\theta', \phi')$ in the LCS by the relation

$$A(\theta, \phi) = A'(\theta', \phi') \quad (7.1-20)$$

with θ' and ϕ' given by (7.1-18) and (7.1-19).

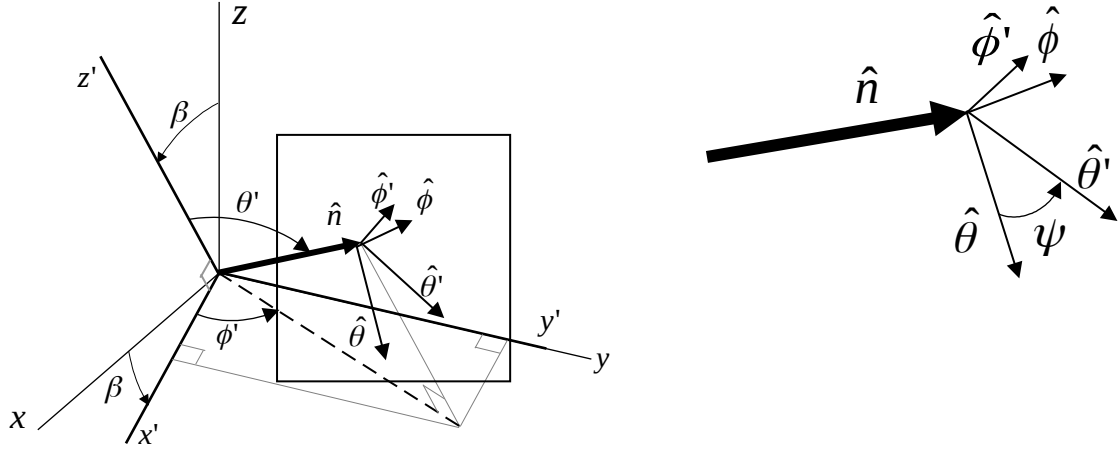


Figure 7.1.4: Definition of angles and unit vectors when the LCS has been rotated an angle β around the y-axis of the GCS

For a mechanical tilt angle β , the global coordinate system field components $F_\theta(\theta, \phi)$ and $F_\phi(\theta, \phi)$, are calculated from the field components $F_{\theta'}(\theta', \phi')$ and $F_{\phi'}(\theta', \phi')$ of the radiation pattern in the local (antenna-fixed) coordinate system as:

$$F_\theta(\theta, \phi) = F_{\theta'}(\theta', \phi') \cos \psi - F_{\phi'}(\theta', \phi') \sin \psi \quad (7.1-21)$$

$$F_\phi(\theta, \phi) = F_{\theta'}(\theta', \phi') \sin \psi + F_{\phi'}(\theta', \phi') \cos \psi \quad (7.1-22)$$

where θ' and ϕ' are defined as in (7.1-18) and (7.1-19), and ψ is defined as:

$$\psi = \arg(\sin \theta \cos \beta - \cos \phi \cos \theta \sin \beta + j \sin \phi \sin \beta). \quad (7.1-23)$$

Note that the equation (7.1-15) is reduced to equation (7.1-23) if both α and γ are zero.

As an example, in the horizontal cut, i.e., for $\theta = 90^\circ$, equations (7.1-18), (7.1-19) and (7.1-23) become

$$\theta' = \arccos(\cos \phi \sin \beta) \quad (7.1-24)$$

$$\phi' = \arg(\cos \phi \cos \beta + j \sin \phi) \quad (7.1-25)$$

$$\psi = \arg(\cos \beta + j \sin \phi \sin \beta) \quad (7.1-26)$$

7.2 Scenarios

The detailed scenario description in this subsection can be used for channel model calibration.

Umi-street canyon and Uma

Details on Umi-street canyon and Uma scenarios are listed in Table 7.2-1.

Table 7.2-1: Evaluation parameters for Umi-street canyon and Uma scenarios

Parameters		Umi – street canyon	Uma
Cell layout		Hexagonal grid, 19 micro sites, 3 sectors per site (ISD = 200m)	Hexagonal grid, 19 macro sites, 3 sectors per site (ISD = 500m)
BS antenna height h_{BS}		10m	25m
UT location	Outdoor/indoor	Outdoor and indoor	Outdoor and indoor
	LOS/NLOS	LOS and NLOS	LOS and NLOS
	Height h_{UT}	Same as 3D-Umi in TR36.873	Same as 3D-Uma in TR36.873
Indoor UT ratio		80%	80%
UT mobility (horizontal plane only)		3km/h	3km/h
Min. BS – UT distance (2D)		10m	35m
UT distribution (horizontal)		Uniform	Uniform

Indoor-office

Details on indoor-office scenarios are listed in Table 7.2-2 and presented in Figure 7.2-1. More details, if necessary, can be added to Figure 7.2-1.

Table 7.2-2: Evaluation parameters for indoor-office scenarios

Parameters		Indoor – office open office	Indoor – office mixed office
Layout	Room size (WxLxH)	120mx50mx3m	
	ISD	20m	
BS antenna height h_{BS}		3 m (ceiling)	
UT location	LOS/NLOS	LOS and NLOS	
	Height h_{UT}	1 m	
UT mobility (horizontal plane only)		3 km/h	
Min. BS – UT distance (2D)		0	
UT distribution (horizontal)		Uniform	

Note: the only difference between the open office and mixed office models in this TR is the line of sight probability.

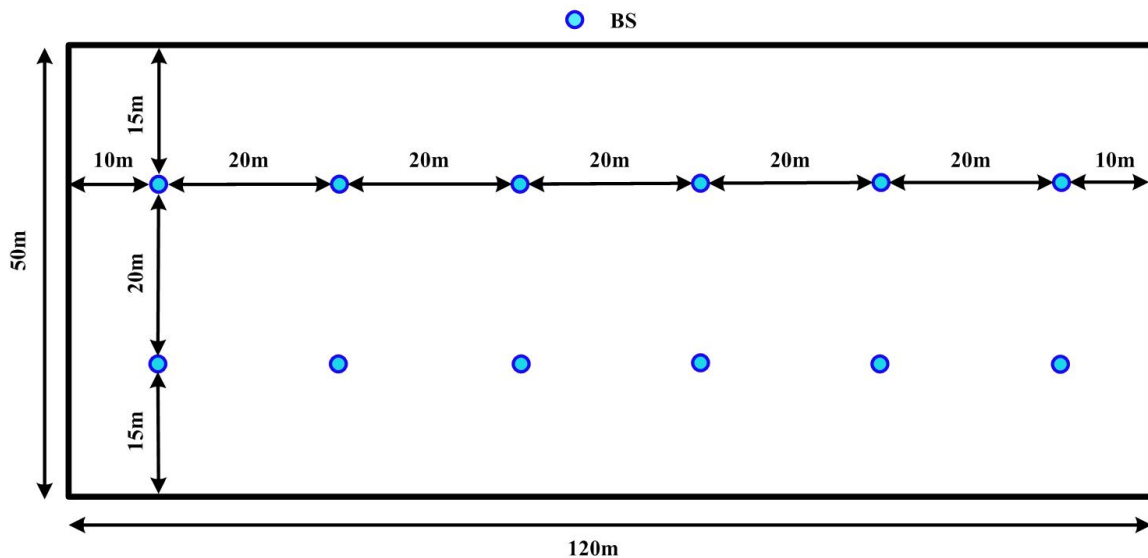


Figure 7.2-1: Layout of indoor office scenarios.

Rma

The rural deployment scenario focuses on larger and continuous coverage. The key characteristics of this scenario are continuous wide area coverage supporting high speed vehicles. This scenario will be noise-limited and/or interference-limited, using macro TRPs. Details of Rma scenario is described in Table 7.2-3.

Table 7.2-3: Evaluation parameters for Rma

Parameters	Rma
Carrier Frequency	Up to 7Ghz
BS height h_{BS}	35m
Layout	Hexagonal grid, 19 Macro sites, 3sectors per site, ISD = 1732m or 5000m
UT height h_{UT}	1.5m
UT distribution	Uniform
Indoor/Outdoor	50% indoor and 50% in car
LOS/NLOS	LOS and NLOS
Min BS- UT distance(2D)	35m

7.3 Antenna modelling

This subsection captures the antenna array structures considered in this SI for calibration.

The BS antenna is modelled by a uniform rectangular panel array, comprising $M_g N_g$ panels, as illustrated in Figure 7.3-1 with M_g being the number of panels in a column and N_g being the number of panels in a row. Furthermore the following properties apply:

- Antenna panels are uniformly spaced in the horizontal direction with a spacing of $d_{g,H}$ and in the vertical direction with a spacing of $d_{g,V}$.
- On each antenna panel, antenna elements are placed in the vertical and horizontal direction, where N is the number of columns, M is the number of antenna elements with the same polarization in each column.
- Antenna numbering on the panel illustrated in Figure 7.3-1 assumes observation of the antenna array from the front (with x-axis pointing towards broad-side and increasing y-coordinate for increasing column number).

- The antenna elements are uniformly spaced in the horizontal direction with a spacing of d_H and in the vertical direction with a spacing of d_V .
- The antenna panel is either single polarized ($P=1$) or dual polarized ($P=2$).

The rectangular panel array antenna can be described by the following tuple (M_g, N_g, M, N, P) .

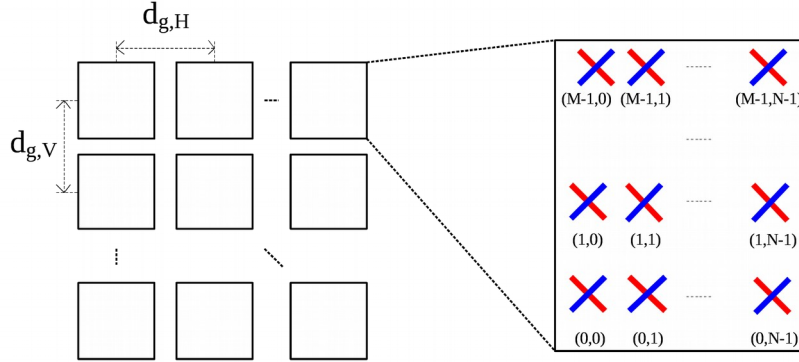


Figure 7.3-1: Cross-polarized panel array antenna model

The antenna radiation power pattern of each antenna element is generated according to Table 7.3-1.

Table 7.3-1: Radiation power pattern of a single antenna element

Parameter	Values
Vertical cut of the radiation power pattern (dB)	$A_{dB}(\theta_{\parallel}, \phi_{\parallel}=0^{\circ}) = -\min_{\theta_{\parallel}} \left[12 \left(\frac{\theta_{\parallel} - 90^{\circ}}{\theta_{3dB}} \right)^2, SLA_V \right]$ <p>with $\theta_{3dB} = 65^{\circ}$, $SLA_V = 30$ dB and $\theta_{\parallel} \in [0^{\circ}, 180^{\circ}]$</p>
Horizontal cut of the radiation power pattern (dB)	$A_{dB}(\theta_{\parallel}=90^{\circ}, \phi_{\parallel}) = -\min_{\phi_{\parallel}} \left[12 \left(\frac{\phi_{\parallel}}{\phi_{3dB}} \right)^2, A_{max} \right]$ <p>with $\phi_{3dB} = 65^{\circ}$, $A_{max} = 30$ dB and $\phi_{\parallel} \in [-180^{\circ}, 180^{\circ}]$</p>
3D radiation power pattern (dB)	$A_{dB}(\theta_{\parallel}, \phi_{\parallel}) = -\min \left[(A_{dB}(\theta_{\parallel}, \phi_{\parallel}=0^{\circ}) + A_{dB}(\theta_{\parallel}=90^{\circ}, \phi_{\parallel})), A_{max} \right]$
Maximum directional gain of an antenna element $G_{E,max}$	8 dBi

7.3.1 Antenna port mapping

Legacy BS array antennas, i.e. uniform linear arrays with fix phase shifts between its M elements to obtain a beamtilt in vertical direction are modelled using complex weights

$$w_m = \frac{1}{\sqrt{M}} \exp \left[-j \frac{2\pi}{\lambda} (m-1) d_V \cos \theta_{tilt} \right] \quad (7.3-1)$$

where $m=1, \dots, M$, is the electrical vertical steering angle defined between 0° and 180° (90° represents perpendicular to the array). λ denotes the wavelength and d_V the vertical element spacing.

7.3.2 Polarized antenna modelling

In general the relationship between radiation field and power pattern is given by:

$$A(\theta, \phi) = |F_{\theta}(\theta, \phi)|^2 + |F_{\phi}(\theta, \phi)|^2. \quad (7.3-2)$$

The following two models represent two options on how to determine the radiation field patterns based on a defined radiation power pattern.

Model-1:

In case of polarized antenna elements assume ζ is the polarization slant angle where $\zeta = 0$ degrees corresponds to a purely vertically polarized antenna element and $\zeta = \pm 45$ degrees correspond to a pair of cross-polarized antenna elements. Then the antenna element field components in θ' and ϕ' direction are given by

$$\begin{bmatrix} F_{\theta'}(\theta, \phi) \\ F_{\phi'}(\theta, \phi) \end{bmatrix} = \begin{bmatrix} +\cos\psi & -\sin\psi \\ +\sin\psi & +\cos\psi \end{bmatrix} \begin{bmatrix} F_{\theta}(\theta, \phi) \\ F_{\phi}(\theta, \phi) \end{bmatrix} \quad (7.3-3)$$

$$\text{where } \cos\psi = \frac{\cos\zeta \sin\theta + \sin\zeta \sin\phi \cos\theta}{\sqrt{1 - (\cos\zeta \cos\theta - \sin\zeta \sin\phi \sin\theta)^2}}, \quad \sin\psi = \frac{\sin\zeta \cos\phi}{\sqrt{1 - (\cos\zeta \cos\theta - \sin\zeta \sin\phi \sin\theta)^2}}.$$

Note that the zenith and the azimuth field components $F_{\theta}(\theta, \phi)$, $F_{\phi}(\theta, \phi)$, $F_{\theta'}(\theta, \phi)$ and $F_{\phi'}(\theta, \phi)$ are defined in terms of the spherical basis vectors of an LCS as defined in Section 7.1. The difference between the single-primed and the double-primed components is that the single-primed field components account for the polarization slant and the double-primed field components do not. For a single polarized antenna (purely vertically polarized antenna) we can write $F_{\theta'}(\theta, \phi) = \sqrt{A(\theta, \phi)}$ and $F_{\phi'}(\theta, \phi) = 0$ where $A(\theta, \phi)$ is the 3D antenna radiation power pattern as a function of azimuth angle ϕ and zenith angle θ in the LCS as defined in Table 7.3-1 converted into linear scale.

Model-2:

In case of polarized antennas, the polarization is modelled as angle-independent in both azimuth and elevation, in an LCS. For a linearly polarized antenna, the antenna element field pattern, in the vertical polarization and in the horizontal polarization, are given by

$$F_{\theta'}(\theta, \phi) = \sqrt{A(\theta, \phi)} \cos(\zeta) \quad (7.3-4)$$

and

$$F_{\phi'}(\theta, \phi) = \sqrt{A(\theta, \phi)} \sin(\zeta), \quad (7.3-5)$$

respectively, where ζ is the polarization slant angle and $A(\theta, \phi)$ is the 3D antenna element power pattern as a function of azimuth angle, ϕ and elevation angle, θ in the LCS. Note that $\zeta = 0$ degrees correspond to a purely vertically polarized antenna element. The vertical and horizontal field directions are defined in terms of the spherical basis vectors, $\hat{\theta}'$ and $\hat{\phi}'$ respectively in the LCS as defined in Section 7.1.2. Also $A(\theta, \phi) = A(\theta, \phi)$, $\theta = \theta$ and $\phi = \phi$ as defined in Table 7.1-1.

7.4 Pathloss, LOS probability and penetration modelling

7.4.1 Pathloss

The pathloss models are summarized in Table 7.4.1-1 and the distance definitions are indicated in Figure 7.4.1-1 and Figure 7.4.1-2. Note that the distribution of the shadow fading is log-normal, and its standard deviation for each scenario is given in Table 7.4.1-1.

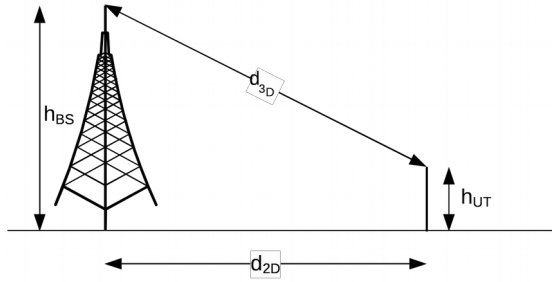


Figure 7.4.1-1: Definition of d_{2D} and d_{3D} for outdoor Uts

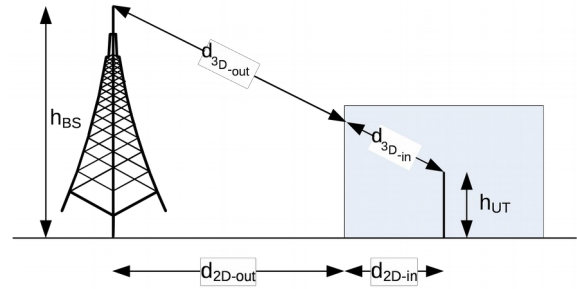


Figure 7.4.1-2: Definition of d_{2D-out} , d_{2D-in} and d_{3D-out} , d_{3D-in} for indoor Uts.

Note that

$$d_{3D-out} + d_{3D-in} = \sqrt{(d_{2D-out} + d_{2D-in})^2 + (h_{BS} - h_{UT})^2} \quad (7.4-1)$$

Table 7.4.1-1: Pathloss models

Scenario	LOS/NLOS	Pathloss [dB], f_c is in GHz and d is in meters ⁽⁶⁾	Shadow fading std [dB]	Applicability range, antenna height default values
RMa	LOS	$PL_{\text{RMa-LOS}} = \begin{cases} PL_1 & 10\text{m} \leq d_{2D} \leq d_{\text{BP}} \\ PL_2 & d_{\text{BP}} \leq d_{2D} \leq 10\text{km} \end{cases}, \text{ see note 5}$ $PL_1 = 20\log_{10}(40\pi d_{3D} f_c / 3) + \min(0.03h^{1.72}, 10)\log_{10}(d_{3D}) - \min(0.044h^{1.72}, 14.77) + 0.002\log_{10}(h)d_{3D}$ $PL_2 = PL_1(d_{\text{BP}}) + 40\log_{10}(d_{3D} / d_{\text{BP}})$	$\sigma_{\text{SF}} = 4$ $\sigma_{\text{SF}} = 6$	$h_{\text{BS}} = 35\text{m}$ $h_{\text{UT}} = 1.5\text{m}$ $W = 20\text{m}$ $h = 5\text{m}$ h = avg. building height W = avg. street width The applicability ranges:
	NLOS	$PL_{\text{RMa-NLOS}} = \max(PL_{\text{RMa-LOS}}, PL'_{\text{RMa-NLOS}})$ for $10\text{m} \leq d_{2D} \leq 5\text{km}$ $PL'_{\text{RMa-NLOS}} = 161.04 - 7.1\log_{10}(W) + 7.5\log_{10}(h) - (24.37 - 3.7(h/h_{\text{BS}})^2)\log_{10}(h_{\text{BS}}) + (43.42 - 3.1\log_{10}(h_{\text{BS}}))(\log_{10}(d_{3D}) - 3) + 20\log_{10}(f_c) - (3.2(\log_{10}(11.75h_{\text{UT}}))^2 - 4.97)$	$\sigma_{\text{SF}} = 8$	$5\text{m} \leq h \leq 50\text{m}$ $5\text{m} \leq W \leq 50\text{m}$ $10\text{m} \leq h_{\text{BS}} \leq 150\text{m}$ $1\text{m} \leq h_{\text{UT}} \leq 10\text{m}$
UMa	LOS	$PL_{\text{UMa-LOS}} = \begin{cases} PL_1 & 10\text{m} \leq d_{2D} \leq d_{\text{BP}} \\ PL_2 & d_{\text{BP}} \leq d_{2D} \leq 5\text{km} \end{cases}, \text{ see note 1}$ $PL_1 = 28.0 + 22\log_{10}(d_{3D}) + 20\log_{10}(f_c)$ $PL_2 = 28.0 + 40\log_{10}(d_{3D}) + 20\log_{10}(f_c) - 9\log_{10}((d'_{\text{BP}})^2 + (h_{\text{BS}} - h_{\text{UT}})^2)$	$\sigma_{\text{SF}} = 4$	$1.5\text{m} \leq h_{\text{UT}} \leq 22.5\text{m}$ $h_{\text{BS}} = 25\text{m}$
	NLOS	$PL_{\text{UMa-NLOS}} = \max(PL_{\text{UMa-LOS}}, PL'_{\text{UMa-NLOS}})$ for $10\text{m} \leq d_{2D} \leq 5\text{km}$ $PL'_{\text{UMa-NLOS}} = 13.54 + 39.08\log_{10}(d_{3D}) + 20\log_{10}(f_c) - 0.6(h_{\text{UT}} - 1.5)$	$\sigma_{\text{SF}} = 6$	$1.5\text{m} \leq h_{\text{UT}} \leq 22.5\text{m}$ $h_{\text{BS}} = 25\text{m}$ Explanations: see note 3
		Optional PL $= 32.4 + 20\log_{10}(f_c) + 30\log_{10}(d_{3D})$	$\sigma_{\text{SF}} = 7.8$	
UMi – Street Canyon	LOS	$PL_{\text{UMi-LOS}} = \begin{cases} PL_1 & 10\text{m} \leq d_{2D} \leq d_{\text{BP}} \\ PL_2 & d_{\text{BP}} \leq d_{2D} \leq 5\text{km} \end{cases}, \text{ see note 1}$ $PL_1 = 32.4 + 21\log_{10}(d_{3D}) + 20\log_{10}(f_c)$ $PL_2 = 32.4 + 40\log_{10}(d_{3D}) + 20\log_{10}(f_c) - 9.5\log_{10}((d'_{\text{BP}})^2 + (h_{\text{BS}} - h_{\text{UT}})^2)$	$\sigma_{\text{SF}} = 4$	$1.5\text{m} \leq h_{\text{UT}} \leq 22.5\text{m}$ $h_{\text{BS}} = 10\text{m}$

InH – Office	NLOS	$PL_{\text{UMi-NLOS}} = \max(PL_{\text{UMi-LOS}}, PL'_{\text{UMi-NLOS}})$ for $10\text{m} \leq d_{2D} \leq 5\text{km}$ $PL'_{\text{UMi-NLOS}} = 35.3\log_{10}(d_{3D}) + 22.4$ $+ 21.3\log_{10}(f_c) - 0.3(h_{\text{UT}} - 1.5)$	$\sigma_{\text{SF}} = 7.82$	$1.5\text{m} \leq h_{\text{UT}} \leq 22.5\text{m}$ $h_{\text{BS}} = 10\text{m}$ Explanations: see note 4
		Optional $PL = 32.4 + 20\log_{10}(f_c) + 31.9\log_{10}(d_{3D})$	$\sigma_{\text{SF}} = 8.2$	
	LOS	$PL_{\text{InH-LOS}} = 32.4 + 17.3\log_{10}(d_{3D}) + 20\log_{10}(f_c)$	$\sigma_{\text{SF}} = 3$	$1\text{m} \leq d_{3D} \leq 100\text{m}$
NLOS	$PL_{\text{InH-NLOS}} = \max(PL_{\text{InH-LOS}}, PL'_{\text{InH-NLOS}})$ $PL'_{\text{InH-NLOS}} = 38.3\log_{10}(d_{3D}) + 17.30 + 24.9\log_{10}(f_c)$	$\sigma_{\text{SF}} = 8.03$	$1\text{m} \leq d_{3D} \leq 86\text{m}$	
	Optional $PL'_{\text{InH-NLOS}} = 32.4 + 20\log_{10}(f_c) + 31.9\log_{10}(d_{3D})$	$\sigma_{\text{SF}} = 8.29$	$1\text{m} \leq d_{3D} \leq 86\text{m}$	

Note 1 : Breakpoint distance $d'_{\text{BP}} = 4 h'_{\text{BS}} h'_{\text{UT}} f_c/c$, where f_c is the centre frequency in Hz, $c = 3.0 \times 10^8$ m/s is the propagation velocity in free space, and h'_{BS} and h'_{UT} are the effective antenna heights at the BS and the UT, respectively. The effective antenna heights h'_{BS} and h'_{UT} are computed as follows: $h'_{\text{BS}} = h_{\text{BS}} - h_{\text{E}}$, $h'_{\text{UT}} = h_{\text{UT}} - h_{\text{E}}$, where h_{BS} and h_{UT} are the actual antenna heights, and h_{E} is the effective environment height. For Umi $h_{\text{E}} = 1.0\text{m}$. For Uma $h_{\text{E}} = 1\text{m}$ with a probability equal to $1/(1+C(d_{2D}, h_{\text{UT}}))$ and chosen from a discrete uniform distribution $\text{uniform}(12, 15, \dots, (h_{\text{UT}} - 1.5))$ otherwise. With $C(d_{2D}, h_{\text{UT}})$ given by

$$C(d_{2D}, h_{\text{UT}}) = \begin{cases} 0 & , h_{\text{UT}} < 13\text{m} \\ \frac{h_{\text{UT}} - 13}{10} g(d_{2D}) & , 13\text{m} \leq h_{\text{UT}} \leq 23\text{m} \end{cases}$$

where

$$g(d_{2D}) = \begin{cases} 0 & , d_{2D} \leq 18\text{m} \\ \frac{5}{4} \left(\frac{d_{2D}}{100} \right)^3 \exp\left(-\frac{d_{2D}}{150} \right) & , 18\text{m} < d_{2D} \end{cases}$$

Note 2 : The applicable frequency range of the PL formula in this table is $0.5 < f_c < f_{\text{H}}$ GHz, where $f_{\text{H}} = 30$ GHz for Rma and $f_{\text{H}} = 100$ GHz for all the other scenarios. It is noted that Rma pathloss model for >7 GHz is validated based on a single measurement campaign conducted at 24 GHz.

Note 3: Uma NLOS pathloss is from TR36.873 with simplified format and $PL_{\text{Uma-LOS}} = \text{Pathloss of Uma LOS outdoor scenario}$.

Note 4: $PL_{\text{Umi-LOS}} = \text{Pathloss of Umi-Street Canyon LOS outdoor scenario}$.

Note 5: Break point distance $d_{\text{BP}} = 2\pi h_{\text{BS}} h_{\text{UT}} f_c/c$, where f_c is the centre frequency in Hz, $c = 3.0 \times 10^8$ m/s is the propagation velocity in free space, and h_{BS} and h_{UT} are the antenna heights at the BS and the UT, respectively.

Note 6: f_c denotes the center frequency normalized by 1GHz, all distance related values are normalized by 1m, unless it is stated otherwise.

7.4.2 LOS probability

The Line-Of-Sight (LOS) probabilities are given in Table 7.4.2-1.

Table 7.4.2-1 LOS probability

Scenario	LOS probability (distance is in meters)
Rma	$P_{LOS} = \begin{cases} 1 & , d_{2D} \leq 10\text{m} \\ \exp\left[-\frac{d_{2D} - 10}{1000}\right] & , 10\text{m} < d_{2D} \end{cases}$
Umi – Street canyon	<p>Outdoor users:</p> $P_{LOS} = \begin{cases} 1 & , d_{2D} \leq 18\text{m} \\ \frac{18}{d_{2D}} + \exp\left[-\frac{d_{2D}}{36}\right] \left(1 - \frac{18}{d_{2D}}\right) & , 18\text{m} < d_{2D} \end{cases}$ <p>Indoor users: Use d_{2D-out} in the formula above instead of d_{2D}</p>
Uma	<p>Outdoor users:</p> $P_{LOS} = \begin{cases} 1 & , d_{2D} \leq 18\text{m} \\ \frac{18}{d_{2D}} + \exp\left[-\frac{d_{2D}}{63}\right] \left(1 - \frac{18}{d_{2D}}\right) + C(h_{UT}) \frac{5}{4} \left(\frac{d_{2D}}{100}\right)^3 \exp\left[-\frac{d_{2D}}{150}\right] & , 18\text{m} < d_{2D} \end{cases}$ <p>where</p> $C(h_{UT}) = \begin{cases} 0 & , h_{UT} \leq 13\text{m} \\ \frac{h_{UT} - 13}{10}^{1.5} & , 13\text{m} < h_{UT} \leq 23\text{m} \end{cases}$ <p>Indoor users: Use d_{2D-out} in the formula above instead of d_{2D}</p>
Indoor – Mixed office	$P_{LOS} = \begin{cases} 1 & , d_{2D} \leq 1.2\text{m} \\ \exp\left[-\frac{d_{2D} - 1.2}{4.7}\right] & , 1.2\text{m} < d_{2D} < 6.5\text{m} \\ \exp\left[-\frac{d_{2D} - 6.5}{32.6}\right] \cdot 0.32 & , 6.5\text{m} \leq d_{2D} \end{cases}$
Indoor – Open office	$P_{LOS}^{Open_office} = \begin{cases} 1 & , d_{2D} \leq 5\text{m} \\ \exp\left[-\frac{d_{2D} - 5}{70.8}\right] & , 5\text{m} < d_{2D} \leq 49\text{m} \\ \exp\left[-\frac{d_{2D} - 49}{211.7}\right] \cdot 0.54 & , 49\text{m} < d_{2D} \end{cases}$
Note:	The LOS probability is derived with assuming antenna heights of 3m for indoor, 10m for Umi, and 25m for Uma

7.4.3 O2I penetration loss

The pathloss incorporating O2I building penetration loss is modelled as in the following:

$$PL = PL_b + PL_{tw} + PL_{in} + N(0, \sigma_p^2) \quad (7.4-2)$$

where PL_b is the basic outdoor path loss given in Section 7.4.1, where d_{3D} is replaced by $(d_{3D-out} + d_{3D-in})$. PL_{tw} is the building penetration loss through the external wall, PL_{in} is the inside loss dependent on the depth into the building, and σ_p is the standard deviation for the penetration loss.

PL_{tw} is characterized as:

$$PL_{tw} = PL_{npi} - 10 \log_{10} \sum_{i=1}^N p_i \times 10^{\frac{L_{material_i}}{-10}} \quad (7.4-3)$$

PL_{npi} is an additional loss is added to the external wall loss to account for non-perpendicular incidence;

$L_{material_i} = a_{material_i} + b_{material_i} \cdot f$, is the penetration loss of material I , example values of which can be found in Table

7.4.3-1. P_i is proportion of i -th materials, where $\sum_{i=1}^N p_i = 1$; and N is the number of materials.

Table 7.4.3-1: Material penetration losses

Material	Penetration loss [dB]
Standard multi-pane glass	$L_{glass} = 2 + 0.2 f$
IRR glass	$L_{IRRglass} = 23 + 0.3 f$
Concrete	$L_{concrete} = 5 + 4 f$
Wood	$L_{wood} = 4.85 + 0.12 f$
Note: f is in GHz	

Table 7.4.3-2 gives PL_{tw} , PL_{in} and σ_p for two O2I penetration loss models. The O2I penetration is UT-specifically generated, and is added to the SF realization in the log domain.

Table 7.4.3-2: O2I penetration loss model

	Path loss through external wall: PL_{tw} in [dB]	Indoor loss: PL_{in} in [dB]	Standard deviation: σ_p in [dB]
Low-loss model	$5 - 10 \log_{10} \left[0.3 \cdot 10^{\frac{-L_{glass}}{10}} + 0.7 \cdot 10^{\frac{-L_{concrete}}{10}} \right]$	$0.5 d_{2D-in}$	4.4
High-loss model	$5 - 10 \log_{10} \left[0.7 \cdot 10^{\frac{-L_{IRRglass}}{10}} + 0.3 \cdot 10^{\frac{-L_{concrete}}{10}} \right]$	$0.5 d_{2D-in}$	6.5

d_{2D-in} is minimum of two independently generated uniformly distributed variables between 0 and 25 m for Uma and Umi-Street Canyon, and between 0 and 10 m for Rma. d_{2D-in} shall be UT-specifically generated.

Both low-loss and high-loss models are applicable to Uma and Umi-Street Canyon.

Only the low-loss model is applicable to Rma.

The composition of low and high loss is a simulation parameter that should be determined by the user of the channel models, and is dependent on the use of metal-coated glass in buildings and the deployment scenarios. Such use is expected to differ in different markets and regions of the world and also may increase over years to new regulations and energy saving initiatives. Furthermore, the use of such high-loss glass currently appears to be more predominant in commercial buildings than in residential buildings in some regions of the world¹.

¹

One example survey for the US market can be found in [5]. The survey does not necessarily be representative for all the scenarios. Other ratios outside of the survey should not be precluded.

The pathloss incorporating O2I car penetration loss is modelled as in the following:

$$PL = PL_b + N(\mu, \sigma_p^2) \quad (7.4-4)$$

where PL_b is the basic outdoor path loss given in Section 7.4.1. $\mu = 9$, and $\sigma_p = 5$. The car penetration loss shall be UT-specifically generated. Optionally, for metallized car windows, $\mu = 20$ can be used. The O2I car penetration loss models are applicable for at least 0.6-60 GHz.

For backwards compatibility with TR 36.873 [3], the following building penetration model should be used for Uma and Umi single-frequency simulations at frequencies below 6 GHz.

Table 7.4.3-3. Building penetration loss model for single-frequency simulations <6 GHz

Parameter	Value
PL_{tw}	20 dB
PL_{in}	$0.5d_{2D-in}$ with d_{2D-in} being a single, link-specific, uniformly distributed variable between 0 and 25 m
σ_p	0 dB
σ_{SF}	7 dB (note: replacing the respective value in Table 7.4.1-1)

7.4.4 Autocorrelation of shadow fading

The long-term (log-normal) fading in the logarithmic scale around the mean path loss PL (dB) is characterized by a Gaussian distribution with zero mean and standard deviation. Due to the slow fading process versus distance Δx (Δx is in the horizontal plane), adjacent fading values are correlated. Its normalized autocorrelation function $R(\Delta x)$ can be described with sufficient accuracy by the exponential function ITU-R Rec. P.1816 [18]

$$R(\Delta x) = e^{-\frac{|\Delta x|}{d_{cor}}} \quad (7.4-5)$$

with the correlation length d_{cor} being dependent on the environment, see the correlation parameters for shadowing and other large scale parameters in Table 7.5-6 (Channel model parameters). In a spatial consistency procedure in Section 7.6.3, the cluster specific random variables are also correlated following the exponential function with respect to correlation distances in the two dimensional horizontal plane.

7.5 Fast fading model

The radio channel realizations are created using the parameters listed in Table 7.5-1. The channel realizations are obtained by a step-wise procedure illustrated in Figure 7.5-1 and described below. It has to be noted that the geometric description covers arrival angles from the last bounce scatterers and respectively departure angles to the first scatterers interacted from the transmitting side. The propagation between the first and the last interaction is not defined. Thus, this approach can model also multiple interactions with the scattering media. This indicates also that e.g., the delay of a multipath component cannot be determined by the geometry. In the following steps, downlink is assumed. For uplink, arrival and departure parameters have to be swapped.

Note: the channel generation in this section is enough for at least the following cases.

- Case 1: For low complexity evaluations
- Case 2: To compare with earlier simulation results,
- Case 3: When none of the additional 3D modelling components are turned on.

For other advanced simulations, e.g., spatially consistency, large bandwidth and arrays, oxygen absorption, blockage, etc., some of the additional modelling components of Section 7.6 should be considered.

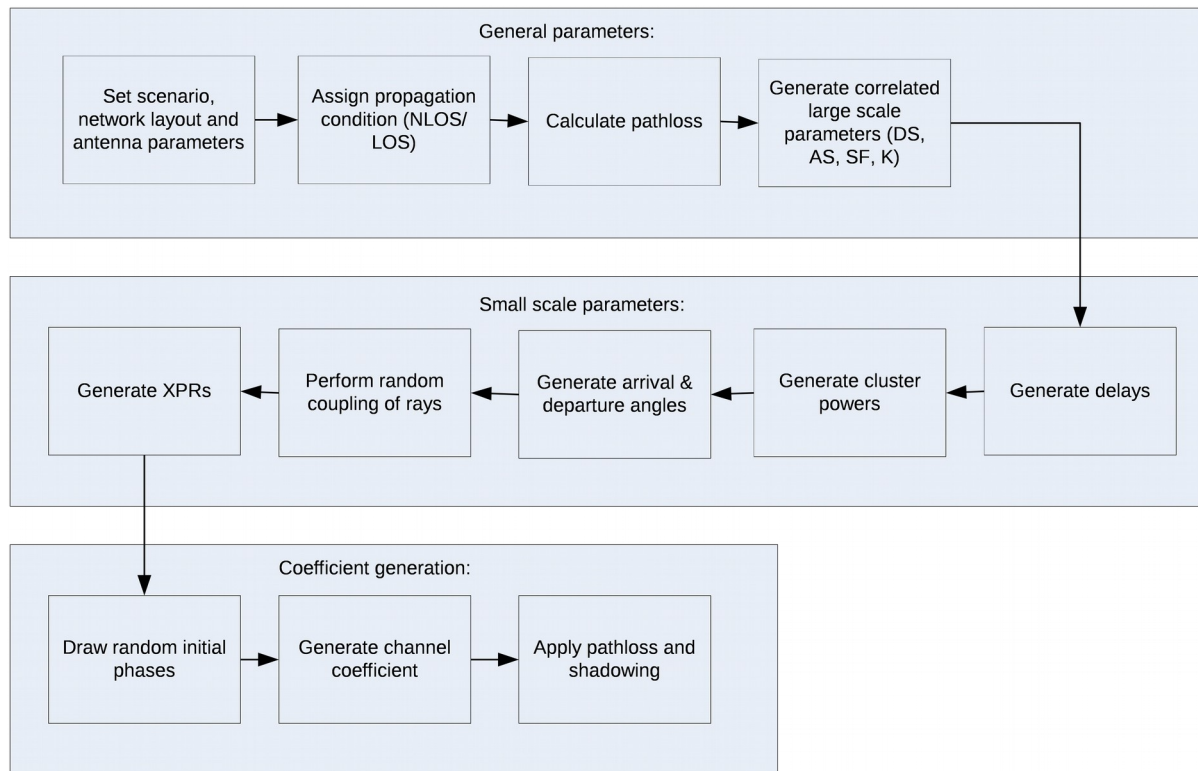


Figure 7.5-1 Channel coefficient generation procedure

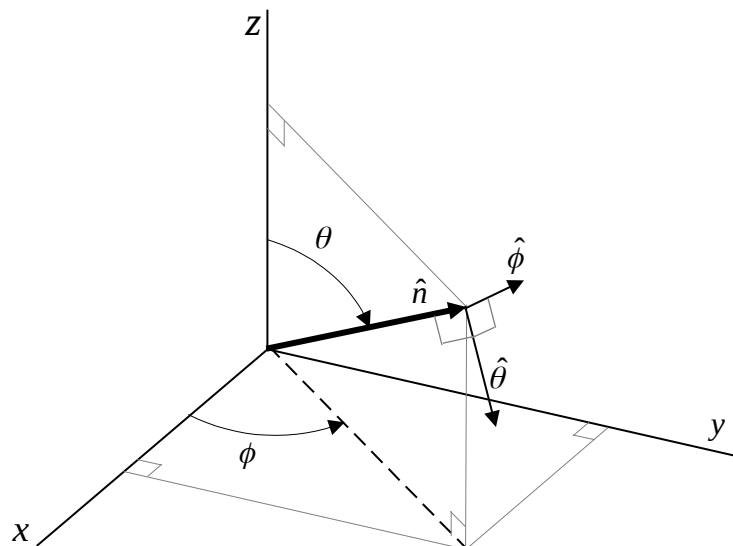


Figure 7.5-2: Definition of a global coordinate system showing the zenith angle θ and the azimuth angle ϕ . $\theta=0^\circ$ points to zenith and $\theta=+90^\circ$ points to the horizon.

The spherical basis vectors $\hat{\theta}$ and $\hat{\phi}$ shown above are defined based on the direction of propagation \hat{n} .

Table 7.5-1: Notations in the global coordinate system (GCS)

Parameter	Notation
LOS AOD	$\phi_{LOS,AOD}$
LOS AOA	$\phi_{LOS,AOA}$
LOS ZOD	$\theta_{LOS,ZOD}$
LOS ZOA	$\theta_{LOS,ZOA}$
AOA for cluster n	$\phi_{n,AOA}$
AOD for cluster n	$\phi_{n,AOD}$
AOA for ray m in cluster n	$\phi_{n,m,AOA}$
AOD for ray m in cluster n	$\phi_{n,m,AOD}$
ZOA for cluster n	$\theta_{n,ZOA}$
ZOD for cluster n	$\theta_{n,ZOD}$
ZOA for ray m in cluster n	$\theta_{n,m,ZOA}$
ZOD for ray m in cluster n	$\theta_{n,m,ZOD}$
Receive antenna element u field pattern in the direction of the spherical basis vector $\hat{\theta}$	$F_{rx,u,\theta}$
Receive antenna element u field pattern in the direction of the spherical basis vector $\hat{\phi}$	$F_{rx,u,\phi}$
Transmit antenna element s field pattern in the direction of the spherical basis vector $\hat{\theta}$	$F_{tx,s,\theta}$
Transmit antenna element s field pattern in the direction of the spherical basis vector $\hat{\phi}$	$F_{tx,s,\phi}$

Step 1: Set environment, network layout, and antenna array parameters

- Choose one of the scenarios (e.g. Uma, Umi-Street Canyon, Rma or InH-Office). Choose a global coordinate system and define zenith angle θ , azimuth angle ϕ , and spherical basis vectors $\hat{\theta}$, $\hat{\phi}$ as shown in Figure 7.3-2. Note: Scenario Rma is for up to 7GHz while others are for up to 100GHz
- Give number of BS and UT
- Give 3D locations of BS and UT, and determine LOS AOD ($\phi_{LOS,AOD}$), LOS ZOD ($\theta_{LOS,ZOD}$), LOS AOA ($\phi_{LOS,AOA}$), and LOS ZOA ($\theta_{LOS,ZOA}$) of each BS and UT in the global coordinate system
- Give BS and UT antenna field patterns F_{rx} and F_{tx} in the global coordinate system and array geometries
- Give BS and UT array orientations with respect to the global coordinate system. BS array orientation is defined by three angles $\Omega_{BS,\alpha}$ (BS bearing angle), $\Omega_{BS,\beta}$ (BS downtilt angle) and $\Omega_{BS,\gamma}$ (BS slant angle). UT array orientation is defined by three angles $\Omega_{UT,\alpha}$ (UT bearing angle), $\Omega_{UT,\beta}$ (UT downtilt angle) and $\Omega_{UT,\gamma}$ (UT slant angle).
- Give speed and direction of motion of UT in the global coordinate system
- Specify system centre frequency f_c and bandwidth B

Note: In case wrapping is used, each wrapping copy of a BS or site should be treated as a separate BS/site considering channel generation.

Large scale parameters:

Step 2: Assign propagation condition (LOS/NLOS) according to Table 7.4.2-1. The propagation conditions for different BS-UT links are uncorrelated.

Also, assign an indoor/outdoor state for each UT. It is noted that all the links from a UT have the same indoor/outdoor state.

Step 3: Calculate pathloss with formulas in Table 7.4.1-1 for each BS-UT link to be modelled.

Step 4: Generate large scale parameters, e.g. delay spread (DS), angular spreads (ASA, ASD, ZSA, ZSD), Ricean K factor (K) and shadow fading (SF) taking into account cross correlation according to Table 7.5-6 and using the procedure described in section 3.3.1 of [14] with the square root matrix $\sqrt{C_{M \times M}(\mathbf{0})}$ being generated using the Cholesky decomposition and the following order of the large scale parameter vector: $\mathbf{s}_M = [s_{SF}, s_K, s_{DS}, s_{ASD}, s_{ASA}, s_{ZSD}, s_{ZSA}]^T$.

These LSPs for different BS-UT links are uncorrelated, but the LSPs for links from co-sited sectors to a UT are the same. In addition, these LSPs for the links of Uts on different floors are uncorrelated.

Limit random RMS azimuth arrival and azimuth departure spread values to 104 degrees, i.e., $ASA = \min(ASA, 104^\circ)$, $ASD = \min(ASD, 104^\circ)$. Limit random RMS zenith arrival and zenith departure spread values to 52 degrees, i.e., $ZSA = \min(ZSA, 52^\circ)$, $ZSD = \min(ZSD, 52^\circ)$.

Small scale parameters:

Step 5: Generate delays .

Delays are drawn randomly from the delay distribution defined in Table 7.5-6. With exponential delay distribution calculate

$$\tau'_n = -r_\tau \text{DS} \ln(X_n), \quad (7.5-1)$$

Where r_τ is the delay distribution proportionality factor, $X_n \sim \text{uniform}(0,1)$, and cluster index $n = 1, \dots, N$. With uniform delay distribution the delay values τ'_n are drawn from the corresponding range. Normalise the delays by subtracting the minimum delay and sort the normalised delays to ascending order:

$$\tau_n = \text{sort}(\tau'_n - \min(\tau'_n)). \quad (7.5-2)$$

In the case of LOS condition, additional scaling of delays is required to compensate for the effect of LOS peak addition to the delay spread. The heuristically determined Ricean K-factor dependent scaling constant is

$$C_\tau = 0.7705 - 0.0433K + 0.0002K^2 + 0.000017K^3, \quad (7.5-3)$$

where K [dB] is the Ricean K-factor as generated in Step 4. The scaled delays

$$\tau_n^{LOS} = \tau_n / C_\tau, \quad (7.5-4)$$

are **not** to be used in cluster power generation.

Step 6: Generate cluster powers P_n .

Cluster powers are calculated assuming a single slope exponential power delay profile. Power assignment depends on the delay distribution defined in Table 7.5-6. With exponential delay distribution the cluster powers are determined by

$$P'_n = \exp\left[-\tau_n \frac{r_\tau - 1}{r_\tau \text{DS}}\right] \cdot 10^{\frac{-Z_n}{10}} \quad (7.5-5)$$

where $Z_n \sim \mathcal{N}(0, \xi^2)$ is the per cluster shadowing term in [dB]. Normalize the cluster powers so that the sum of all cluster powers is equal to one, i.e.,

$$P_n = \frac{P'_n}{\sum_{n=1}^N P'_n} \quad (7.5-6)$$

In the case of LoS condition an additional specular component is added to the first cluster. Power of the single LoS ray is:

$$P_{1,LOS} = \frac{K_R}{K_R + 1} \quad (7.5-7)$$

and the cluster powers are not normalized as in equation (7.5-6) , but:

$$P_n = \frac{1}{K_R + 1} \frac{P_n^{\square}}{\sum_{n=1}^N P_n'} + \delta(n-1)P_{1,LOS} \quad (7.5-8)$$

where $\delta(\cdot)$ is Dirac's delta function and K_R is the Ricean K -factor as generated in Step 4 converted to linear scale. These power values are used *only* in equations (7.5-9) and (7.5-14), but *not* in equation (7.5-22).

Assign the power of each ray within a cluster as P_n / M , where M is the number of rays per cluster.

Remove clusters with less than -25 dB power compared to the maximum cluster power. The scaling factors need not be changed after cluster elimination.

Step 7: Generate arrival angles and departure angles for both azimuth and elevation.

The composite PAS in azimuth of all clusters is modelled as wrapped Gaussian (see Table 7.5-6). The AOAs are determined by applying the inverse Gaussian function (7.5-9) with input parameters P_n and RMS angle spread ASA

$$\phi_{n,AOA}' = \frac{2(ASA/1.4)\sqrt{-\ln(P_n/\max(P_n))}}{C_\phi}, \quad (7.5-9)$$

with C_ϕ defined as

$$C_\phi = \begin{cases} C_\phi^{\text{NLOS}} \cdot (1.1035 - 0.028K - 0.002K^2 + 0.0001K^3) & \text{, for LOS} \\ C_\phi^{\text{NLOS}} & \text{, for NLOS} \end{cases} \quad (7.5-10)$$

where C_ϕ^{NLOS} is defined as a scaling factor related to the total number of clusters and is given in Table 7.5-2:

Table 7.5-2: Scaling factors for AOA, AOD generation

# clusters	4	5	8	10	11	12	14	15	16	19	20
C_ϕ^{NLOS}	0.779	0.860	1.018	1.090	1.123	1.146	1.190	1.211	1.226	1.273	1.289

In the LOS case, constant C_ϕ also depends on the Ricean K -factor K in [dB], as generated in Step 4. Additional scaling of the angles is required to compensate for the effect of LOS peak addition to the angle spread.

Assign positive or negative sign to the angles by multiplying with a random variable X_n with uniform distribution to the discrete set of $\{1, -1\}$, and add component $Y_n \sim N(0, (ASA/7)^2)$ to introduce random variation

$$\phi_{n,AOA} = X_n \phi_{n,AOA}' + Y_n + \phi_{LOS,AOA}, \quad (7.5-11)$$

where $\phi_{LOS,AOA}$ is the LOS direction defined in the network layout description, see Step1c.

In the LOS case, substitute (7.5-11) by (7.5-12) to enforce the first cluster to the LOS direction $\phi_{LOS,AOA}$

$$\phi_{n,AOA} = (X_n \phi_{n,AOA}' + Y_n) - (X_1 \phi_{1,AOA}' + Y_1 - \phi_{LOS,AOA}) \quad (7.5-12)$$

Finally add offset angles α_m from Table 7.5-3 to the cluster angles

$$\phi_{n,m,AOA} = \phi_{n,AOA} + C_{ASA} \alpha_m, \quad (7.5-13)$$

where C_{ASA} is the cluster-wise rms azimuth spread of arrival angles (cluster ASA) in Table 7.5-6.

Table 7.5-3: Ray offset angles within a cluster, given for rms angle spread normalized to 1

Ray number m	Basis vector of offset angles α_m
1,2	± 0.0447
3,4	± 0.1413
5,6	± 0.2492
7,8	± 0.3715
9,10	± 0.5129
11,12	± 0.6797
13,14	± 0.8844
15,16	± 1.1481
17,18	± 1.5195
19,20	± 2.1551

The generation of AOD ($\phi_{n,m,AOD}$) follows a procedure similar to AOA as described above.

The generation of ZOA assumes that the composite PAS in the zenith dimension of all clusters is Laplacian (see Table 7.5-6). The ZOAs are determined by applying the inverse Laplacian function (7.5-14) with input parameters P_n and RMS angle spread ZSA

$$\theta'_{n,ZOA} = - \frac{ZSA \ln(P_n / \max(P_n))}{C_\theta}, \quad (7.5-14)$$

with C_θ defined as

$$C_\theta = \begin{cases} C_\theta^{\text{NLOS}} \cdot (1.3086 + 0.0339K - 0.0077K^2 + 0.0002K^3) & , \text{ for LOS} \\ C_\theta^{\text{NLOS}} & , \text{ for NLOS} \end{cases}, \quad (7.5-15)$$

Where C_θ^{NLOS} is a scaling factor related to the total number of clusters and is given in Table 7.5-4:

Table 7.5-4: Scaling factors for ZOA, ZOD generation

# clusters	8	10	11	12	19	20
C_θ^{NLOS}	0.889	0.957	1.031	1.104	1.184	1.178

In the LOS case, constant C_θ also depends on the Ricean K-factor K in [dB], as generated in Step 4. Additional scaling of the angles is required to compensate for the effect of LOS peak addition to the angle spread.

Assign positive or negative sign to the angles by multiplying with a random variable X_n with uniform distribution to the discrete set of $\{1, -1\}$, and add component $Y_n \sim N(0, (ZSA/7)^2)$ to introduce random variation

$$\theta_{n,ZOA} = X_n \theta'_{n,ZOA} + Y_n + \bar{\theta}_{ZOA}, \quad (7.5-16)$$

where $\bar{\theta}_{ZOA} = 90^\circ$ if the BS-UT link is O2I and $\bar{\theta}_{ZOA} = \theta_{LOS,ZOA}$ otherwise. The LOS direction is defined in the network layout description, see Step1c.

In the LOS case, substitute (7.5-16) by (7.5-17) to enforce the first cluster to the LOS direction $\theta_{LOS,ZOA}$

$$\theta_{n,ZOA} = (X_n \theta'_{n,ZOA} + Y_n) - (X_1 \theta'_{1,ZOA} + Y_1 - \theta_{LOS,ZOA}). \quad (7.5-17)$$

Finally add offset angles α_m from Table 7.5-3 to the cluster angles

$$\theta_{n,m,ZOA} = \theta_{n,ZOA} + c_{ZSA} \alpha_m, \quad (7.5-18)$$

where c_{ZSA} is the cluster-wise rms spread of ZOA (cluster ZSA) in Table 7.5-6. Assuming that $\theta_{n,m,ZOA}$ is wrapped within $[0, 360^\circ]$, if $\theta_{n,m,ZOA} \in [180^\circ, 360^\circ]$, then $\theta_{n,m,ZOA}$ is set to $(360^\circ - \theta_{n,m,ZOA})$.

The generation of ZOD follows the same procedure as ZOA described above except equation (7.5-16) is replaced by

$$\theta_{n,ZOD} = X_n \theta'_{n,ZOD} + Y_n + \theta_{LOS,ZOD} + \mu_{offset,ZOD}, \quad (7.5-19)$$

where variable X_n is with uniform distribution to the discrete set of $\{1, -1\}$, $Y_n \sim N(0, (ZSD/7)^2)$, $\mu_{offset,ZOD}$ is given in Tables 7.5-6/7/8 and equation (7.5-18) is replaced by

$$\theta_{n,m,ZOD} = \theta_{n,ZOD} + (3/8)(10^{\mu_{lgZSD}}) \alpha_m \quad (7.5-20)$$

where μ_{lgZSD} is the mean of the ZSD log-normal distribution.

In the LOS case, the generation of ZOD follows the same procedure as ZOA described above using equation (7.5-17).

Step 8: Coupling of rays within a cluster for both azimuth and elevation

Couple randomly AOD angles $\phi_{n,m,AOD}$ to AOA angles $\phi_{n,m,AOA}$ within a cluster n , or within a sub-cluster in the case of two strongest clusters (see Step 11 and Table 7.5-3). Couple randomly ZOD angles $\theta_{n,m,ZOD}$ with ZOA angles $\theta_{n,m,ZOA}$ using the same procedure. Couple randomly AOD angles $\phi_{n,m,AOD}$ with ZOD angles $\theta_{n,m,ZOD}$ within a cluster n or within a sub-cluster in the case of two strongest clusters.

Step 9: Generate the cross polarization power ratios

Generate the cross polarization power ratios (XPR) κ for each ray m of each cluster n . XPR is log-Normal distributed. Draw XPR values as

$$\kappa_{n,m} = 10^{X/10}, \quad (7.5-21)$$

where $X \sim N(\mu_{XPR}, \sigma_{XPR}^2)$ is Gaussian distributed with σ_{XPR} and μ_{XPR} from Table 7.5-6

The outcome of Steps 1-9 shall be identical for all the links from co-sited sectors to a UT.

Coefficient generation:

Step 10: Draw initial random phases

Draw random initial phase $\left[\Phi_{n,m}^{\theta\theta}, \Phi_{n,m}^{\theta\phi}, \Phi_{n,m}^{\phi\theta}, \Phi_{n,m}^{\phi\phi} \right]$ for each ray m of each cluster n and for four different polarisation combinations $(\theta\theta, \theta\phi, \phi\theta, \phi\phi)$. The distribution for initial phases is uniform within $(-\pi, \pi)$.

Step 11: Generate channel coefficients for each cluster n and each receiver and transmitter element pair u, s .

The method described below is used at least for *drop-based evaluations* irrespective of UT speeds. Relevant cases for drop-based evaluations are:

- Case 1: For low complexity evaluations

- Case 2: To compare with earlier simulation results,
- Case 3: When none of the additional modeling components are turned on.
- Case 4: When spatial consistency and/or blockage is modeled for MU-MIMO simulations
- Other cases are not precluded

For the $N - 2$ weakest clusters, say $n = 3, 4, \dots, N$, the channel coefficients are given by:

$$H_{u,s,n}^{\text{NLOS}}(t) = \sqrt{\frac{P_n}{M}} \sum_{m=1}^M \begin{bmatrix} F_{rx,u,\theta}(\theta_{n,m,ZOA}, \phi_{n,m,AOA}) \\ F_{rx,u,\phi}(\theta_{n,m,ZOA}, \phi_{n,m,AOA}) \end{bmatrix}^T \begin{bmatrix} \exp(j\Phi_{n,m}^{\theta\theta}) & \sqrt{\kappa_{n,m}^{-1}} \exp(j\Phi_{n,m}^{\theta\phi}) \\ \sqrt{\kappa_{n,m}^{-1}} \exp(j\Phi_{n,m}^{\phi\theta}) & \exp(j\Phi_{n,m}^{\phi\phi}) \end{bmatrix} \begin{bmatrix} F_{tx,s,\theta}(\theta_{n,m,ZOD}, \phi_{n,m,AOD}) \\ F_{tx,s,\phi}(\theta_{n,m,ZOD}, \phi_{n,m,AOD}) \end{bmatrix} \exp\left[\frac{j2\pi(\hat{r}_{rx,n,m}^T \cdot \bar{d}_{rx,u})}{\lambda_0}\right] \exp\left[\frac{j2\pi(\hat{r}_{tx,n,m}^T \cdot \bar{d}_{tx,s})}{\lambda_0}\right] \exp\left[j2\pi \frac{\hat{r}_{rx,n,m}^T \cdot \bar{v}}{\lambda_0} t\right] \quad (7.5-22)$$

where $F_{rx,u,\theta}$ and $F_{rx,u,\phi}$ are the field patterns of receive antenna element u according to (7.1-11) and in the direction of the spherical basis vectors, $\hat{\theta}$ and $\hat{\phi}$ respectively, $F_{tx,s,\theta}$ and $F_{tx,s,\phi}$ are the field patterns of transmit antenna element s in the direction of the spherical basis vectors, $\hat{\theta}$ and $\hat{\phi}$ respectively. Note that the patterns are given in the GCS and therefore include transformations with respect to antenna orientation as described in Section 7.1. $\hat{r}_{rx,n,m}$ is the spherical unit vector with azimuth arrival angle $\phi_{n,m,AOA}$ and elevation arrival angle $\theta_{n,m,ZOA}$, given by

$$\hat{r}_{rx,n,m} = \begin{bmatrix} \sin \theta_{n,m,ZOA} \cos \phi_{n,m,AOA} \\ \sin \theta_{n,m,ZOA} \sin \phi_{n,m,AOA} \\ \cos \theta_{n,m,ZOA} \end{bmatrix}, \quad (7.5-23)$$

where n denotes a cluster and m denotes a ray within cluster n . $\hat{r}_{tx,n,m}$ is the spherical unit vector with azimuth departure angle $\phi_{n,m,AOD}$ and elevation departure angle $\theta_{n,m,ZOD}$, given by

$$\hat{r}_{tx,n,m} = \begin{bmatrix} \sin \theta_{n,m,ZOD} \cos \phi_{n,m,AOD} \\ \sin \theta_{n,m,ZOD} \sin \phi_{n,m,AOD} \\ \cos \theta_{n,m,ZOD} \end{bmatrix}, \quad (7.5-24)$$

where n denotes a cluster and m denotes a ray within cluster n . Also, $\bar{d}_{rx,u}$ is the location vector of receive antenna element u and $\bar{d}_{tx,s}$ is the location vector of transmit antenna element s , $\kappa_{n,m}$ is the cross polarisation power ratio in linear scale, and λ_0 is the wavelength of the carrier frequency. If polarisation is not considered, the 2x2 polarisation matrix can be replaced by the scalar $\exp(j\Phi_{n,m})$ and only vertically polarised field patterns are applied.

The Doppler frequency component depends on the arrival angles (AOA, ZOA), and the UT velocity vector \bar{v} with speed v , travel azimuth angle ϕ_v , elevation angle θ_v and is given by

$$v_{n,m} = \frac{\hat{r}_{rx,n,m}^T \cdot \bar{v}}{\lambda_0}, \text{ where } \bar{v} = v \begin{bmatrix} \sin \theta_v \cos \phi_v & \sin \theta_v \sin \phi_v & \cos \theta_v \end{bmatrix}^T. \quad (7.5-25)$$

For the two strongest clusters, say $n = 1$ and 2, rays are spread in delay to three sub-clusters (per cluster), with fixed delay offset. The delays of the sub-clusters are

$$\begin{aligned}
\tau_{n,1} &= \tau_n \\
\tau_{n,2} &= \tau_n + 1.28 \, c_{DS} \\
\tau_{n,3} &= \tau_n + 2.56 \, c_{DS}
\end{aligned} \tag{7.5-26}$$

where c_{DS} is cluster delay spread specified in Table 7.5-6. When intra-cluster delay spread is unspecified (i.e., N/A) the value 3.91 ns is used; it is noted that this value results in the legacy behaviour with 5 and 10 ns sub-cluster delays

Twenty rays of a cluster are mapped to sub-clusters as presented in Table 7.5-5 below. The corresponding offset angles are taken from Table 7.5-3 with mapping of Table 7.5-5.

Table 7.5-5: Sub-cluster information for intra cluster delay spread clusters

sub-cluster # i	mapping to rays R_i	Power $ R_i /M$	delay offset $\tau_{n,i} - \tau_n$
$i = 1$	$R_1 = [1,2,3,4,5,6,7,8,19,20]$	10/20	0
$i = 2$	$R_2 = [9,10,11,12,17,18]$	6/20	$1.28 \, c_{DS}$
$i = 3$	$R_3 = [13,14,15,16]$	4/20	$2.56 \, c_{DS}$

Then, the channel impulse response is given by:

$$H_{u,s}^{\text{NLOS}}(\tau, t) = \sum_{n=1}^2 \sum_{i=1}^3 \sum_{m \in R_i} H_{u,s,n,m}^{\text{NLOS}}(t) \delta(\tau - \tau_{n,i}) + \sum_{n=3}^N H_{u,s,n}^{\text{NLOS}}(t) \delta(\tau - \tau_n) \tag{7.5-27}$$

where $H_{u,s,n}^{\text{NLOS}}(t)$ is given in (7.5-22) and $H_{u,s,n,m}^{\text{NLOS}}(t)$ defined as:

$$\begin{aligned}
H_{u,s,n,m}^{\text{NLOS}}(t) = & \sqrt{\frac{P_n}{M}} \begin{bmatrix} F_{rx,u,\theta}(\theta_{n,m,ZOA}, \phi_{n,m,AOA}) \\ F_{rx,u,\phi}(\theta_{n,m,ZOA}, \phi_{n,m,AOA}) \end{bmatrix}^T \begin{bmatrix} \exp(j\Phi_{n,m}^{\theta\theta}) & \sqrt{\kappa_{n,m}^{-1}} \exp(j\Phi_{n,m}^{\theta\phi}) \\ \sqrt{\kappa_{n,m}^{-1}} \exp(j\Phi_{n,m}^{\phi\theta}) & \exp(j\Phi_{n,m}^{\phi\phi}) \end{bmatrix} \\
& \begin{bmatrix} F_{tx,s,\theta}(\theta_{n,m,ZOD}, \phi_{n,m,AOD}) \\ F_{tx,s,\phi}(\theta_{n,m,ZOD}, \phi_{n,m,AOD}) \end{bmatrix} \exp \left[j2\pi \frac{\hat{r}_{rx,n,m}^T \cdot \bar{d}_{rx,u}}{\lambda_0} \right] \exp \left[j2\pi \frac{\hat{r}_{tx,n,m}^T \cdot \bar{d}_{tx,s}}{\lambda_0} \right] \exp \left[j2\pi \frac{\hat{r}_{rx,n,m}^T \cdot \bar{v}}{\lambda_0} t \right]
\end{aligned} \tag{7.5-28}$$

In the LOS case, determine the LOS channel coefficient by:

$$\begin{aligned}
H_{u,s,1}^{\text{LOS}}(t) = & \begin{bmatrix} F_{rx,u,\theta}(\theta_{LOS,ZOA}, \phi_{LOS,AOA}) \\ F_{rx,u,\phi}(\theta_{LOS,ZOA}, \phi_{LOS,AOA}) \end{bmatrix}^T \begin{bmatrix} 1 & 0 \\ 0 & -1 \end{bmatrix} \begin{bmatrix} F_{tx,s,\theta}(\theta_{LOS,ZOD}, \phi_{LOS,AOD}) \\ F_{tx,s,\phi}(\theta_{LOS,ZOD}, \phi_{LOS,AOD}) \end{bmatrix} \\
& \cdot \exp \left[-j2\pi \frac{d_{3D}}{\lambda_0} \right] \exp \left[j2\pi \frac{\hat{r}_{rx,LOS}^T \cdot \bar{d}_{rx,u}}{\lambda_0} \right] \exp \left[j2\pi \frac{\hat{r}_{tx,LOS}^T \cdot \bar{d}_{tx,s}}{\lambda_0} \right] \exp \left[j2\pi \frac{\hat{r}_{rx,LOS}^T \cdot \bar{v}}{\lambda_0} t \right]
\end{aligned} \tag{7.5-29}$$

where $\delta(\cdot)$ is the Dirac's delta function and K_R is the Ricean K-factor as generated in Step 4 converted to linear scale.

Then, the channel impulse response is given by adding the LOS channel coefficient to the NLOS channel impulse response and scaling both terms according to the desired K-factor K_R as

$$H_{u,s}^{\text{LOS}}(\tau, t) = \sqrt{\frac{1}{K_R + 1}} H_{u,s}^{\text{NLOS}}(\tau, t) + \sqrt{\frac{K_R}{K_R + 1}} H_{u,s,1}^{\text{LOS}}(t) \delta(\tau - \tau_1). \tag{7.5-30}$$

Step 12: Apply pathloss and shadowing for the channel coefficients.

Table 7.5-6 Part-1: Channel model parameters for Umi-Street Canyon and Uma

Scenarios		Umi – Street Canyon			Uma		
		LOS	NLOS	O2I	LOS	NLOS	O2I
Delay spread (DS) lgDS=log ₁₀ (DS/1s)	μ_{lgDS}	$-0.24 \log_{10}(1+f_c) - 7.14$	$-0.24 \log_{10}(1+f_c) - 6.83$	-6.62	$-6.955 - 0.0963 \log_{10}(f_c)$	$-6.28 - 0.204 \log_{10}(f_c)$	-6.62
	σ_{lgDS}	0.38	$0.16 \log_{10}(1+f_c) + 0.28$	0.32	0.66	0.39	0.32
AoD spread (ASD) lgASD=log ₁₀ (ASD/1°)	μ_{lgASD}	$-0.05 \log_{10}(1+f_c) + 1.21$	$-0.23 \log_{10}(1+f_c) + 1.53$	1.25	$1.06 + 0.1114 \log_{10}(f_c)$	$1.5 - 0.1144 \log_{10}(f_c)$	1.25
	σ_{lgASD}	0.41	$0.11 \log_{10}(1+f_c) + 0.33$	0.42	0.28	0.28	0.42
AoA spread (ASA) lgASA=log ₁₀ (ASA/1°)	μ_{lgASA}	$-0.08 \log_{10}(1+f_c) + 1.73$	$-0.08 \log_{10}(1+f_c) + 1.81$	1.76	1.81	$2.08 - 0.27 \log_{10}(f_c)$	1.76
	σ_{lgASA}	$0.014 \log_{10}(1+f_c) + 0.28$	$0.05 \log_{10}(1+f_c) + 0.3$	0.16	0.20	0.11	0.16
ZoA spread (ZSA) lgZSA=log ₁₀ (ZSA/1°)	μ_{lgZSA}	$-0.1 \log_{10}(1+f_c) + 0.73$	$-0.04 \log_{10}(1+f_c) + 0.92$	1.01	0.95	$-0.3236 \log_{10}(f_c) + 1.512$	1.01
	σ_{lgZSA}	$-0.04 \log_{10}(1+f_c) + 0.34$	$-0.07 \log_{10}(1+f_c) + 0.41$	0.43	0.16	0.16	0.43
Shadow fading (SF) [dB]	σ_{SF}	See Table 7.4.1-1	See Table 7.4.1-1	7	See Table 7.4.1-1	See Table 7.4.1-1	7
K-factor (K) [dB]	μ_K	9	N/A	N/A	9	N/A	N/A
	σ_K	5	N/A	N/A	3.5	N/A	N/A
Cross-Correlations	ASD vs DS	0.5	0	0.4	0.4	0.4	0.4
	ASA vs DS	0.8	0.4	0.4	0.8	0.6	0.4
	ASA vs SF	-0.4	-0.4	0	-0.5	0	0
	ASD vs SF	-0.5	0	0.2	-0.5	-0.6	0.2
	DS vs SF	-0.4	-0.7	-0.5	-0.4	-0.4	-0.5
	ASD vs ASA	0.4	0	0	0	0.4	0
	ASD vs K	-0.2	N/A	N/A	0	N/A	N/A
	ASA vs K	-0.3	N/A	N/A	-0.2	N/A	N/A
	DS vs K	-0.7	N/A	N/A	-0.4	N/A	N/A
Cross-Correlations ¹⁾	SF vs K	0.5	N/A	N/A	0	N/A	N/A
	ZSD vs SF	0	0	0	0	0	0
	ZSA vs SF	0	0	0	-0.8	-0.4	0
	ZSD vs K	0	N/A	N/A	0	N/A	N/A
	ZSA vs K	0	N/A	N/A	0	N/A	N/A
	ZSD vs DS	0	-0.5	-0.6	-0.2	-0.5	-0.6
	ZSA vs DS	0.2	0	-0.2	0	0	-0.2
	ZSD vs ASD	0.5	0.5	-0.2	0.5	0.5	-0.2
	ZSA vs ASD	0.3	0.5	0	0	-0.1	0
	ZSD vs ASA	0	0	0	-0.3	0	0
	ZSA vs ASA	0	0.2	0.5	0.4	0	0.5
	ZSD vs ZSA	0	0	0.5	0	0	0.5
Delay scaling parameter r_τ		3	2.1	2.2	2.5	2.3	2.2
XPR [dB]	μ_{XPR}	9	8.0	9	8	7	9
	σ_{XPR}	3	3	5	4	3	5
Number of clusters N		12	19	12	12	20	12
Number of rays per cluster M		20	20	20	20	20	20

Cluster DS (C_{DS}) in [ns]	5	11	11	$\max(0.25, 6.5622 - 3.4084 \log_{10}(f_c))$	$\max(0.25, 6.5622 - 3.4084 \log_{10}(f_c))$	11
Cluster ASD (C_{ASD}) in [deg]	3	10	5	5	2	5
Cluster ASA (C_{ASA}) in [deg]	17	22	8	11	15	8
Cluster ZSA (C_{ZSA}) in [deg]	7	7	3	7	7	3
Per cluster shadowing std ζ [dB]	3	3	4	3	3	4
Correlation distance in the horizontal plane [m]	DS	7	10	10	30	40
	ASD	8	10	11	18	50
	ASA	8	9	17	15	50
	SF	10	13	7	37	50
	K	15	N/A	N/A	12	N/A
	ZSA	12	10	25	15	50
	ZSD	12	10	25	15	50

f_c is carrier frequency in GHz; d_{2D} is BS-UT distance in km.

NOTE 1: DS = rms delay spread, ASD = rms azimuth spread of departure angles, ASA = rms azimuth spread of arrival angles, ZSD = rms zenith spread of departure angles, ZSA = rms zenith spread of arrival angles, SF = shadow fading, and K = Ricean K-factor.

NOTE 2: The sign of the shadow fading is defined so that positive SF means more received power at UT than predicted by the path loss model.

NOTE 3: All large scale parameters are assumed to have no correlation between different floors.

NOTE 4: The following notation for mean ($\mu_{\log X} = \text{mean}\{\log_{10}(X)\}$) and standard deviation ($\sigma_{\log X} = \text{std}\{\log_{10}(X)\}$) is used for logarithmized parameters X .

NOTE 5: For all considered scenarios the AoD/AoA distributions are modelled by a wrapped Gaussian distribution, the ZoD/ZoA distributions are modelled by a Laplacian distribution and the delay distribution is modelled by an exponential distribution.

NOTE 6: For Ura and frequencies below 6 GHz, use $f_c = 6$ when determining the values of the frequency-dependent LSP values

NOTE 7: For Umi and frequencies below 2 GHz, use $f_c = 2$ when determining the values of the frequency-dependent LSP values

Table 7.5-6 Part-2: Channel model parameters for Rma (up to 7GHz) and Indoor-Office

Scenarios		Rma		Indoor-Office	
		LOS	NLOS	LOS	NLOS
Delay spread (DS)	μ_{lgDS}	-7.49	-7.43	$-0.01 \log_{10}(1+f_c) - 7.692$	$-0.28 \log_{10}(1+f_c) - 7.173$
lgDS=log ₁₀ (DS/1s)	σ_{lgDS}	0.55	0.48	0.18	$0.10 \log_{10}(1+f_c) + 0.055$
AoD spread (ASD)	μ_{lgASD}	0.90	0.95	1.60	1.62
lgASD=log ₁₀ (ASD/1°)	σ_{lgASD}	0.38	0.45	0.18	0.25
AoA spread (ASA)	μ_{lgASA}	1.52	1.52	$-0.19 \log_{10}(1+f_c) + 1.781$	$-0.11 \log_{10}(1+f_c) + 1.863$
lgASA=log ₁₀ (ASA/1°)	σ_{lgASA}	0.24	0.13	$0.12 \log_{10}(1+f_c) + 0.119$	$0.12 \log_{10}(1+f_c) + 0.059$
ZoA spread (ZSA)	μ_{lgZSA}	0.60	0.88	$-0.26 \log_{10}(1+f_c) + 1.44$	$-0.15 \log_{10}(1+f_c) + 1.387$
lgZSA=log ₁₀ (ZSA/1°)	σ_{lgZSA}	0.16	0.16	$-0.04 \log_{10}(1+f_c) + 0.264$	$-0.09 \log_{10}(1+f_c) + 0.746$
Shadow fading (SF) [dB]	σ_{SF}	See Table 7.4.1-1.		See Table 7.4.1-1.	
K-factor (K) [dB]	μ_K	7	N/A	7	N/A
	σ_K	4	N/A	4	N/A
Cross-Correlations	ASD vs DS	0	-0.4	0.6	0.4
	ASA vs DS	0	0	0.8	0
	ASA vs SF	0	0	-0.5	-0.4
	ASD vs SF	0	0.6	-0.4	0
	DS vs SF	-0.5	-0.5	-0.8	-0.5
	ASD vs ASA	0	0	0.4	0
	ASD vs K	0	N/A	0	N/A
	ASA vs K	0	N/A	0	N/A
	DS vs K	0	N/A	-0.5	N/A
	SF vs K	0	N/A	0.5	N/A
Cross-Correlations ¹⁾	ZSD vs SF	0	0	0.2	0
	ZSA vs SF	-0.8	-0.4	0.3	0
	ZSD vs K	0	N/A	0	N/A
	ZSA vs K	0	N/A	0.1	N/A
	ZSD vs DS	0	-0.5	0.1	-0.27
	ZSA vs DS	0	0	0.2	-0.06
	ZSD vs ASD	0.5	0.5	0.5	0.35
	ZSA vs ASD	0	-0.1	0	0.23
	ZSD vs ASA	0	0	0	-0.08
	ZSA vs ASA	0	0	0.5	0.43
	ZSD vs ZSA	0	0	0	0.42
Delay scaling parameter r_τ		3.8	1.7	3.6	3
XPR [dB]	μ_{XPR}	12	7	11	10
	σ_{XPR}	4	3	4	4
Number of clusters		11	10	15	19
Number of rays per cluster		20	20	20	20

Cluster DS (C_{DS}) in [ns]	N/A	N/A	N/A	N/A
Cluster ASD (C_{ASD}) in [deg]	2	2	5	5
Cluster ASA (C_{ASA}) in [deg]	3	3	8	11
Cluster ZSA (C_{ZSA}) in [deg]	3	3	9	9
Per cluster shadowing std ζ [dB]	3	3	6	3
Correlation distance in the horizontal plane [m]	DS	50	36	8
	ASD	25	30	7
	ASA	35	40	5
	SF	37	120	10
	K	40	N/A	4
	ZSA	15	50	4
	ZSD	15	50	4
f_c is carrier frequency in GHz; d_{2D} is BS-UT distance in km. NOTE 1: DS = rms delay spread, ASD = rms azimuth spread of departure angles, ASA = rms azimuth spread of arrival angles, ZSD = rms zenith spread of departure angles, ZSA = rms zenith spread of arrival angles, SF = shadow fading, and K = Ricean K-factor. NOTE 2: The sign of the shadow fading is defined so that positive SF means more received power at UT than predicted by the path loss model. NOTE 3: The following notation for mean ($\mu_{\lg X} = \text{mean}\{\log_{10}(X)\}$) and standard deviation ($\sigma_{\lg X} = \text{std}\{\log_{10}(X)\}$) is used for logarithmized parameters X . NOTE 4: For Rma O2I the same parameters are used as for outdoor links, depending on the LOS condition of the outdoor link part. NOTE 5: For all considered scenarios the AoD/AoA distributions are modelled by a wrapped Gaussian distribution, the ZoD/ZoA distributions are modelled by a Laplacian distribution and the delay distribution is modelled by an exponential distribution. NOTE 6: For InH and frequencies below 6 GHz, use $f_c = 6$ when determining the values of the frequency-dependent LSP values				

Table 7.5-7: ZSD and ZoD offset parameters for Uma

Scenarios		LOS	NLOS
ZoD spread (ZSD) $\lg ZSD = \log_{10}(ZSD/1^\circ)$	$\mu_{\lg ZSD}$	$\max[-0.5, -2.1(d_{2D}/1000)$ $-0.01(h_{UT} - 1.5) + 0.75]$	$\max[-0.5, -2.1(d_{2D}/1000)$ $-0.01(h_{UT} - 1.5) + 0.9]$
	$\sigma_{\lg ZSD}$	0.40	0.49
ZoD offset	$\mu_{\text{offset,ZoD}}$	0	$e(f_c) \cdot 10^{\{a(f_c) \log_{10}(\max(b(f_c), d_{2D}))$ $+ c(f_c) - 0.07(h_{UT} - 1.5)\}}$
Note: For NLOS ZoD offset: $a(f_c) = 0.208 \log_{10}(f_c) - 0.782$; $b(f_c) = 25$; $c(f_c) = -0.13 \log_{10}(f_c) + 2.03$; $e(f_c) = 7.66 \log_{10}(f_c) - 5.96$.			

Table 7.5-8: ZSD and ZoD offset parameters for Umi – Street Canyon

Scenarios		LOS	NLOS
ZoD spread (ZSD) $\lg ZSD = \log_{10}(ZSD/1^\circ)$	$\mu_{\lg ZSD}$	$\max[-0.21, -14.8(d_{2D}/1000)$ $+ 0.01 h_{UT} - h_{BS} + 0.83]$	$\max[-0.5, -3.1(d_{2D}/1000)$ $+ 0.01 \max(h_{UT} - h_{BS}, 0) + 0.2]$
	$\sigma_{\lg ZSD}$	0.35	0.35
ZoD offset	$\mu_{\text{offset,ZoD}}$	0	$-10^{\{-1.5 \log_{10}(\max(10, d_{2D})) + 3.3\}}$

Table 7.5-9: ZSD and ZoD offset parameters for Rma

Scenarios		LOS	NLOS
ZoD spread (ZSD) $\lg ZSD = \log_{10}(ZSD/1^\circ)$	$\mu_{\lg ZSD}$	-0.52	-0.52
	$\sigma_{\lg ZSD}$	0.40	0.49
ZoD offset	$\mu_{\text{offset,ZoD}}$	0	$\arctan((35-5)/d_{2D}) - \arctan((35-1.5)/d_{2D})$

Table 7.5-10: ZSD and ZoD offset parameters for Indoor-Office

Scenarios		LOS	NLOS
ZoD spread (ZSD) $\lg ZSD = \log_{10}(ZSD/1^\circ)$	$\mu_{\lg ZSD}$	$-1.43 \log_{10}(1 + f_c) + 2.228$	1.08
	$\sigma_{\lg ZSD}$	$0.13 \log_{10}(1 + f_c) + 0.30$	0.36
ZoD offset	$\mu_{\text{offset,ZoD}}$	0	0

Notes for Table 7.5-7, 7.5-8, 7.5-9, 7.5-10:

NOTE 1: f_c is center frequency in GHz; d_{2D} is BS-UT distance in m.

NOTE 2: h_{BS} and h_{UT} are antenna heights in m for BS and UT **respectively**.

NOTE 3: The following notation for mean ($\mu_{\lg X} = \text{mean}\{\log_{10}(X)\}$) and standard deviation ($\sigma_{\lg X} = \text{std}\{\log_{10}(X)\}$) is used for logarithmized parameters X.

NOTE 4: For frequencies below 6 GHz, use $f_c = 6$ when determining the values of the frequency-dependent ZSD and ZoD offset parameters in Table 7.5-7 and 7.5-10

NOTE 5: The ZSD parameters for O2I links are the same parameters that are used for outdoor links, depending on the LOS condition of the outdoor link part.

7.6 Additional modelling components

The additional modelling components in this section are to support advanced simulations, such as simulations with very large arrays and large bandwidth, simulations affected by oxygen absorption (frequencies between 53 and 67 GHz), simulations in which spatial consistency is important (e.g. high number of closely located user), simulations of mobility,

and simulations of blockage effects. These modelling components affect some of the steps between Step 1 and Step 12 in Section 7.5.

These extensions are computationally more expensive and might not be required in all evaluation cases.

7.6.1 Oxygen absorption

Oxygen absorption loss is applied to the cluster responses generated in Step 11 in Section 7.5. The additional loss, $OL_n(f_c)$ for cluster n at centre frequency f_c is modelled as:

$$OL_n(f_c) = \frac{\alpha(f_c)}{1000} \cdot (d_{3D} + c \cdot (\tau_n + \tau_\Delta)) \quad [\text{dB}] \quad (7.6-1)$$

where:

- $\alpha(f_c)$ is frequency dependent oxygen loss (dB/km) characterized in Table 7.6.1-1;
- c is the speed of light (m/s); and d_{3D} is the distance (m);
- τ_n is the n -th cluster delay (s) in Step 11 in Section 7.5;
- τ_Δ is 0 in the LOS case and $\min(\tau_n)$ otherwise, where $\min(\tau_n)$ is the minimum delay in Step 5.

For centre frequencies not specified in this table, the frequency dependent oxygen loss $\alpha(f_c)$ is obtained from a linear interpolation between two loss values corresponding to the two adjacent centre frequencies of the centre frequency f_c .

Table 7.6.1-1 Frequency dependent oxygen loss $\alpha(f)$ [dB/km]

f in [GHz]	0-52	53	54	55	56	57	58	59	60	61	62	63	64	65	66	67	68-100
$\alpha(f)$ in [dB/km]	0	1	2.2	4	6.6	9.7	12.6	14.6	15	14.6	14.3	10.5	6.8	3.9	1.9	1	0

For large channel bandwidth, first transform the time-domain channel response of each cluster (all rays within one cluster share common oxygen absorption loss for simplicity) into frequency-domain channel response, and apply the oxygen absorption loss to the cluster's frequency-domain channel response for frequency $f_c + \Delta f$ within the considered bandwidth. The oxygen loss, $OL_n(f_c + \Delta f)$ for cluster n at frequency $f_c + \Delta f$ is modelled as:

$$OL_n(f_c + \Delta f) = \frac{\alpha(f_c + \Delta f)}{1000} \cdot (d_{3D} + c \cdot (\tau_n + \tau_\Delta)) \quad [\text{dB}] \quad (7.6-2)$$

where:

- $\alpha(f_c + \Delta f)$ is the oxygen loss (dB/km) at frequency $f_c + \Delta f$ characterized in Table 7.6.1-1. Note that Δf is in $[-B/2, B/2]$, where B is the bandwidth. Linear interpolation is applied for frequencies not provided in Table 7.6.1-1.

The final frequency-domain channel response is obtained by the summation of frequency-domain channel responses of all clusters.

Time-domain channel response is obtained by the reverse transform from the obtained frequency-domain channel response.

7.6.2 Large bandwidth and large antenna array

7.6.2.1 Modelling of the propagation delay

The modelling in this section applies only when the bandwidth B is greater than c/D Hz, where

- D is the maximum antenna aperture in either azimuth or elevation (m)
- c is the speed of light (m/s)

Each ray within a cluster for a given u (Rx) and s (Tx) has unique time of arrival (TOA). The channel coefficient generation step (step 11 in Section 7.5) is updated to model individual rays. In this case, the channel response of ray m in cluster n for a link between Rx antenna u and Tx antenna s at delay τ at time t is given by:

$$\begin{aligned}
 H_{u,s,n,m}^{\text{NLOS}}(t;\tau) = & \sqrt{P_{n,m}} \begin{bmatrix} F_{rx,u,\theta}(\theta_{n,m,ZOA}, \phi_{n,m,AOA}) \\ F_{rx,u,\phi}(\theta_{n,m,ZOA}, \phi_{n,m,AOA}) \end{bmatrix}^T \begin{bmatrix} \exp(j\Phi_{n,m}^{\theta\theta}) \\ \sqrt{\kappa_{n,m}^{-1}} \exp(j\Phi_{n,m}^{\theta\phi}) \\ \sqrt{\kappa_{n,m}^{-1}} \exp(j\Phi_{n,m}^{\phi\theta}) \\ \exp(j\Phi_{n,m}^{\phi\phi}) \end{bmatrix} \sqrt{\kappa_{n,m}^{-1}} \exp(j\Phi_{n,m}^{\theta\phi}) \\
 & \begin{bmatrix} F_{tx,s,\theta}(\theta_{n,m,ZOD}, \phi_{n,m,AOD}) \\ F_{tx,s,\phi}(\theta_{n,m,ZOD}, \phi_{n,m,AOD}) \end{bmatrix} \exp\left\{ \frac{j2\pi(\hat{r}_{rx,n,m}^T \cdot \bar{d}_{rx,u})}{\lambda(f)} \right\} \exp\left\{ \frac{j2\pi(\hat{r}_{tx,n,m}^T \cdot \bar{d}_{tx,s})}{\lambda(f)} \right\} \\
 & \cdot \exp\left\{ j2\pi \frac{\hat{r}_{rx,n,m}^T \cdot \bar{v}}{\lambda_0} t \right\} \delta(\tau - \tau_{n,m})
 \end{aligned} \quad (7.6-3)$$

with $\lambda(f)$ is the wavelength on frequency $f \in [f_c - \frac{B}{2}, f_c + \frac{B}{2}]$, which can be implemented by user's own method.

The delay (TOA) for ray m in cluster n for a link between Rx antenna u and Tx antenna s is given by:

$$\tau_{u,s,n,m} = \tau_{n,m} - \frac{1}{c} \hat{r}_{rx,n,m}^T \cdot \bar{d}_{rx,u} - \frac{1}{c} \hat{r}_{tx,n,m}^T \cdot \bar{d}_{tx,s} \quad (7.6-4)$$

Note that Equation (7.6-3) only considers the delays $\tau_{n,m}$ intentionally. If unequal ray powers are considered, $P_{n,m}$ are generated according to Section 7.6.2.2. Otherwise, ray powers are equal within a cluster, i.e., $P_{n,m} = P_n / M$ for all m . Note: this model is developed assuming plane wave propagation.

7.6.2.2 Modelling of intra-cluster angular and delay spreads

With large antenna arrays or large bandwidths, the angle and/or delay resolution can be larger than what the fast fading model in Section 7.5 is designed to support. To model this effect, the following modifications to Step 7 in Section 7.5 can be optionally used.

2017. The offset angles α_m in (7.5-13), (7.5-18) and (7.5-20) are generated independently per cluster and ray using:

$$\alpha_{n,m} | \text{AOA, AOD, ZOA, ZOD} \sim \text{unif}(-2, 2) \quad (7.6-5)$$

where $\text{unif}(a, b)$ denotes the continuous uniform distribution in the interval $[a, b]$. These random variables may further be modelled as spatially consistent with correlation distance equal to the cluster-specific random variable correlation distance of Table 7.6.3.1-2.

2. The relative delay of m -th ray is given by $\tau_{n,m}^{\text{rel}} = \tau_{n,m}^{\text{abs}} - \min(\tau_{n,i}^{\text{abs}})_{i=1}^M$, where n is the cluster index,

$\tau_{n,m}^{\text{abs}} \sim \text{unif}(0, 2C_{\text{DS}})$, the cluster DS C_{DS} is given in Table 7.5-6. These random variables may further be modelled as spatially consistent with correlation distance equal to the cluster-specific random variable correlation distance of Table 7.6.3.1-2. In this case, the sub-cluster mapping according to (7.5-26) and Table 7.5-5 shall not be applied. The delays to be used in Equation (7.6-3) are given by $\tau_{n,m} = \tau_n + \tau_{n,m}^{\text{rel}}$.

3. Ray powers are determined unequally by the following process:

The power of m -th ray in n -th cluster is given by $P_{n,m} = P_n \cdot \frac{P_{n,m}^{\text{rel}}}{\sum_{m=1}^M P_{n,m}^{\text{rel}}}$ for $m = 1, \dots, M$, where

$$P_{n,m} = \exp\left[-\frac{\tau'_{n,m}}{c_{DS}}\right] \exp\left[-\frac{\sqrt{2}|\alpha_{n,m,AOA}|}{c_{ASA}}\right] \exp\left[-\frac{\sqrt{2}|\alpha_{n,m,AOD}|}{c_{ASD}}\right] \cdot \exp\left[-\frac{\sqrt{2}|\alpha_{n,m,ZOA}|}{c_{ZSA}}\right] \exp\left[-\frac{\sqrt{2}|\alpha_{n,m,ZOD}|}{c_{ZSD}}\right] \quad (7.6-6)$$

and c_{DS} , c_{ASA} , c_{ASD} , and c_{ZSA} are respectively the intra-cluster delay spread and the corresponding intra-cluster angular spread that are given in Table 7.5-6. The cluster zenith spread of departure is given by

$$c_{ZSD} = \frac{3}{8} 10^{\mu_{lgZSD}}, \quad (7.6-7)$$

with μ_{lgZSD} being defined in Tables 7.5-7, 7.5-8, 7.5-9, and 7.5-10.

4. The number of rays per cluster shall be calculated as follows:

$$M = \min\left[\max(M_t M_{AOD} M_{ZOD}, 20), M_{\max}\right] \quad (7.6-8)$$

where:

- $M_t = \lceil 4kc_{DS}B \rceil$
- $M_{AOD} = \lceil 4kc_{ASD}D_h/57.3 \rceil$
- $M_{ZOD} = \lceil 4kc_{ZSD}D_v/57.3 \rceil$
- M_{\max} is the upper limit of M , and it should be selected by the user of channel model based on the trade-off between simulation complexity and accuracy.
- D_h and D_v are the array size in m in horizontal and vertical dimension, B is bandwidth in Hz
- k is a “sparseness” parameter with value 0.5.

It is noted that each MPC may have different AOD, ZOD, and delay.

7.6.3 Spatial consistency

7.6.3.1 Spatial consistency procedure

A new procedure, namely a *spatial consistency procedure*, can be used for both cluster-specific and ray-specific random variables to be generated in various channel generation steps in Section 7.5, so that they are spatially consistent for drop-based simulations. Alternatively, this can be used together with Procedure B described in Section 7.6.3.2 for spatially consistent mobility simulations.

The procedure can be considered as a 2D random process (in the horizontal plane) given the UT locations based on the parameter-specific correlation distance values for spatial consistency, specified in Table 7.6.3.1-2. The cluster specific random variables include:

- Cluster specific random delay in step 5;
- Cluster specific shadowing in step 6; and
- Cluster specific offset for AoD/AoA/ZoD/ZoA in step 7.
- Cluster specific sign for AoD/AoA/ZoD/ZoA in step 7.
- Optionally in case of large bandwidth as described in Section 7.6.2.2 the procedure may apply as well for the parameters of rays within a cluster.

The procedure shall apply to each cluster before sorting the delay. Cluster specific sign for AoD/AoA/ZoD/ZoA in step 7 shall be kept unchanged per simulation drop even if UT position changes during simulation. The ray specific random variables include:

- Random coupling of rays in step 8;
- XPR in step 9; and
- Random phase in step 10.

The random coupling of rays in step 8 and the intra-cluster delays in step 11 shall be kept unchanged per simulation drop even if UT position changes during simulation.

Table 7.6.3.1-2 Correlation distance for spatial consistency

Correlation distance in [m]	Rma			Umi			Uma			Indoor
	LOS	NLOS	O2I	LOS	NLOS	O2I	LOS	NLOS	O2I	
Cluster and ray specific random variables	50	60	15	12	15	15	40	50	15	10
LOS/NLOS state	60			50			50			10
Indoor/outdoor state	50			50			50			N/A

7.6.3.2 Spatially-consistent UT mobility modelling

For mobility simulation enhancement, two alternative spatial consistency procedures – Procedure A and Procedure B – are described as follows. The procedures presented below consider the downlink direction same as in Section 7.5.

Procedure A:

For $t_0=0$ when a UT is dropped into the network, spatially consistent powers/delays/angles of clusters are generated according to Section 7.6.3.1.

At t_0+t , update channel cluster power/delay/angles based on UT channel cluster power/delay/angles, moving speed moving direction and UT position at t_0 .

Cluster delay is updated as:

$$\tau_n(t_0 + t) = \tau_n(t_0) - \frac{\hat{r}_{rx,n}(t_0)^T \bar{v}(t_0)}{C} t \quad (7.6-9)$$

where C is the speed of light, $\bar{v}(t_0) = v [\cos(\phi_v(t_0)) \quad \sin(\phi_v(t_0)) \quad 0]^T$ is the UT velocity vector on the horizontal plane, v is the speed of the UT, and ϕ_v is UT moving direction on the horizontal plane. Also,

$$\hat{r}_{rx,n}(t_0) = \begin{bmatrix} \sin(\theta_{n,ZOA}(t_0)) \cos(\phi_{n,AOA}(t_0)) \\ \sin(\theta_{n,ZOA}(t_0)) \sin(\phi_{n,AOA}(t_0)) \\ \cos(\theta_{n,ZOA}(t_0)) \end{bmatrix}. \quad (7.6-10)$$

where $\theta_{n,ZOA}$ and $\phi_{n,AOA}$ are cluster specific arrival and departure angles.

Cluster power is updated using Step 6 with cluster delay .

Cluster departure angles ($\theta_{n,ZOD}$ and $\phi_{n,AOD}$) and arrival angles ($\theta_{n,ZOA}$ and $\phi_{n,AOA}$) are updated as

$$\phi_{n,AOD}(t_0 + t) = \phi_{n,AOD}(t_0) + \frac{vt \sin(\phi_v(t_0) - \phi_{n,AOD}(t_0) + \phi'_{n,AOD})}{d_{2D}(t_0)} \frac{180}{\pi} \quad (7.6-11)$$

$$\theta_{n,ZOD}(t_0 + t) = \theta_{n,ZOD}(t_0) - \frac{vt \cos(\phi_v(t_0) - \phi_{n,AOD}(t_0) + \theta'_{n,ZOD})}{d_{3D}(t_0)} \frac{180}{\pi} \quad (7.6-12)$$

and

$$\phi_{n,AOA}(t_0 + t) = \phi_{n,AOA}(t_0) - \frac{vt \sin(\phi_v(t_0) - \phi_{n,AOA}(t_0) + \phi'_{n,AOA})}{d_{2D}(t_0)} \frac{180}{\pi} \quad (7.6-13)$$

$$\theta_{n,ZOA}(t_0 + t) = \theta_{n,ZOA}(t_0) - \frac{vt \cos(\phi_v(t_0) - \phi_{n,AOA}(t_0) + \theta'_{n,ZOA})}{d_{3D}(t_0)} \frac{180}{\pi} \quad (7.6-14)$$

where d_{2D} is 2D distance between Tx/Rx; d_{3D} is 3D distance between Tx/Rx; $\theta'_{n,ZOD}$, $\phi'_{n,AOD}$, $\theta'_{n,ZOA}$ and $\phi'_{n,AOA}$ are cluster specific reflection surface angles. These angles equal 0 for LOS path and are generated using spatially consistent random numbers with uniform distribution $U(-180^\circ, 180^\circ)$ and 50m correlation distance for $\theta'_{n,ZOD}$ and $\phi'_{n,AOD}$; and $U(-90^\circ, 90^\circ)$ and 100m correlation distance for $\theta'_{n,ZOA}$ and $\phi'_{n,AOA}$.

Procedure B:

In procedure B, spatial or time evolution of the channel is obtained by generating channel realizations separately for all links to different Rx positions using Steps 1-12 of Section 7.5 together with the spatially consistent procedure of Section 7.6.3.1. In the case of mobility these positions may be a function of time along one or more Rx trajectories. Furthermore, to ensure that the spatial or time evolution of delays and angles are within reasonable limits, Steps 5, 6, and 7 in Section 7.5 should be replaced by the below procedure.

Note: For implementation purposes, LSPs and SSPs may be interpolated within the coherence length or time of the respective parameter.

Step 5: Generate delays τ_n , with $n \in [1, N]$.

N delays are drawn randomly from a uniform distribution.

$$\tau'_n \sim \text{unif}(0, 2 \cdot 10^{\mu_{\text{lgDS}} + \sigma_{\text{lgDS}}}) \quad (7.6-15)$$

Normalise the delays by subtracting the minimum delay: $\tau_n = \tau'_n - \min(\tau'_n)$. The autocorrelation distance for τ_n is $2C \cdot 10^{\mu_{\text{lgDS}} + \sigma_{\text{lgDS}}}$.

In the case of LOS, set the delay of the first cluster τ_1 to 0.

Step 6: Generate N arrival angles and departure angles for both azimuth and elevation using (7.6-16) instead of (7.5-9) and (7.5-14).

$$\phi'_{n,AOA} \sim 2 \cdot 10^{\mu_{\text{lgASA}} + \sigma_{\text{lgASA}}} \text{unif}(-1, 1) \quad (7.6-16)$$

with $n \in [1, N]$. This step is repeated independently for AOD, AOA, ZOD, and ZOA with corresponding maximum angles for the uniform distribution. In case of LOS, set the angle of the first cluster ($\phi'_{1,AOA}$, etc) to 0..

The autocorrelation distances are for AOD, and ZOD, while they are fixed to 50m for AOA, and ZOA.

Offset angles etc are applied in the modified Step 7b below after cluster powers have been calculated

Step 7: Generate cluster powers

Cluster powers are calculated assuming a single slope exponential power profile and Laplacian angular power profiles. The cluster powers are determined by

$$P_n^{\square} = \exp\left[\frac{-\tau_n^{\square}}{\text{DS}}\right] \exp\left[\frac{-\sqrt{2}|\phi_{n,\text{AOA}}^{\square}|}{\text{ASA}}\right] \exp\left[\frac{-\sqrt{2}|\phi_{n,\text{AOD}}^{\square}|}{\text{ASD}}\right] \cdot \exp\left[\frac{-\sqrt{2}|\theta_{n,\text{ZOA}}^{\square}|}{\text{ZSA}}\right] \exp\left[\frac{-\sqrt{2}|\theta_{n,\text{ZOD}}^{\square}|}{\text{ZSD}}\right] \cdot 10^{\frac{-Z_n}{10}} \quad (7.6-17)$$

where $Z_n \sim N(0, \xi^2)$ (autocorrelation distance same as for shadow fading) is the per cluster shadowing term in [dB].

Delay spread **DS** and angular spreads **ASA**, **ASD**, **ZSA**, **ZSD** are generated in Step 4 of Section 7.5.

Normalize the cluster powers so that the sum of all cluster powers is equal to one, i.e.,

$$P_n = \frac{P_n^{\square}}{\sum_{n=1}^N P_n^{\square}} \quad (7.6-17a)$$

In the case of LoS condition, substitute **DS** with $\sqrt{1+K_R/2} \cdot \text{DS}$ and $\{\text{ASA}, \text{ASD}, \text{ZSA}, \text{ZSD}\}$ with $\{\sqrt{1+K_R} \cdot \text{ASA}, \sqrt{1+K_R} \cdot \text{ASD}, \sqrt{1+K_R} \cdot \text{ZSA}, \sqrt{1+K_R} \cdot \text{ZSD}\}$ respectively to preserve the delay and angular spreads. K_R is the Ricean K-factor as generated in Step 4 converted to linear scale. Furthermore, an additional specular component is added to the first cluster. Power of the single LoS ray is:

$$P_{1,\text{LOS}} = \frac{K_R}{K_R + 1} \quad (7.6-17b)$$

and the cluster powers are not normalized as in equation (7.6-17a), but:

$$P_n = \frac{1}{K_R + 1} \frac{P_n^{\square}}{\sum_{n=1}^N P_n^{\square}} + \delta(n-1)P_{1,\text{LOS}} \quad (7.6-17c)$$

where $\delta(\cdot)$ is Dirac's delta function.

Assign the power of each ray within a cluster as P_n/M , where M is the number of rays per cluster.

Step 7b: Apply offset angles

The ray AOA angles are determined by

$$\phi_{n,m,\text{AOA}} = \phi_{n,\text{AOA}}^{\square} + \phi_{\text{LOS},\text{AOA}} + c_{\text{ASA}}\alpha_m \quad (7.6-17d)$$

where $\phi_{\text{LOS},\text{AOA}}$ is the LOS direction defined in the network layout description, see Step1c.

The generation of AOD ($\phi_{n,m,\text{AOD}}$) follows a procedure similar to AOA as described above.

The ZOA angles are determined by

$$\theta_{n,m,\text{ZOA}} = \theta_{n,\text{ZOA}}^{\square} + \bar{\theta}_{\text{ZOA}} + c_{\text{ZSA}}\alpha_m \quad (7.6-17e)$$

where $\bar{\theta}_{\text{ZOA}} = 90^\circ$ if the BS-UT link is O2I and $\bar{\theta}_{\text{ZOA}} = \theta_{\text{LOS},\text{ZOA}}$ otherwise. The LOS direction is defined in the network layout description, see Step1c.

The ZOA angles are determined by

$$\theta_{n,m,ZOD} = \phi'_{n,ZOD} + \theta_{LOS,ZOD} + \mu_{offset,ZOD} + (3/8)(10^{\mu_{lgZSD}})\alpha_m \quad (7.6-17f)$$

where μ_{lgZSD} is the mean of the ZSD log-normal distribution.

Some of the delay and angle spreads and standard deviations used in equations (7.6-15) and (7.6-16) may be frequency-dependent. In the case of multi-frequency simulations according to Section 7.6.5, the largest value among all the simulated frequencies should be used in (7.6-15) and (7.6-16) so that the cluster and ray delays and angles (but not the powers or the resulting delay or angular spreads) are the same for all frequencies.

7.6.3.3 LOS/NLOS, indoor states and O2I parameters

The LOS state can be determined according to the spatial consistency procedure for random variables as mentioned in Section 7.6.3.1, by comparing a realization of a random variable generated with distance-dependent LOS probability. If the realization is less than the LOS probability, the state is LOS; otherwise NLOS. Decision of LOS and NLOS status should be used in Step 2 in Section 7.5 if this advanced simulation is performed.

The same procedure can be applied for determining the indoor state, with the indoor probability instead of the LOS probability.

The correlation distance for LOS state and indoor/outdoor is specified in Table 7.6.3.1-2.

The indoor distance can be modeled as the minimum of two spatially consistent uniform random variables within (0, 25) meters with correlation distance 25m.

Note in case the UT is in an indoor state, the pathloss model changes and a penetration loss is considered. For details on the model, see Section 7.4.3. Here, the focus is on modeling aspects with respect to spatial consistency. As described in Section 7.4.3, the penetration loss deviation σ_p represents variations within and between buildings of the same type. For spatial consistency this can be modeled as a spatially consistent random variable with correlation distance 10m, see Section 7.6.3.1. The “building type” is determined using a spatially consistent uniform random variable with correlation distance 50 m. The building type is determined by comparing the random variable with P_1 , where P_1 is the probability of the building type with low loss penetration. If the realization of the random variable is less than P_1 , the building type is low loss; otherwise the building type is high loss.

The cluster-specific and ray-specific random variables as defined in Section 7.6.3.1 on the same floor are generated in the spatial consistency modeling; otherwise, these variables across different floors are uncorrelated.

In case there is a transition from LOS to NLOS due to UT mobility, there will be a hard transition in the channel response. This is because pathloss and LS parameters are different for these states, leading automatically to very different channel realizations. To circumvent such hard transitions the optional soft LOS state can be considered to determine the PL and the channel impulse responses containing characteristics of both LOS and NLOS. Soft LOS state is generated by floating numbers between 0 (NLOS) and 1 (LOS) in the spatial consistency modeling. The value of is determined by

$$LOS_{soft} = \frac{1}{2} + \frac{1}{\pi} \arctan \left[\sqrt{\frac{20}{\lambda}} (G + F(d)) \right], \quad (7.6-18)$$

where:

- is a spatially consistent Gaussian random variable with correlation distance according to Table 7.6.3.1-2;
- ; and
- is the distance dependent LOS probability function.

After is obtained, Steps 2-12 of the channel coefficient generation described in Section 7.5 are performed twice, once with the propagation condition in step 2 set as LOS and once with the propagation condition in Step 2 set as NLOS. The resulting channel coefficients are denoted as H^{LOS} and H^{NLOS} respectively, where H^{LOS} is generated with the LOS path loss formula and channel model parameters while is H^{NLOS} generated using the NLOS path loss formula

and channel model parameters. The channel matrix H with soft LOS state is determined from a linear combination of H^{LOS} and H^{NLOS} as:

$$H(\text{LOS}_{\text{soft}}) = H^{\text{LOS}} \text{LOS}_{\text{soft}} + H^{\text{NLOS}} \sqrt{1 - \text{LOS}_{\text{soft}}^2} \quad (7.6-19)$$

It is noted that soft indoor/outdoor states are not 510dellin in this TR. The model thus doesn't support move between indoor/outdoor states in mobility simulations.

7.6.4 Blockage

Blockage modelling is an add-on feature to the channel model. The method described in the following applies only when this feature is turned on. In addition, the temporal variability of the blockage modelling parameters is on-demand basis. It is also noted that the modeling of the blockage does not change LOS/NLOS state of each link.

When blockage model is applied, the channel generation in section 7.5 should have several additional steps between Step 9 and 10 as illustrated in Figure 7.6.4-1.

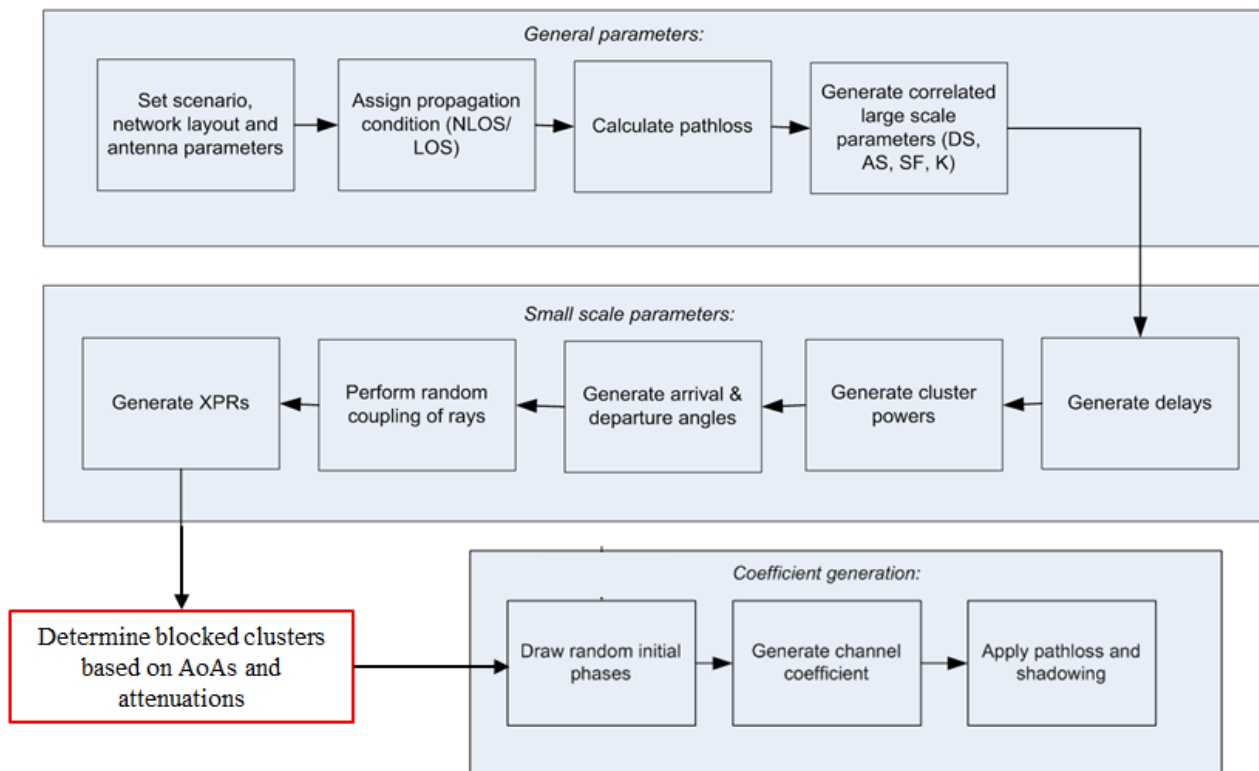


Figure.7.6.4-1 Channel generation procedure with blockage model

Two alternative models (Model A and Model B) are provided for the blockage modelling. Both approaches have their own use cases. Model A is applicable when a generic and computationally efficient blockage modelling is desired. Model B is applicable when a specific and more realistic blocking modelling is desired.

7.6.4.1 Blockage model A

Model A adopts a stochastic method for capturing human and vehicular blocking.

Step a: Determine the number of blockers

Multiple 2-dimensional (2D) angular blocking regions, in terms of centre angle, azimuth and elevation angular span are generated around the UT. There is one self-blocking region, and $K = 4$ non-self-blocking regions, where K may be

changed for certain scenarios (e.g., higher blocker density). Note that the self-blocking component of the model is important in capturing the effects of human body blocking.

Step b: Generate the size and location of each blocker

For self-blocking, the blocking region in UT LCS is defined in terms of elevation and azimuth angles, $(\theta'_{sb}, \phi'_{sb})$ and azimuth and elevation angular span (x_{sb}, y_{sb}) .

$$\left(\theta', \phi' \right) \left| \theta'_{sb} - \frac{y_{sb}}{2} \leq \theta' \leq \theta'_{sb} + \frac{y_{sb}}{2}, \phi'_{sb} - \frac{x_{sb}}{2} \leq \phi' \leq \phi'_{sb} + \frac{x_{sb}}{2} \right. \quad (7.6-20)$$

where the parameters are described in Table 7.6.4.1-1.

Table 7.6.4.1-1: Self-blocking region parameters.

	ϕ'_{sb}	x_{sb}	θ'_{sb}	y_{sb}
Portrait mode	260°	120°	100°	80°
Landscape mode	40°	160°	110°	75°

For non-self-blocking $k = 1, \dots, 4$, the blocking region in GCS is defined by

$$\left(\theta, \phi \right) \left| \theta_k - \frac{y_k}{2} \leq \theta \leq \theta_k + \frac{y_k}{2}, \phi_k - \frac{x_k}{2} \leq \phi \leq \phi_k + \frac{x_k}{2} \right. \quad (7.6-21)$$

where the parameters are described in Table 7.6.4.1-2, as well as the distance r between the UT and the blocker.

Table 7.6.4.1-2: Blocking region parameters.

Blocker index ($k = 1, \dots, 4$)	ϕ_k	x_k	θ_k	y_k	r
InH scenario	Uniform in $[0^\circ, 360^\circ]$	Uniform in $[15^\circ, 45^\circ]$	90°	Uniform in $[5^\circ, 15^\circ]$	2 m
Umi, Uma, Rma scenarios	Uniform in $[0^\circ, 360^\circ]$	Uniform in $[5^\circ, 15^\circ]$	90°	5°	10 m

Step c: Determine the attenuation of each cluster due to blockers

The attenuation of each cluster due to self-blocking corresponding to the centre angle pair $(\theta'_{sb}, \phi'_{sb})$, is 30 dB provided that and Otherwise, the attenuation is 0 dB.

The attenuation of each cluster due to the non-self-blocking regions ($k=1, \dots, 4$) is given by

$$L_{dB} = -20 \log_{10} (1 - (F_{A_1} + F_{A_2})(F_{Z_1} + F_{Z_2})) \quad (7.6-22)$$

provided that and . Otherwise, the attenuation is 0 dB. The terms in the above equation are given as

$$F_{A_1|A_2|Z_1|Z_2} = \frac{\tan^{-1} \left(\pm \frac{\pi}{2} \sqrt{\frac{\pi}{\lambda} r \frac{1}{\cos(A_1|A_2|Z_1|Z_2)} - 1} \right)}{\pi} \quad (7.6-23)$$

where

$$A_1 = \phi_{AOA} - \phi_k + \frac{x_k}{2}, \quad (7.6-24)$$

$$A_2 = \phi_{\text{AOA}} - \left\lfloor \phi_k - \frac{x_k}{2} \right\rfloor, \quad (7.6-25)$$

$$Z_1 = \theta_{\text{ZOA}} - \left\lfloor \theta_k + \frac{y_k}{2} \right\rfloor, \quad (7.6-26)$$

$$Z_2 = \theta_{\text{ZOA}} - \left\lfloor \theta_k - \frac{y_k}{2} \right\rfloor. \quad (7.6-27)$$

In the above formula for $F_{A_1|A_2|Z_1|Z_2}$, λ is the wavelength. The appropriate signs (\pm) within the \tan^{-1} term are described in Table 7.6.4.1-3.

Table 7.6.4.1-3: Description of signs

	$-y_k < \theta_{\text{ZOA}} - \theta_k \leq \frac{y_k}{2}$	$-\frac{y_k}{2} < \theta_{\text{ZOA}} - \theta_k < \frac{y_k}{2}$	$\frac{y_k}{2} < \theta_{\text{ZOA}} - \theta_k < y_k$
$\frac{x_k}{2} < \phi_{\text{AOA}} - \phi_k \leq x_k$	(-, +) for (A_1, A_2) (+, -) for (Z_1, Z_2)	(-, +) for (A_1, A_2) (+, +) for (Z_1, Z_2)	(-, +) for (-, +) for
$-\frac{x_k}{2} < \phi_{\text{AOA}} - \phi_k \leq \frac{x_k}{2}$	(+, +) for (A_1, A_2) (+, -) for (Z_1, Z_2)	(+, +) for (A_1, A_2) (+, +) for	(+, +) for (-, +) for
$-x_k < \phi_{\text{AOA}} - \phi_k \leq -\frac{x_k}{2}$	(+, -) for (+, -) for	(+, -) for (+, +) for	(+, -) for (-, +) for

Step d: Spatial and temporal consistency of each blocker

The centre of the blocker is generated based on a uniformly distributed random variable, which is temporally and spatially consistent. The two-dimensional autocorrelation function can be described with sufficient accuracy by the exponential function

$$R(\Delta_x, \Delta_t) = \exp \left\{ - \left(\frac{|\Delta_x|}{d_{\text{corr}}} + \frac{|\Delta_t|}{t_{\text{corr}}} \right) \right\} \quad (7.6-28)$$

The spatial correlation distance for the random variable determining the centre of the blocker is given in Table 7.6.4.1-4 for different scenarios.

Table 7.6.4.1-4: Spatial correlation distance for different scenarios.

Spatial correlation distance d_{corr} in [m] for the random variable determining the centre of the blocker	Umi			Uma			Rma			InH	
	LOS	NLOS	O2I	LOS	NLOS	O2I	LOS	NLOS	O2I	LOS	NLOS
	10	10	5	10	10	5	10	10	5	5	5

The correlation time, where v is the speed of the moving blocker.

Note: The rectangular blocker description is chosen for self-blocking region with the specific choices of d_{corr} assumed here. Generalization of this description to other choices should be done with care as the rectangular description may not be accurate.

7.6.4.2 Blockage model B

Model B adopts a geometric method for capturing e.g., human and vehicular blocking.

Step a: Determine blockers

A number, K , of blockers are modelled as rectangular screens that are physically placed on the map. Each screen has the dimension by height (h_k) and width (w_k), with the screen centre at coordinate (x_k, y_k, z_k) .

Note:

- The number of blockers (K), their vertical and horizontal extensions (h_k and w_k), locations (x_k, y_k, z_k) , density, and movement pattern (if non-stationary) are all simulation assumptions, to allow different blocking scenarios to be constructed depending on the need of the particular simulation study.

Recommended parameters for typical blockers are provided in Table 7.6.4.2-5.

- The blocking effect diminishes with increasing distance to the blocker. For implementation purposes it may be sufficient to consider only the K nearest blockers or the blockers closer than some distance from a specific UT.

Table 7.6.4.2-5: Recommended blocker parameters

	Typical set of blockers	Blocker dimensions	Mobility pattern
Indoor; Outdoor	Human	Cartesian: w=0.3m; h=1.7m	Stationary or up to 3 km/h
Outdoor	Vehicle	Cartesian: w=4.8m; h=1.4m	Stationary or up to 100 km/h

Step b: Determine the blockage attenuation per sub-path

Attenuation caused by each blocker to each sub-path is modelled using a simple knife edge diffraction model and is given by

$$L_{dB} = -20 \log_{10} (1 - (F_{h_1} + F_{h_2})(F_{w_1} + F_{w_2})) \quad (7.6-29)$$

where F_{h_1} , F_{h_2} , F_{w_1} , and F_{w_2} account for knife edge diffraction at the four edges, and are given by

$$F_{h_1|h_2|w_1|w_2} = \begin{cases} \frac{\tan^{-1} \left(\pm \frac{\pi}{2} \sqrt{\frac{\pi}{\lambda} (D1_{h_1|h_2|w_1|w_2} + D2_{h_1|h_2|w_1|w_2} - r)} \right)}{\pi}, & \text{for direct path in LOS} \\ \frac{\tan^{-1} \left(\pm \frac{\pi}{2} \sqrt{\frac{\pi}{\lambda} (D1_{h_1|h_2|w_1|w_2} - r')} \right)}{\pi}, & \text{for all other paths} \end{cases} \quad (7.6-30)$$

where λ is the wave length. As shown in Figure 7.6.4.2-2, $D1_{h_1|h_2|w_1|w_2}$ and $D2_{h_1|h_2|w_1|w_2}$ are the projected (onto the side and top view planes) distances between the receiver and four edges of the corresponding blocker, and r and r' are the projected (onto the side and top view planes) distances between the transmitter and four edges of the corresponding blocker. The side view plane is perpendicular to the horizontal ground plane. The top view is perpendicular to the side view. For each cluster, the blocker screen is rotated around its centre such that the arrival direction of the corresponding path is always perpendicular to the screen. It should be noted that different rotations are required for each individual sub-path. Meanwhile, the base and top edges of the screens are always parallel to the horizontal plane. As the screen is perpendicular to each sub-path, r is the distance between the transmitter and receiver for the direct path in LOS, and r' is the distance between the blocker screen and receiver, projected onto the incoming sub-path direction, for all the other (NLOS) paths. In the equation of $F_{h_1|h_2|w_1|w_2}$, the plus and minus signs are determined in such a way that, as shown in Figure 7.6.4.2-2,

- if the sub-path (terminated at the receiver or transmitter) does not intersect the screen in side view, minus sign is applied for the shortest path among $D1_{h1}$ and $D1_{h2}$ in the NLoS case ($D1_{h1} + D2_{h1}$ and $D1_{h2} + D2_{h2}$ in the LoS case) and plus sign is applied for the other edge.
- if the sub-path (terminated at the receiver or transmitter) does not intersect the screen in top view, minus sign is applied for the shortest path among $D1_{w1}$ and $D1_{w2}$ in the NLoS case ($D1_{w1} + D2_{w1}$ and $D1_{w2} + D2_{w2}$ for the LoS case) and plus sign is applied for the other edge.
- if the sub-path intersects the screen plus signs are applied for both edges.

For the case of multiple screens the total loss is given by summing the losses of each contributing screen in dB units.

The model according to option B is consistent in time, frequency and space, and is more appropriate to be used for simulations with arbitrarily designated blocker density.

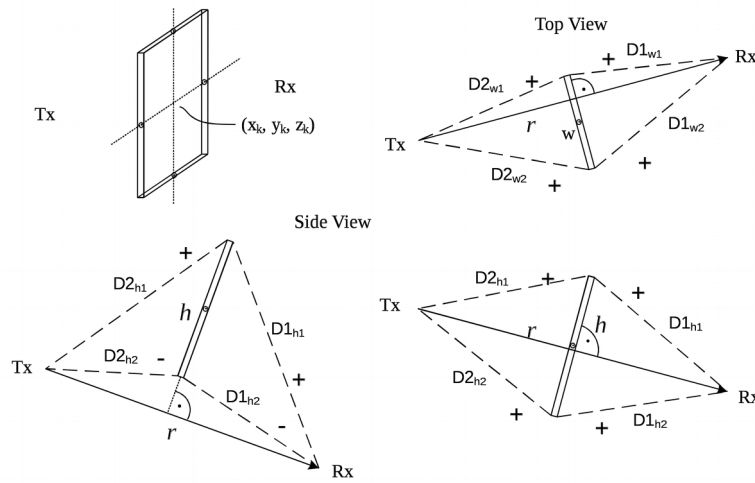


Figure 7.6.4.2(a): Illustration of the geometric relation among blocker, receiver and transmitter for the LOS path

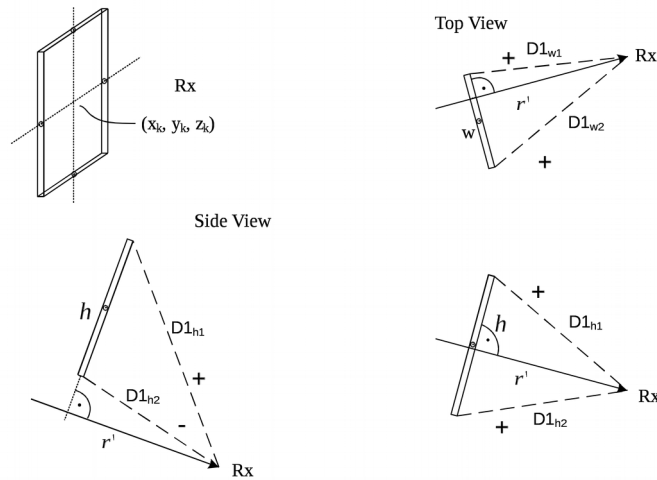


Figure 7.6.4.2(b): Illustration of the geometric relation between blocker and receiver for NLOS paths

7.6.5 Correlation modelling for multi-frequency simulations

This section describes how to generate parameters to reflect correlation across different frequencies for a BS-UT link, for simulations involved with multiple frequencies.

For those simulations, the steps in Section 7.5 should be revised according to the following:

- The parameters generated in Step 1 are the same for all the frequencies, except for antenna patterns, array geometries, system center frequency and bandwidth.
- Propagation conditions generated in Step 2 are the same for all the frequencies. It is noted that soft LOS states may be different due to frequency dependent function.
- The parameters generated in Step 4 are the same for all the frequencies, except for possibly frequency-dependent scaling of e.g. delay spread and angular spreads according to the LSP tables. I.e. let x be a random variable drawn from a Gaussian distribution: $x \sim N(0,1)$. Then the delay spread at frequency f is $DS(f) = 10^{(\mu_{gDS}(f) + \sigma_{gDS}(f) \cdot x)}$, where the same value of x is used for all frequencies. A corresponding procedure applies to each of the angular spreads.
- The cluster delays and angles resulting from Steps 5-7 are the same for all frequency bands
- Per-cluster shadowing Z_n in Step 6 are independently generated for the frequency bands.
- Cluster powers in Step 6 may be frequency-dependent.
- Steps 8-11 are independently applied for the frequency bands.

In addition, when blockage is modeled according to Section 7.6.4, the positions of blockers are the same across all the frequencies.

Note: The requirements above may not be fully aligned with the behavior of the model according to Section 7.5, since cluster delays and angles will be frequency-dependent in scenarios where the DS or AS is frequency-dependent. The procedure below may alternatively be used to ensure that cluster delays and angles are frequency-independently generated.

7.6.5.1 Alternative channel generation method

The alternative method replaces Steps 5-7 in Section 7.5 with the below Steps 5'-7'. The inputs to the alternative method are the delay and angular spreads determined according to Step 4 at an anchor frequency, e.g. 2 GHz: DS_0 , ASD_0 , ASA_0 , ZSD_0 , ZSA_0 , the delay and angular spreads determined according to Step 4 at a frequency of interest: DS , ASD , ASA , ZSD , ZSA , and the number of clusters N from Table 7.5-6.

Step 5': Generate nominal delays τ'_n and angles $\phi'_{AOD,n}$, $\phi'_{AOA,n}$, $\theta'_{ZOD,n}$, $\theta'_{ZOA,n}$

Generate N delays from a single-sided exponential distribution with zero mean and standard deviation of $r DS_0$, according to $\tau'_n = -r DS_0 \ln(X_n)$ with $X_n \sim \text{unif}(0,1)$.

Generate N AODs from a wrapped Gaussian distribution with zero mean and standard deviation of $r ASD_0$, according to $\phi'_{AOD,n} = \arg(\exp(-j r ASD_0 Y_n))$ with $Y_n \sim N(0,1)$.

Generate N AOA from a wrapped Gaussian distribution with zero mean and standard deviation of $r ASA_0$, according to $\phi'_{AOA,n} = \arg(\exp(-j r ASA_0 Z_n))$ with $Z_n \sim N(0,1)$.

Generate N ZODs from a wrapped Laplacian distribution with zero mean and standard deviation of $r ZSD_0$, according to $\theta'_{ZOD,n} = \arg(\exp(-j r ZSD_0 \text{sgn}(V_n - 0.5) \ln(1 - 2|V_n - 0.5|)/\sqrt{2}))$ with $V_n \sim \text{unif}(0,1)$.

Generate N ZOAs from a wrapped Laplacian distribution with zero mean and standard deviation of $r \cdot ZSA_0$, according to $\theta'_{ZOA,n} = \arg(\exp(-j r \cdot ZSA_0 \cdot \text{sgn}(W_n - 0.5) \ln(1 - 2|W_n - 0.5|)/\sqrt{2}))$ with $W_n \sim \text{unif}(0, 1)$.

R is a proportionality factor, $r=1.5$. The principal value of the \arg function should be used, e.g. $(-180, 180)$.

In case of LOS, set $\tau'_1=0$, $\phi'_{AOD,1}=0$, $\phi_{AOA,1}=0$, $\theta'_{ZOD,1}=0$, and $\theta_{ZOA,1}=0$.

Step 6': Generate cluster powers P_n

Generate cluster powers as

$$P_n = \exp\left[-\tau_n g_{DS} - \left|\frac{\phi_{AOD,n} g_{ASD}}{\sqrt{2}}\right|^2 - \left|\frac{\phi_{AOA,n} g_{ASA}}{\sqrt{2}}\right|^2 - \sqrt{2}|\theta_{ZOD,n}|g_{ZSD} - \sqrt{2}|\theta'_{ZOA,n}|g_{ZSA}\right] \cdot 10^{-Q_n/10} \quad (7.6.30a)$$

where $Q_n \sim N(0, \xi^2)$ is the per cluster shadowing term in [dB] and

$$g_{DS} = \frac{\max(r \cdot DS_0 - DS, 0)}{DS \cdot r \cdot DS_0} \quad (7.6.30b)$$

$$g_{ASD} = \frac{\sqrt{\max((r \cdot ASD_0)^2 - ASD^2, 0)}}{ASD \cdot r \cdot ASD_0} \quad (7.6.30c)$$

$$g_{ASA} = \frac{\sqrt{\max((r \cdot ASA_0)^2 - ASA^2, 0)}}{ASA \cdot r \cdot ASA_0} \quad (7.6.30d)$$

$$g_{ZSD} = \frac{\max(r \cdot ZSD_0 - ZSD, 0)}{ZSD \cdot r \cdot ZSD_0} \quad (7.6.30e)$$

$$g_{ZSA} = \frac{\max(r \cdot ZSA_0 - ZSA, 0)}{ZSA \cdot r \cdot ZSA_0} \quad (7.6.30f)$$

Normalize the cluster powers so that the sum of all cluster powers is equal to one, i.e.,

$$P_n = \frac{P'_n}{\sum_{n=1}^N P'_n} \quad (7.6.30g)$$

or, in the case of LOS, so that

$$P_n = \frac{1}{1+K_R} \frac{P'_n}{\sum_{n=1}^N P'_n} + \frac{K_R}{1+K_R} \delta(n-1) \quad (7.6.30h)$$

where K is the K-factor converted to linear scale.

Step 7': Generate delays τ_n and angles $\phi_{AOD,n}$, $\phi_{AOA,n}$, $\theta_{ZOD,n}$, $\theta_{ZOA,n}$

$$\tau_n = \begin{cases} \tau_n^{\square} & , \text{for NLOS} \\ \sqrt{1 + \frac{K_R}{2}} \tau_n^{\prime} & , \text{for LOS} \end{cases} \quad (7.6.30i)$$

$$\phi_{n,m,\text{AOA}} = \begin{cases} \phi_{n,\text{AOA}}^{\square} + \phi_{\text{LOS,AOA}} + c_{\text{ASA}} \alpha_m & , \text{for NLOS} \\ \sqrt{1 + K_R} \phi_{n,\text{AOA}}^{\prime} + \phi_{\text{LOS,AOA}} + c_{\text{ASA}} \alpha_m & , \text{for LOS} \end{cases} \quad (7.6.30j)$$

$$\phi_{n,m,\text{AOD}} = \begin{cases} \phi_{n,\text{AOD}}^{\square} + \phi_{\text{LOS,AOD}} + c_{\text{ASD}} \alpha_m & , \text{for NLOS} \\ \sqrt{1 + K_R} \phi_{n,\text{AOD}}^{\prime} + \phi_{\text{LOS,AOD}} + c_{\text{ASD}} \alpha_m & , \text{for LOS} \end{cases} \quad (7.6.30k)$$

$$\theta_{n,m,\text{ZOA}} = \begin{cases} \theta_{n,\text{ZOA}}^{\square} + \theta_{\text{LOS,ZOA}} + c_{\text{ZSA}} \alpha_m & , \text{for NLOS} \\ \sqrt{1 + K_R} \theta_{n,\text{ZOA}}^{\prime} + \theta_{\text{LOS,ZOA}} + c_{\text{ZSA}} \alpha_m & , \text{for LOS} \end{cases} \quad (7.6.30l)$$

$$\theta_{n,m,\text{ZOD}} = \begin{cases} \theta_{n,\text{ZOD}}^{\square} + \theta_{\text{LOS,ZOD}} + c_{\text{ZSD}} \alpha_m & , \text{for NLOS} \\ \sqrt{1 + K_R} \theta_{n,\text{ZOD}}^{\square} + \theta_{\text{LOS,ZOD}} + c_{\text{ZSD}} \alpha_m & , \text{for LOS} \end{cases} \quad (7.6.30m)$$

Repeat Steps 6'-7' for each frequency of interest, reusing the delays and angles from Step 5' for all frequencies.

Note: The resulting delay and angular spreads of channels generated with this alternative method will be similar but not identical to when using Steps 5-7 in section 7.5.

7.6.6 Time-varying Doppler shift

The Doppler shift generally depends on the time evolution of the channel as it is defined as the derivative of the channels phase over time. It can be the result from Tx, Rx, or scatterer movement. The more general form of the exponential Doppler term as used in Equation (7.5-22) is given by

$$\exp \left[j 2 \pi \int_{t_0}^t \frac{\hat{\mathbf{r}}_{rx,n,m}^T(\tilde{t}) \cdot \mathbf{v}(\tilde{t})}{\lambda_0} d\tilde{t} \right] \quad (7.6-31)$$

Here, $\hat{\mathbf{r}}_{rx,n,m}(\mathbf{t})$ is the normalized vector that points into the direction of the incoming wave as seen from the Rx at time \mathbf{t} . $\mathbf{v}(\mathbf{t})$ denotes the velocity vector of the Rx at time \mathbf{t} , while t_0 denotes a reference point in time that defines the initial phase, e.g. $t_0 = 0$.

Note that Equation (7.5-22) only holds for time-invariant Doppler shift, i.e. $\hat{\mathbf{r}}_{rx,n,m}^T(\mathbf{t}) \cdot \mathbf{v}(\mathbf{t}) = \hat{\mathbf{r}}_{rx,n,m}^T \cdot \mathbf{v}$.

7.6.7 UT rotation

UT rotation modelling is an add-on feature. When modelled, step 1 in Section 7.5 shall consider UT rotational motion.

Step 1:

Add: h) Give rotational motion of UT in terms of its bearing angle, downtilt angle and slant angle.

7.6.8 Explicit ground reflection model

In case the ground reflection shall be modelled explicitly, Equation (7.5-30) has to be replaced by

$$H_{u,s}^{\text{LOS}}(\tau, t) = \sqrt{\frac{1}{K_R + 1}} H_{u,s}^{\text{NLOS}}(\tau - \tau_{\text{LOS}}, t) + \sqrt{\frac{K_R}{K_R + 1}} \left[H_{u,s,1}^{\text{LOS}}(t) \delta(\tau - \tau_{\text{LOS}}) + \frac{d_{3D}}{d_{\text{GR}}} H_{u,s}^{\text{GR}}(t) \delta(\tau - \tau_{\text{GR}}) \right] \quad (7.6-32)$$

with the delays for the ground reflected and the LOS paths being defined by their lengths, according to the Tx-Rx separation d_{2D} and the Tx and Rx heights h_{tx} and h_{rx} respectively, as

$$\tau_{\text{GR}} = \frac{d_{\text{GR}}}{c} = \frac{\sqrt{(h_{\text{tx}} + h_{\text{rx}})^2 + d_{2D}^2}}{c}, \quad (7.6-33)$$

and

$$\tau_{\text{LOS}} = \frac{d_{3D}}{c} = \frac{\sqrt{(h_{\text{tx}} - h_{\text{rx}})^2 + d_{2D}^2}}{c}. \quad (7.6-34)$$

The channel coefficient for the ground reflected path is given by

$$H_{u,s}^{\text{GR}}(t) = \begin{bmatrix} F_{\text{rx},u,\theta}(\theta_{\text{GR,ZOA}}, \phi_{\text{GR,AOA}}) \\ F_{\text{rx},u,\phi}(\theta_{\text{GR,ZOA}}, \phi_{\text{GR,AOA}}) \end{bmatrix}^T \begin{bmatrix} R_{\parallel}^{\text{GR}} & 0 \\ 0 & -R_{\perp}^{\text{GR}} \end{bmatrix} \begin{bmatrix} F_{\text{tx},s,\theta}(\theta_{\text{GR,ZOD}}, \phi_{\text{GR,AOD}}) \\ F_{\text{tx},s,\phi}(\theta_{\text{GR,ZOD}}, \phi_{\text{GR,AOD}}) \end{bmatrix} \cdot \exp\left[-j2\pi \frac{d_{\text{GR}}}{\lambda_0}\right] \exp\left[j2\pi \frac{\hat{r}_{\text{rx,GR}}^T \bar{d}_{\text{rx},u}}{\lambda_0}\right] \exp\left[j2\pi \frac{\hat{r}_{\text{tx,GR}}^T \bar{d}_{\text{tx},s}}{\lambda_0}\right] \exp\left[j2\pi \frac{\hat{r}_{\text{rx,GR}}^T \bar{v}}{\lambda_0} t\right] \quad (7.6-35)$$

with the normalized vectors pointing towards the ground reflection point from the Tx

$$\hat{r}_{\text{tx,GR}} = e_r(\theta_{\text{GR,ZOD}}, \phi_{\text{GR,AOD}}) = \begin{bmatrix} \sin \theta_{\text{GR,ZOD}} \cos \phi_{\text{GR,AOD}} \\ \sin \theta_{\text{GR,ZOD}} \sin \phi_{\text{GR,AOD}} \\ \cos \theta_{\text{GR,ZOD}} \end{bmatrix} \quad (7.6-36)$$

and from the Rx side

$$\hat{r}_{\text{rx,GR}} = e_r(\theta_{\text{GR,ZOA}}, \phi_{\text{GR,AOA}}) = \begin{bmatrix} \sin \theta_{\text{GR,ZOA}} \cos \phi_{\text{GR,AOA}} \\ \sin \theta_{\text{GR,ZOA}} \sin \phi_{\text{GR,AOA}} \\ \cos \theta_{\text{GR,ZOA}} \end{bmatrix}. \quad (7.6-37)$$

The angles for the ground reflected path are given by the geometry assuming a flat surface with its normal pointing into z-direction. The angles at the Tx side can be determined by

$$\theta_{\text{GR,ZOD}} = 180^\circ - \text{atan}\left[\frac{d_{2D}}{h_{\text{tx}} + h_{\text{rx}}}\right] \quad (7.6-37a)$$

$$\phi_{\text{GR,AOD}} = \phi_{\text{LOS,AOD}} \quad (7.6-37b)$$

and at the Rx side by

$$\theta_{\text{GR,ZOA}} = \theta_{\text{GR,ZOD}} \quad (7.6-37c)$$

$$\phi_{\text{GR,AOA}} = \phi_{\text{GR,AOD}} + 180^\circ. \quad (7.6-37d)$$

The reflection coefficients for parallel and perpendicular polarization on the ground, cf. [21], are given by

$$R_{\parallel}^{\text{GR}} = \frac{\frac{\varepsilon_{\text{GR}}}{\varepsilon_0} \cos(\theta_{\text{GR,ZOD}}) + \sqrt{\frac{\varepsilon_{\text{GR}}}{\varepsilon_0} - \sin^2(\theta_{\text{GR,ZOD}})}}{\frac{\varepsilon_{\text{GR}}}{\varepsilon_0} \cos(\theta_{\text{GR,ZOD}}) - \sqrt{\frac{\varepsilon_{\text{GR}}}{\varepsilon_0} - \sin^2(\theta_{\text{GR,ZOD}})}}, \quad (7.6-38)$$

and

$$R_{\perp}^{\text{GR}} = \frac{\cos(\theta_{\text{GR,ZOD}}) + \sqrt{\frac{\varepsilon_{\text{GR}}}{\varepsilon_0} - \sin^2(\theta_{\text{GR,ZOD}})}}{\cos(\theta_{\text{GR,ZOD}}) - \sqrt{\frac{\varepsilon_{\text{GR}}}{\varepsilon_0} - \sin^2(\theta_{\text{GR,ZOD}})}}, \quad (7.6-39)$$

with the complex relative permittivity of the ground material given by

$$\frac{\varepsilon_{\text{GR}}}{\varepsilon_0} = \varepsilon_r - j \frac{\sigma}{2\pi f_c \varepsilon_0}. \quad (7.6-40)$$

The electric constant ε_0 is given by $8.854187817... \times 10^{-12} \text{ F}\cdot\text{m}^{-1}$.

For applicable frequency ranges, the real relative permittivity can be modelled by

$$\varepsilon_r = a_\varepsilon \left[\frac{f_c}{10^9} \right]^{b_\varepsilon}, \quad (7.6-41)$$

while the conductivity in [S/m] may be modelled by

$$\sigma = c_\sigma \left[\frac{f_c}{10^9} \right]^{d_\sigma}, \quad (7.6-42)$$

with f_c being the center frequency in Hz.

A selection of material properties from [19] is given below. Since the simplified models for conductivity and relative permittivity are only applicable for frequencies between 1 and 10 GHz, Figure 7.6.8-1 presents curves up to 100 GHz at least for very, medium dry and wet ground, cf. [20].

Table 7.6.8-1 Material properties [19]

Material class	Relative permittivity		Conductivity		Frequency range in [GHz]
	a_ϵ	b_ϵ	c_σ	d_σ	
Concrete	5.31	0	0.0326	0.8095	1-100
Brick	3.75	0	0.038	0	1-10
Plasterboard	2.94	0	0.0116	0.7076	1-100
Wood	1.99	0	0.0047	1.0718	0.001-100
Floorboard	3.66	0	0.0044	1.3515	50-100
Metal	1	0	10^7	0	1-100
Very dry ground	3	0	0.00015	2.52	1-10
Medium dry ground	15	-0.1	0.035	1.63	1-10
Wet ground	30	-0.4	0.15	1.30	1-10

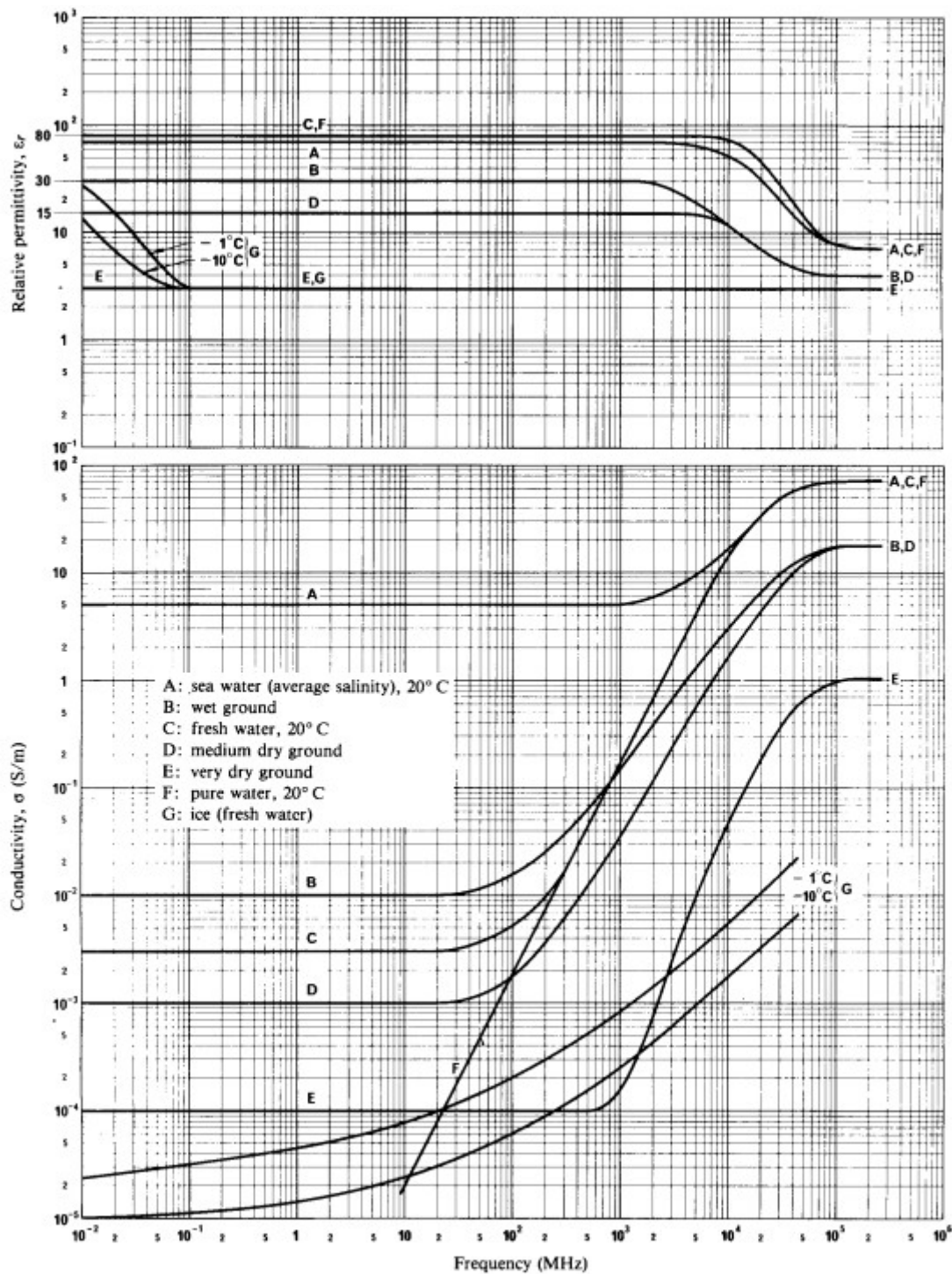


Figure 7.6.8-1: Relative permittivity and conductivity as a function of frequency [20]

7.7 Channel models for link-level evaluations

7.7.1 Clustered Delay Line (CDL) models

The CDL models are defined for the full frequency range from 0.5 GHz to 100 GHz with a maximum bandwidth of 2 GHz. CDL models can be implemented by e.g., coefficient generation Step 10 and Step 11 in Section 7.5 or generating TDL model using spatial filter from Section 7.7.4. Three CDL models, namely CDL-A, CDL-B and CDL-C are constructed to represent three different channel profiles for NLOS while CDL-D and CDL-E are constructed for LOS, the parameters of which can be found respectively in Table 7.7.1-1, Table 7.7.1-2, Table 7.7.1-3, Table 7.7.1-4 and Table 7.7.1-5.

Each CDL model can be scaled in delay so that the model achieves a desired RMS delay spread, according to the procedure described in Section 7.7.3. Each CDL model can also be scaled in angles so that the model achieves desired angle spreads, according to the procedure described in Section 7.7.5.1.

For LOS channel models, the K-factor of CDL-D and CDL-E can be set to a desired value following the procedure described in Section 7.7.6.

For 3D modelling effect of beamforming in a simplified way, a brick-wall window can be applied to a delay-scaled CDL model. The power shall be normalized after applying the window. A TDL model for simplified evaluations can be obtained from the CDL model, according to this method.

The following step by step procedure should be used to generate channel coefficients using the CDL models.

Step 1: Generate departure and arrival angles

Generate arrival angles of azimuth using the following equation

$$\phi_{n,m,AOA} = \phi_{n,AOA} + c_{ASA} \alpha_m, \quad (7.7-0a)$$

Where $\phi_{n,AOA}$ is the cluster AOA and c_{ASA} is the cluster-wise rms azimuth spread of arrival angles (cluster ASA) in Tables 7.7.1.1 – 7.7.1.5 below, and α_m is the ray offset angles within a cluster given by Table 7.5-3. If angular scaling according to Section 7.7.5.1 is used, this is applied to the ray angles $\phi_{n,m,AOA}$. The generation of AOD ($\phi_{n,m,AOD}$), ZSA ($\theta_{n,m,ZOA}$), and ZSD ($\theta_{n,m,ZOD}$) follows a procedure similar to AOA as described above.

Step 2: Coupling of rays within a cluster for both azimuth and elevation

Couple randomly AOD angles $\phi_{n,m,AOD}$ to AOA angles $\phi_{n,m,AOA}$ within a cluster n . Couple randomly ZOD angles $\theta_{n,m,ZOD}$ with ZOA angles $\theta_{n,m,ZOA}$ using the same procedure. Couple randomly AOD angles $\phi_{n,m,AOD}$ with ZOD angles $\theta_{n,m,ZOD}$ within a cluster n .

Step 3: Generate the cross polarization power ratios

Generate the cross polarization power ratios (XPR) κ for each ray m of each cluster n as

$$\kappa_{n,m} = 10^{X/10}, \quad (7.7-0b)$$

where X is the per-cluster XPR in dB from Tables 7.7.1.1 – 7.7.1.5.

Step 4: Coefficient generation

Follow the same procedure as in Steps 10 and 11 in Section 7.5, with the exception that all clusters are treated as “weaker cluster”, i.e. no further sub-clusters in delay should be generated. Additional clusters representing delay spread of the stronger clusters are already provided in Tables 7.7.1.1 – 7.7.1.5.

Table 7.7.1-1. CDL-A

Cluster #	Normalized delay	Power in [dB]	AoD in [°]	AoA in [°]	ZoD in [°]	ZoA in [°]
1	0.0000	-13.4	-178.1	51.3	50.2	125.4
2	0.3819	0	-4.2	-152.7	93.2	91.3
3	0.4025	-2.2	-4.2	-152.7	93.2	91.3
4	0.5868	-4	-4.2	-152.7	93.2	91.3
5	0.4610	-6	90.2	76.6	122	94
6	0.5375	-8.2	90.2	76.6	122	94
7	0.6708	-9.9	90.2	76.6	122	94
8	0.5750	-10.5	121.5	-1.8	150.2	47.1
9	0.7618	-7.5	-81.7	-41.9	55.2	56
10	1.5375	-15.9	158.4	94.2	26.4	30.1
11	1.8978	-6.6	-83	51.9	126.4	58.8
12	2.2242	-16.7	134.8	-115.9	171.6	26
13	2.1718	-12.4	-153	26.6	151.4	49.2
14	2.4942	-15.2	-172	76.6	157.2	143.1
15	2.5119	-10.8	-129.9	-7	47.2	117.4
16	3.0582	-11.3	-136	-23	40.4	122.7
17	4.0810	-12.7	165.4	-47.2	43.3	123.2
18	4.4579	-16.2	148.4	110.4	161.8	32.6
19	4.5695	-18.3	132.7	144.5	10.8	27.2
20	4.7966	-18.9	-118.6	155.3	16.7	15.2
21	5.0066	-16.6	-154.1	102	171.7	146
22	5.3043	-19.9	126.5	-151.8	22.7	150.7
23	9.6586	-29.7	-56.2	55.2	144.9	156.1
Per-Cluster Parameters						
Parameter	C_{ASD}	C_{ASA}	C_{ZSD}	C_{ZSA}	XPR	
Unit	0	0	0	0	dB	
Value	5	11	3	3	10	

Table 7.7.1-2. CDL-B

Cluster #	Normalized delay	Power in [dB]	AoD in [°]	AoA in [°]	ZoD in [°]	ZoA in [°]
1	0.0000	0	9.3	-173.3	105.8	78.9
2	0.1072	-2.2	9.3	-173.3	105.8	78.9
3	0.2155	-4	9.3	-173.3	105.8	78.9
4	0.2095	-3.2	-34.1	125.5	115.3	63.3
5	0.2870	-9.8	-65.4	-88.0	119.3	59.9
6	0.2986	-1.2	-11.4	155.1	103.2	67.5
7	0.3752	-3.4	-11.4	155.1	103.2	67.5
8	0.5055	-5.2	-11.4	155.1	103.2	67.5
9	0.3681	-7.6	-67.2	-89.8	118.2	82.6
10	0.3697	-3	52.5	132.1	102.0	66.3
11	0.5700	-8.9	-72	-83.6	100.4	61.6
12	0.5283	-9	74.3	95.3	98.3	58.0
13	1.1021	-4.8	-52.2	103.7	103.4	78.2
14	1.2756	-5.7	-50.5	-87.8	102.5	82.0
15	1.5474	-7.5	61.4	-92.5	101.4	62.4
16	1.7842	-1.9	30.6	-139.1	103.0	78.0
17	2.0169	-7.6	-72.5	-90.6	100.0	60.9
18	2.8294	-12.2	-90.6	58.6	115.2	82.9
19	3.0219	-9.8	-77.6	-79.0	100.5	60.8
20	3.6187	-11.4	-82.6	65.8	119.6	57.3
21	4.1067	-14.9	-103.6	52.7	118.7	59.9
22	4.2790	-9.2	75.6	88.7	117.8	60.1
23	4.7834	-11.3	-77.6	-60.4	115.7	62.3
Per-Cluster Parameters						
Parameter	C_{ASD}	C_{ASA}	C_{ZSD}	C_{ZSA}	XPR	
Unit	0	0	0	0	dB	
Value	10	22	3	7	8	

Table 7.7.1-3. CDL-C

Cluster #	Normalized delay	Power in [dB]	AoD in [°]	AoA in [°]	ZoD in [°]	ZoA in [°]
1	0	-4.4	-46.6	-101	97.2	87.6
2	0.2099	-1.2	-22.8	120	98.6	72.1
3	0.2219	-3.5	-22.8	120	98.6	72.1
4	0.2329	-5.2	-22.8	120	98.6	72.1
5	0.2176	-2.5	-40.7	-127.5	100.6	70.1
6	0.6366	0	0.3	170.4	99.2	75.3
7	0.6448	-2.2	0.3	170.4	99.2	75.3
8	0.6560	-3.9	0.3	170.4	99.2	75.3
9	0.6584	-7.4	73.1	55.4	105.2	67.4
10	0.7935	-7.1	-64.5	66.5	95.3	63.8
11	0.8213	-10.7	80.2	-48.1	106.1	71.4
12	0.9336	-11.1	-97.1	46.9	93.5	60.5
13	1.2285	-5.1	-55.3	68.1	103.7	90.6
14	1.3083	-6.8	-64.3	-68.7	104.2	60.1
15	2.1704	-8.7	-78.5	81.5	93.0	61.0
16	2.7105	-13.2	102.7	30.7	104.2	100.7
17	4.2589	-13.9	99.2	-16.4	94.9	62.3
18	4.6003	-13.9	88.8	3.8	93.1	66.7
19	5.4902	-15.8	-101.9	-13.7	92.2	52.9
20	5.6077	-17.1	92.2	9.7	106.7	61.8
21	6.3065	-16	93.3	5.6	93.0	51.9
22	6.6374	-15.7	106.6	0.7	92.9	61.7
23	7.0427	-21.6	119.5	-21.9	105.2	58
24	8.6523	-22.8	-123.8	33.6	107.8	57
Per-Cluster Parameters						
Parameter	C _{ASD}	C _{ASA}	C _{ZSD}	C _{ZSA}	XPR	
Unit	0	0	0	0	dB	
Value	2	15	3	7	7	

Table 7.7.1-4. CDL-D.

Cluster #	Cluster PAS	Normalized Delay	Power in [dB]	AoD in [°]	AoA in [°]	ZoD in [°]	ZoA in [°]
1	Specular(LOS path)	0	-0.2	0	-180	98.5	81.5
	Laplacian	0	-13.5	0	-180	98.5	81.5
2	Laplacian	0.035	-18.8	89.2	89.2	85.5	86.9
3	Laplacian	0.612	-21	89.2	89.2	85.5	86.9
4	Laplacian	1.363	-22.8	89.2	89.2	85.5	86.9
5	Laplacian	1.405	-17.9	13	163	97.5	79.4
6	Laplacian	1.804	-20.1	13	163	97.5	79.4
7	Laplacian	2.596	-21.9	13	163	97.5	79.4
8	Laplacian	1.775	-22.9	34.6	-137	98.5	78.2
9	Laplacian	4.042	-27.8	-64.5	74.5	88.4	73.6
10	Laplacian	7.937	-23.6	-32.9	127.7	91.3	78.3
11	Laplacian	9.424	-24.8	52.6	-119.6	103.8	87
12	Laplacian	9.708	-30.0	-132.1	-9.1	80.3	70.6
13	Laplacian	12.525	-27.7	77.2	-83.8	86.5	72.9
Per-Cluster Parameters							
Parameter	C _{ASD}	C _{ASA}	C _{ZSD}	C _{ZSA}	XPR		
Unit	0	0	0	0	dB		
Value	5	8	3	3	11		

Table 7.7.1-5. CDL-E.

Cluster #	Cluster PAS	Normalized Delay	Power in [dB]	AoD in [°]	AoA in [°]	ZoD in [°]	ZoA in [°]
1	Specular (LOS path)	0.000	-0.03	0	-180	99.6	80.4
	Laplacian	0.000	-22.03	0	-180	99.6	80.4
2	Laplacian	0.5133	-15.8	57.5	18.2	104.2	80.4
3	Laplacian	0.5440	-18.1	57.5	18.2	104.2	80.4
4	Laplacian	0.5630	-19.8	57.5	18.2	104.2	80.4
5	Laplacian	0.5440	-22.9	-20.1	101.8	99.4	80.8
6	Laplacian	0.7112	-22.4	16.2	112.9	100.8	86.3
7	Laplacian	1.9092	-18.6	9.3	-155.5	98.8	82.7
8	Laplacian	1.9293	-20.8	9.3	-155.5	98.8	82.7
9	Laplacian	1.9589	-22.6	9.3	-155.5	98.8	82.7
10	Laplacian	2.6426	-22.3	19	-143.3	100.8	82.9
11	Laplacian	3.7136	-25.6	32.7	-94.7	96.4	88
12	Laplacian	5.4524	-20.2	0.5	147	98.9	81
13	Laplacian	12.0034	-29.8	55.9	-36.2	95.6	88.6
14	Laplacian	20.6419	-29.2	57.6	-26	104.6	78.3
Per-Cluster Parameters							
Parameter	C_{ASD}		C_{ASA}	C_{ZSD}	C_{ZSA}	XPR	
Unit	o		o	o	o	dB	
Value	5		11	3	7	8	

7.7.2 Tapped Delay Line (TDL) models

The TDL models for simplified evaluations, e.g., for non-MIMO evaluations, are defined for the full frequency range from 0.5 GHz to 100 GHz with a maximum bandwidth of 2 GHz.

Three TDL models, namely TDL-A, TDL-B and TDL-C, are constructed to represent three different channel profiles for NLOS while TDL-D and TDL-E are constructed for LOS, the parameters of which can be found respectively in Table 7.7.2-1, Table 7.7.2-2, Table 7.7.2-3, Table 7.7.2-4 and Table 7.7.2-5.

The Doppler spectrum for each tap is characterized by a classical (Jakes) spectrum shape and a maximum Doppler shift f_D where $f_D = |\vec{v}|/\lambda_0$. Due to the presence of a LOS path, the first tap in TDL-D and TDL-E follows a Ricean fading distribution. For those taps the Doppler spectrum additionally contains a peak at the Doppler shift $f_s = 0.7 f_D$ with an amplitude such that the resulting fading distribution has the specified K-factor.

Each TDL model can be scaled in delay so that the model achieves a desired RMS delay spread, according to the procedure described in Section 7.7.3.

For LOS channel models, the K-factor of TDL-D and TDL-E can be set to a desired value following the procedure described in Section 7.7.6.

Table 7.7.2-1. TDL-A

Tap #	Normalized delay	Power in [dB]	Fading distribution
1	0.0000	-13.4	Rayleigh
2	0.3819	0	Rayleigh
3	0.4025	-2.2	Rayleigh
4	0.5868	-4	Rayleigh
5	0.4610	-6	Rayleigh
6	0.5375	-8.2	Rayleigh
7	0.6708	-9.9	Rayleigh
8	0.5750	-10.5	Rayleigh
9	0.7618	-7.5	Rayleigh
10	1.5375	-15.9	Rayleigh
11	1.8978	-6.6	Rayleigh
12	2.2242	-16.7	Rayleigh
13	2.1718	-12.4	Rayleigh
14	2.4942	-15.2	Rayleigh
15	2.5119	-10.8	Rayleigh
16	3.0582	-11.3	Rayleigh
17	4.0810	-12.7	Rayleigh
18	4.4579	-16.2	Rayleigh
19	4.5695	-18.3	Rayleigh
20	4.7966	-18.9	Rayleigh
21	5.0066	-16.6	Rayleigh
22	5.3043	-19.9	Rayleigh
23	9.6586	-29.7	Rayleigh

Table 7.7.2-2. TDL-B

Tap #	Normalized delay	Power in [dB]	Fading distribution
1	0.0000	0	Rayleigh
2	0.1072	-2.2	Rayleigh
3	0.2155	-4	Rayleigh
4	0.2095	-3.2	Rayleigh
5	0.2870	-9.8	Rayleigh
6	0.2986	-1.2	Rayleigh
7	0.3752	-3.4	Rayleigh
8	0.5055	-5.2	Rayleigh
9	0.3681	-7.6	Rayleigh
10	0.3697	-3	Rayleigh
11	0.5700	-8.9	Rayleigh
12	0.5283	-9	Rayleigh
13	1.1021	-4.8	Rayleigh
14	1.2756	-5.7	Rayleigh
15	1.5474	-7.5	Rayleigh
16	1.7842	-1.9	Rayleigh
17	2.0169	-7.6	Rayleigh
18	2.8294	-12.2	Rayleigh
19	3.0219	-9.8	Rayleigh
20	3.6187	-11.4	Rayleigh
21	4.1067	-14.9	Rayleigh
22	4.2790	-9.2	Rayleigh
23	4.7834	-11.3	Rayleigh

Table 7.7.2-3. TDL-C

Tap #	Normalized delays	Power in [dB]	Fading distribution
1	0	-4.4	Rayleigh
2	0.2099	-1.2	Rayleigh
3	0.2219	-3.5	Rayleigh
4	0.2329	-5.2	Rayleigh
5	0.2176	-2.5	Rayleigh
6	0.6366	0	Rayleigh
7	0.6448	-2.2	Rayleigh
8	0.6560	-3.9	Rayleigh
9	0.6584	-7.4	Rayleigh
10	0.7935	-7.1	Rayleigh
11	0.8213	-10.7	Rayleigh
12	0.9336	-11.1	Rayleigh
13	1.2285	-5.1	Rayleigh
14	1.3083	-6.8	Rayleigh
15	2.1704	-8.7	Rayleigh
16	2.7105	-13.2	Rayleigh
17	4.2589	-13.9	Rayleigh
18	4.6003	-13.9	Rayleigh
19	5.4902	-15.8	Rayleigh
20	5.6077	-17.1	Rayleigh
21	6.3065	-16	Rayleigh
22	6.6374	-15.7	Rayleigh
23	7.0427	-21.6	Rayleigh
24	8.6523	-22.8	Rayleigh

Table 7.7.2-4. TDL-D.

Tap #	Normalized delay	Power in [dB]	Fading distribution
1	0	-0.2	LOS path
	0	-13.5	Rayleigh
2	0.035	-18.8	Rayleigh
3	0.612	-21	Rayleigh
4	1.363	-22.8	Rayleigh
5	1.405	-17.9	Rayleigh
6	1.804	-20.1	Rayleigh
7	2.596	-21.9	Rayleigh
8	1.775	-22.9	Rayleigh
9	4.042	-27.8	Rayleigh
10	7.937	-23.6	Rayleigh
11	9.424	-24.8	Rayleigh
12	9.708	-30.0	Rayleigh
13	12.525	-27.7	Rayleigh

NOTE: The first tap follows a Ricean distribution with a K-factor of $K_1 = 13.3$ dB and a mean power of 0dB.

Table 7.7.2-5. TDL-E.

Tap #	Normalized delay	Power in [dB]	Fading distribution
1	0	-0.03	LOS path
	0	-22.03	Rayleigh
2	0.5133	-15.8	Rayleigh
3	0.5440	-18.1	Rayleigh
4	0.5630	-19.8	Rayleigh
5	0.5440	-22.9	Rayleigh
6	0.7112	-22.4	Rayleigh
7	1.9092	-18.6	Rayleigh
8	1.9293	-20.8	Rayleigh
9	1.9589	-22.6	Rayleigh
10	2.6426	-22.3	Rayleigh
11	3.7136	-25.6	Rayleigh
12	5.4524	-20.2	Rayleigh
13	12.0034	-29.8	Rayleigh
14	20.6519	-29.2	Rayleigh

NOTE: The first tap follows a Ricean distribution with a K-factor of $K_1 = 22$ dB and a mean power of 0dB.

7.7.3 Scaling of delays

The RMS delay spread values of both CDL and TDL models are normalized and they can be scaled in delay so that a desired RMS delay spread can be achieved. The scaled delays can be obtained according to the following equation:

$$\tau_{n,\text{scaled}} = \tau_{n,\text{model}} \cdot \text{DS}_{\text{desired}} \quad (7.7-1)$$

in which

$\tau_{n,\text{model}}$ is the normalized delay value of the n th cluster in a CDL or a TDL model

$\tau_{n,\text{scaled}}$ is the new delay value (in [ns]) of the n th cluster

$\text{DS}_{\text{desired}}$ is the wanted delay spread (in [ns])

The example scaling parameters are selected according to Table 7.7.3-1 where the values have been chosen such that the RMS delay spreads span the range observed in measurements corresponding to the typical 5G evaluation scenarios. For information purposes, examples of such RMS delay spreads for the different scenarios are given in Table 7.7.3-2 where the “short-delay profile” corresponds to the median RMS delay spread for LOS scenarios, while “normal-delay profile” and “long-delay profile” correspond to the median and the 90th percentile RMS delay spread for NLOS scenarios according to the channel parameters in Table 7.5-6. It can therefore be understood that a particular RMS delay spread in Table 7.7.3-1 may occur in any scenario; however certain values may be more likely in some scenarios than in others.

The example parameters given in Table 7.7.3-1 does not preclude the use of other scaling values if this is found appropriate, for instance if additional scenarios are introduced or if e.g. the effect of beamforming needs to be captured in a TDL. Both of these examples can potentially result in an increased range of experienced RMS delay spreads.

Table 7.7.3-1. Example scaling parameters for CDL and TDL models.

Model	$\text{DS}_{\text{desired}}$
Very short delay spread	10 ns
Short delay spread	30 ns
Nominal delay spread	100 ns
Long delay spread	300 ns
Very long delay spread	1000 ns

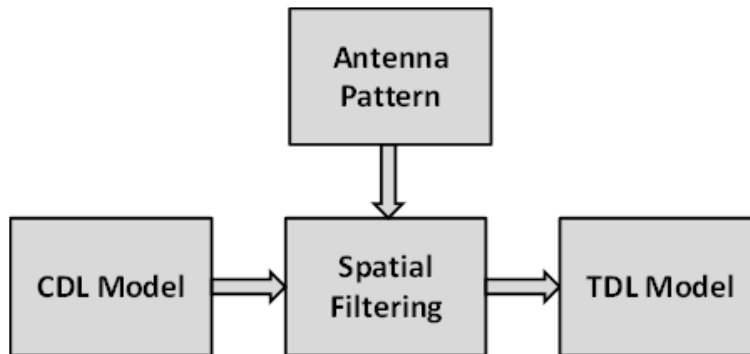
Table 7.7.3-2. Scenario specific scaling factors – for information only

Proposed Scaling Factor $DS_{desired}$ in [ns]		Frequency [GHz]						
		2	6	15	28	39	60	70
Indoor office	Short-delay profile	20	16	16	16	16	16	16
	Normal-delay profile	39	30	24	20	18	16	16
	Long-delay profile	59	53	47	43	41	38	37
Umi Street-canyon	Short-delay profile	65	45	37	32	30	27	26
	Normal-delay profile	129	93	76	66	61	55	53
	Long-delay profile	634	316	307	301	297	293	291
Uma	Short-delay profile	93	93	85	80	78	75	74
	Normal-delay profile	363	363	302	266	249	228	221
	Long-delay profile	1148	1148	955	841	786	720	698
Rma & Rma O2I	Short-delay profile	32	32	N/A	N/A	N/A	N/A	N/A
	Normal-delay profile	37	37	N/A	N/A	N/A	N/A	N/A
	Long-delay profile	153	153	N/A	N/A	N/A	N/A	N/A
Umi / Uma O2I	Normal-delay profile	240						
	Long-delay profile	616						

7.7.4 Spatial filter for generating TDL channel model

The TDL models described in Section 7.7.2 are generated from the CDL models assuming ideal isotropic antennas at both Tx and Rx. It is also possible to generate TDL models by assuming non-isotropic antennas like directive horn antennas or array antennas.

The basic idea to generate a TDL model based on a filtered CDL model is shown in Figure 7.7.4-1 below.

**Figure 7.7.4-1 The basic idea for filtering the CDL model to TDL model.**

7.7.4.1 Exemplary filters/antenna patterns

Note that any filter/pattern can be applied on a CDL to derive a TDL for evaluating directional algorithms.

Example 1: Isotropic pattern

$$F_{\{tx,rx\}}(\theta, \phi) = 1 \quad (7.7-2)$$

Example 2: Rectangular mask

$$F_{\{tx,rx\}}(\theta, \phi, BW) = \begin{cases} 1, & |\theta - 90^\circ| \leq \frac{BW}{2} \text{ \& } |\phi| \leq \frac{BW}{2} \\ 0, & \text{otherwise.} \end{cases} \quad (7.7-3)$$

with BW denotes beamwidth.

Example 3: Simplified antenna pattern given in [ITU-R M.2135]



Figure 7.7.4-2 Simplified antenna pattern [ITU-R M.2135].

7.7.4.2 Generation procedure

1. The following steps are needed to generate tapped delay line (TDL) models: Choose a CDL model (e.g. CDL-A). Note that the models may be scaled according to Section 7.7.5.1 prior to the filtering in order to represent different angular spreads.
2. Choose spatial filters F'_{tx} and F'_{rx} defined in LCS
3. Transform the spatial filter into GCS to obtain F_{tx} and F_{rx} such that the pointing direction (θ_p, ϕ_p) is centered within the filter. The pointing direction may be defined
 - a. by the dominant path $(\theta_p, \phi_p) = (\theta_i, \phi_i)$ with , where P_n^{CDL} denotes the CDL cluster power values
 - b. Or an arbitrary direction
4. Calculate TDL cluster power values given the following equation

$$P_n^{TDL} = P_n^{CDL} |F_{rx}(\theta_n, \phi_n) F_{tx}(\theta_n, \phi_n)|^2 \quad (7.7-4)$$

7.7.5 Extension for MIMO simulations

Extended MIMO link-level channel models can be constructed according to two alternative methods described in the following subsections.

7.7.5.1 CDL extension: Scaling of angles

The angle values of CDL models are fixed, which is not very suitable for MIMO simulations for several reasons; The PMI statistics can become biased, and a fixed precoder may perform better than open-loop and on par with closed-loop or reciprocity beamforming. Furthermore, a CDL only represents a single channel realization. The predefined angle values in the CDL models can be generalized by introducing angular translation and scaling. By translation, mean angle can be changed to $\mu_{\phi, \text{desired}}$ and angular spread can be changed by scaling. The translated and scaled ray angles can be obtained according to the following equation:

$$\phi_{n, \text{scaled}} = \frac{AS_{\text{desired}}}{AS_{\text{model}}} (\phi_{n, \text{model}} - \mu_{\phi, \text{model}}) + \mu_{\phi, \text{desired}} \quad (7.7-5)$$

in which:

$\phi_{n, \text{model}}$ is the tabulated CDL ray angle

AS_{model} is the rms angular spread of the tabulated CDL including the offset ray angles, calculated using the angular spread definition in Annex A

$\mu_{\phi,\text{model}}$ is the mean angle of the tabulated CDL

$\mu_{\phi,\text{desired}}$ is the desired mean angle

AS_{desired} is the desired rms angular spread

$\phi_{n,\text{scaled}}$ is the resulting scaled ray angle.

The angular scaling is applied on the ray angles including offsets from the tabulated cluster angles. Typical angular spreads for different scenarios can be obtained from the system-level model.

Example scaling values are:

- AoD spread (ASD) for each CDL model: {5, 10, 15, 25} degrees.
- AoA spread (ASA) for each CDL model: {30, 45, 60} degrees.
- ZoA spread (ZSA) for each CDL model: {5, 10, 15} degrees.
- ZoD spread (ZSD) for each CDL model: {1, 3, 5} degrees.

The angular scaling and translation can be applied to some or all of the azimuth and zenith angles of departure and arrival.

Note: The azimuth angles may need to be wrapped around to be within [0, 360] degrees, while the zenith angles may need to be clipped to be within [0, 180] degrees.

7.7.5.2 TDL extension: Applying a correlation matrix

The TDLs and the spatial-filtered TDLs can be used with the correlation matrices for MIMO link-level simulations. Typical correlation parameters can be derived from 1) delay & angular scaled CDLs with antenna array assumptions, 2) system-level model with antenna array assumptions, or 3) by selecting extreme cases, e.g. uncorrelated, highly correlated etc. For example, these following options can be considered:

- 1) Zero correlation (IID channel coefficients) can be used for any number of antenna elements
- 2) The correlation matrix construction method from 3GPP TS36.101/104 [15][16] can be used for linear and planar (single- or dual-polarized) arrays.
 - Other correlation parameters α , β , γ than those specified in 3GPP TS36.101/104 [15][16] and extensions to larger antenna arrays can be considered. For typical scenarios, α and β will be in the range 0-1
 - A representative set of values is {0,0.7,0.9,0.99}

Note: This approach can be applied to TDLs derived from spatially filtered CDLs to emulate hybrid BF system

Note: Other methodologies could also be developed, e.g.

- - extending the 3GPP TS36.101/104 [15][16] procedure to planar arrays or more elements
- - using CDLs in combination with array assumptions to derive per-tap correlation matrices as in [17].
- - using the system-level model in combination with array assumptions to derive per-tap or per-channel correlation matrices

7.7.6 K-factor for LOS channel models

For the LOS channel models of CDL/TDL-D and CDL/TDL-E, the K-factor values may be changed by the user. Mean and standard deviation of K-factor values can be found in Table 7.5-6, although other values may also be used.

If the K-factor of a model shall be changed to K_{desired} [dB], the cluster powers for the Laplacian clusters (in case of CDL) or the tap powers for the Rayleigh fading taps (in case of TDL) are determined by

$$P_{n,scaled} = P_{n,model} - K_{desired} + K_{model}, \quad (7.7.6-1)$$

where $P_{n,scaled}$ and $P_{n,model}$ denote the scaled and the model path power (as given in the tables) of tap/cluster n . The model's K-factor K_{model} is defined as

$$K_{model} = P_{1,model}^{LOS} - 10 \log_{10} \left[\sum_{n=1}^N 10^{P_{n,model}/10} \right]. \quad (7.7.6-2)$$

After scaling the powers, the delay spread needs to be re-normalized. This is done through the two steps below.

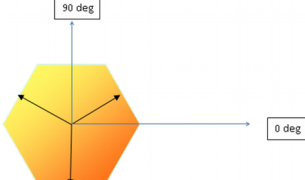
- 1) Calculate the actual RMS delay spread after the K-factor adjustment.
- 2) Divide the delays by that value to obtain DS = 1.

7.8 Channel model calibration

7.8.1 Large scale calibration

For large scale calibration, fast fading is not modeled. The calibration parameters can be found in Table 7.8-1. The calibration results can be found in R1-165974.

Table 7.8-1: Simulation assumptions for large scale calibration

Parameter	Values
Scenarios	Uma, Umi-Street Canyon, Indoor-office
Sectorization	3 sectors per cell site: 30, 150 and 270 degrees 
BS antenna configurations	Mg = Ng = 1; (M,N,P) = (10,1,1), dV = 0.5lambda
BS port mapping	The 10 elements are mapped to a single CRS port
BS antenna electrical downtilting	102 degrees for Uma and Umi Street Canyon 110 degrees for indoor
Antenna virtualization	DFT precoding according to TR 36.897 with application of panning and tilting angles
BS Tx power	44 dBm for Umi-Street Canyon, 49 for Uma at 6GHz 35 dBm at 30GHz and 70 GHz for Uma and Umi-Street canyon 24 dBm for Indoor for all carrier frequencies
Bandwidth	20MHz for 6GHz, and 100MHz for 30Ghz and 70 GHz
UT antenna configurations	1 element (vertically polarized), Isotropic antenna gain pattern
Handover margin (for calibration)	0dB
UT distribution	Following TR36.873 for Uma and Umi, (3D dropping) uniform dropping for indoor with minimum distance (2D) of 0 m
UT attachment	Based on pathloss considering LOS angle
UT noise figure	9 dB
Fast fading channel	Fast fading channel is not modelled
O2I penetration loss	50% low loss and 50% high loss
Carrier Frequency	6 GHz, 30 GHz, 70GHz
Wrapping method for Uma and Umi	geographical distance based wrapping (mandatory) radio distance (optional)
Metrics	1) Coupling loss – serving cell (based on LOS pathloss) 2) Geometry (based on LOS pathloss) with and without white noise

7.8.2 Full calibration

The calibration parameters for full calibration including the fast fading modeling can be found in Table 7.8-2.

Unspecified parameters in Table 7.8-2 are the same as those in Table 7.8-1. When P=2, X-pol (+/-45 degree) is used for BS antenna configuration 1 and X-pol (0/+90 degree) is used for UT antenna configuration. The calibration results can be found in R1-165975.

Table 7.8-2: Simulation assumptions for full calibration

Parameter	Values
Scenarios	3D-Uma, 3D-Umi-street Canyon, Indoor-office
Carrier Frequency	6 GHz, 30 GHz, 60GHz, 70GHz
Bandwidth	20MHz for 6GHz, and 100MHz for 30GHz, 60 GHz and 70 GHz
BS Tx power	44 dBm for Umi-Street Canyon, 49 for Uma at 6GHz 35 dBm at 30GHz, 60 GHz and 70 GHz for Uma and Umi-Street canyon 24 dBm for Indoor for all carrier frequencies
BS antenna configurations	Config 1: M=4,N=4,P=2, Mg=1, Ng =2, dH = dV = 0.5lambda, d _{H,g} =d _{V,g} =2.5lambda ... calibration metrics 1), 2), 3) are calibrated Config 2: Mg=Ng=1, M=N=2, P = 1 ... calibration metrics 1), 2), 4) are calibrated
BS port mapping	Config 1: all 16 elements for each polarization on each panel are mapped to a single CRS port; panning angles of the two subarrays: (0,0) degs; same downtilt angles as used for the large-scale calibrations Config 2: each antenna element is mapped to one CRS port
UT antenna configurations	Mg=Ng=1, M=N=1, P=2
UT distribution	Following TR36.873 for Uma and Umi, (3D dropping) uniform dropping for indoor with minimum distance (2D) of 0 m
UT attachment	Based on RSRP (formula) from CRS port 0
Polarized antenna modelling	Model-2 in TR36.873
UT array orientation	$\Omega_{UT,\alpha}$ uniformly distributed on [0,360] degree, $\Omega_{UT,\beta} = 90$ degree, $\Omega_{UT,\gamma} = 0$ degree
UT antenna pattern	Isotropic
Metrics	1) Coupling loss – serving cell
	2) Wideband SIR before receiver without noise
	3) CDF of Delay Spread and Angle Spread (ASD, ZSD, ASA, ZSA) from the serving cell (according to circular angle spread definition of TR 25.996)
	4) CDF of largest (1 st) PRB singular values (serving cell) at t=0 plotted in 10*log10 scale. CDF of smallest (2 nd) PRB singular values (serving cell) at t=0 plotted in 10*log10 scale. CDF of the ratio between the largest PRB singular value and the smallest PRB singular value (serving cell) at t=0 plotted in 10*log10 scale. Note: The PRB singular values of a PRB are the eigenvalues of the mean covariance matrix in the PRB.

7.8.3 Calibration of additional features

The calibration parameters for the calibration of oxygen absorption, large bandwidth and large antenna array, spatial consistency, and blockage can be respectively found in Table 7.8-3, 7.8-4, 7.8-5, and 7.8-6. Unspecified parameters in these tables are the same as those in Tables 7.8-1 and 7.8-2. When P=2, X-pol (+/-45 degree) is used for BS antenna configuration 1 and X-pol (0/+90 degree) is used for UT antenna configuration. The calibration results can be found in R1-1700990.

Table 7.8-3: Simulation assumptions for calibration for oxygen absorption

Parameter	Values
Scenarios	3D-Umi-street Canyon
Carrier Frequency	60 GHz
BS antenna configurations	$M=4, N=4, P=2, M_g=1, N_g=2, d_H = d_V = 0.5\lambda, d_{H,g}=d_{V,g}=2.5\lambda$
BS port mapping	all 16 elements for each polarization on each panel are mapped to a single CRS port; panning angles of the two subarrays: (0,0) degs; same downtilt angles as used for the large-scale calibrations
Calibration method	Drop multiple users in the multiple cells randomly, and collect the following metrics for each user after attachment.
Metrics	1) CDF of coupling loss (serving cell) 2) Wideband SINR before receiver – determined from RSRP (formula) from CRS port 0 3) CDF of Delay Spread from the serving cell

Table 7.8-4: Simulation assumptions for calibration for large bandwidth and large antenna array

Parameter	Values
Scenarios	3D-Umi-street Canyon
Carrier Frequency	30GHz
Bandwidth	2GHz
BS antenna configurations	$M=8, N=8, P=2, M_g=1, N_g=4, d_H = d_V = 0.5\lambda, d_{H,g}=d_{V,g}=4\lambda$
BS port mapping	all 64 elements for each polarization on each panel are mapped to a single CRS port; panning angles of the two subarrays: (0,0) degs; same downtilt angles as used for the large-scale calibrations
The number of rays per cluster	$N_{MPC} = 40$
Calibration method	Drop multiple users in the multiple cells randomly, and collect the following metrics for each user after attachment.
Metrics	1) CDF of coupling loss (serving cell) 2) Wideband SINR before receiver – determined from RSRP (formula) from CRS port 0 3) CDF of largest (1^{st}) PRB singular values (serving cell) at $t=0$ plotted in $10 \cdot \log_{10}$ scale

Table 7.8-5: Simulation assumptions for calibration for spatial consistency

Parameter	Values
Scenarios	3D-Umi-street Canyon
Carrier Frequency	30 GHz
BS antenna configurations	M=4,N=4,P=2, Mg=1, Ng =2, $d_H = d_V = 0.5\lambda$, $d_{H,g}=d_{V,g}=2.5\lambda$
BS port mapping	all 16 elements for each polarization on each panel are mapped to a single CRS port; panning angles of the two subarrays: (0,0) degs; same downtilt angles as used for the large-scale calibrations
UE distribution	Following TR36.873, 3D dropping uniform dropping for indoor with minimum distance of 0 m For Config1: 100% UE indoor and in the 1 st floor For Config2: 100% UE outdoor
Mobility	Config1: UE is stationary Config2: UE is moving with random direction and fixed speed, e.g., 30 km/h
Calibration method	For Config1: Drop multiple UEs in a single cell, determine all permutations of pairs of UEs, collect the variables for each pair and bin them into certain distance ranges, e.g., 1m/2m/10m, to get enough samples. Collect the following metrics 1) –6). For Config2: Drop multiple users in the single cell, and collect metric 1)-2) and 7)-9) for each user after attachment.
Metrics	1) CDF of coupling loss (serving cell) 2) Wideband SINR before receiver – determined from RSRP (formula) from CRS port 0 3) Cross-correlation coefficient of delay for the third cluster between paired UEs, see note 1 4) Cross-correlation coefficient of AoA for the third cluster between paired UEs 5) Cross-correlation coefficient of LoS/NLoS status between paired UEs 6) Cross correlation coefficient of the channel response in Step 11 on the first non-DC subcarrier in an OFDM symbol on antenna port 0 received on the first UE antenna over multiple realizations between paired UEs 7) CDF of average varying rate of power for the third cluster, see note 2 8) CDF of average varying rate of delay for the third cluster (ns) 9) CDF of average varying rate of AoA for the third cluster (degree)
NOTE 1	For the UT pair at a certain distance range, the variables collected by two UEs can be denoted as X and Y, respectively, then the cross-correlation coefficient for real number can be written as $\frac{[E(XY)-E(X)E(Y)]}{\sqrt{[E(X^2)-E(X)^2]}\sqrt{[E(Y^2)-E(Y)^2]}}$, the cross-correlation coefficient for complex number can be written as $\frac{ [E(XY^*)-E(X)E(Y)^*] }{\sqrt{[E(XX^*)-E(X)E(X)^*]}\sqrt{[E(YY^*)-E(Y)E(Y)^*]}}$.
NOTE 2	For the average varying rate, we assume the collecting interval, e.g., 100ms, and then get the samples for a certain UE, the varying rate can be written as the standard variance of the samples per 100ms.

Table 7.8-6: Simulation assumptions for calibration for blockage

Parameter	Values
Scenarios	Umi-street Canyon
Carrier Frequency	30 GHz
BS antenna configurations	$M=4, N=4, P=2, M_g=1, N_g=2, d_H = d_V = 0.5\lambda, d_{H,g}=d_{V,g}=2.5\lambda$
BS port mapping	all 16 elements for each polarization on each panel are mapped to a single CRS port; panning angles of the two subarrays: (0,0) degs; same downtilt angles as used for the large-scale calibrations
Calibration method	<p>For Model A: Drop multiple users in the multiple cells, and collect the following metrics 1) – 3) for each user after attachment. Optional self-blocking feature is made mandatory in the Landscape mode only for calibration purposes.</p> <p>For Model B: Drop a BS in (0,0,30) and a UT in (100,0,1.5), Jump directly to step 11 and replace the channel with CDL-E. Drop a blocking screen of size $h=10\text{m}$, $w = 2\text{m}$ in (80,10,1.5) Move the UT from (100,0,1.5) to (100,20,1.5) in small increments. For each UT position, translate all the AoDs and AoAs of CDL-E such that the specular (LOS path) of CDL-E is pointing along the direct path between the BS and UT. Collect metric 4)</p>
Metrics	<ol style="list-style-type: none"> 1) CDF of coupling loss (serving cell) 2) Wideband SINR before receiver – determined from RSRP (formula) from CRS port 0 3) CDF of ASA from the serving cell 4) RSRP as a function of UT position

8 Map-based hybrid channel model (Alternative channel model methodology)

Map-based hybrid model is composed of a deterministic component following, e.g., METIS work [6] and a stochastic component following mainly the model described in section 7. The channel model methodology described in this section is an alternative to the methodology specified in section 7, and can be used if:

- The system performance is desired to be evaluated or predicted with the use of digital map to take into account the impacts from environmental structures and materials.

The map-based hybrid model defined in this section is not calibrated and can be used per company basis.

8.1 Coordinate system

The same coordinate system as defined in section 7.1 is applied.

8.2 Scenarios

The same scenarios as in section 7.2 can be applied.

8.3 Antenna modelling

The same antenna modelling as defined in section 7.3 can be applied.

8.4 Channel generation

The radio channels are created using the deterministic ray-tracing upon a digitized map and emulating certain stochastic components according to the statistic parameters listed in Table 7.5-6 to Table 7.5-10 [Note: Not all parameters listed in these tables are used in hybrid model]. The channel realizations are obtained by a step-wise procedure illustrated in

Figure 8.4-1 and described below. In the following steps, downlink is assumed. For uplink, arrival and departure parameters have to be swapped.

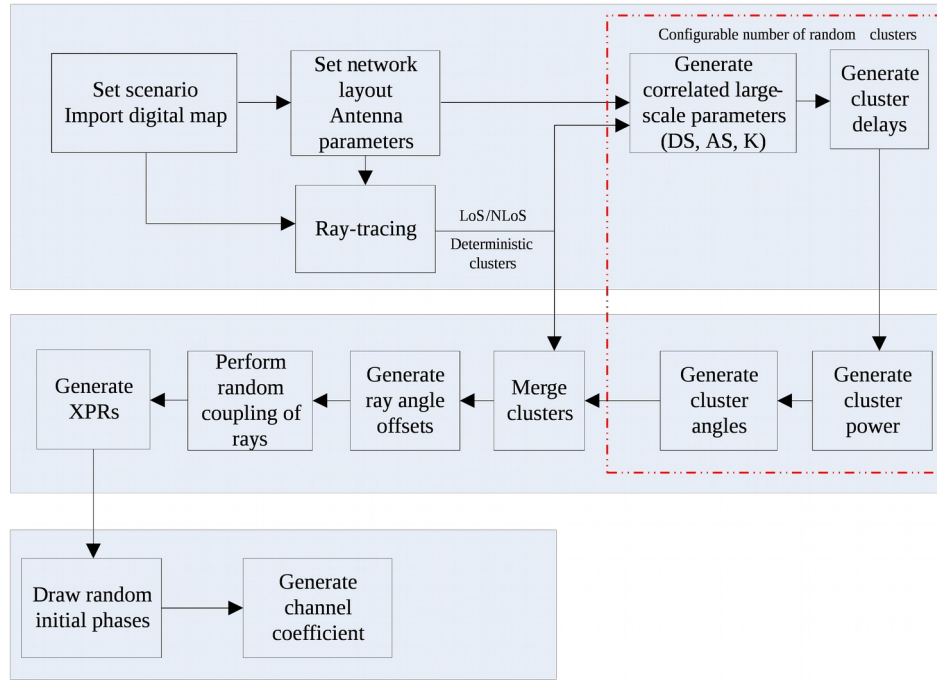


Figure 8.4-1: Channel coefficient generation procedure

Step-wise procedure:

Step 1: Set environment and import digitized map accordingly

- a) Choose scenario. Choose a global coordinate system and define zenith angle θ , azimuth angle ϕ , and spherical basis vectors $\hat{\theta}$, $\hat{\phi}$ as shown in Figure 7.5-2.
- b) Import digitized map according to the chosen scenario. The digitized map should at least contain the following information:
 - The 3D geometric information for each of major structures involving with buildings or rooms. The external building walls and internal room walls are represented by surfaces and identified by the coordinates of the vertices on each wall.
 - The material and thickness of each wall as well as the corresponding electromagnetic properties including permittivity and conductivity.
 - Random small objects in certain scenarios (e.g, Umi outdoor)

The format of digitized map, including additional information besides above-mentioned, is per implementation wise and out of scope of this description.

Step 2: Set network layout, and antenna array parameters

- a) Give number of BS and UT.
- b) Give 3D locations of BS and UT, and calculate LOS AOD ($\phi_{LOS,AOD}$), LOS ZOD ($\theta_{LOS,ZOD}$), LOS AOA ($\phi_{LOS,AOA}$), LOS ZOA ($\theta_{LOS,ZOA}$) of each BS and UT in the global coordinate system
- c) Give BS and UT antenna field patterns F_{rx} and F_{tx} in the global coordinate system and array geometries
- d) Give BS and UT array orientations with respect to the global coordinate system. BS array orientation is defined by three angles $\Omega_{BS,\alpha}$ (BS bearing angle), $\Omega_{BS,\beta}$ (BS downtilt angle) and $\Omega_{BS,\gamma}$ (BS slant angle). UT array orientation is defined by three angles $\Omega_{UT,\alpha}$ (UT bearing angle), $\Omega_{UT,\beta}$ (UT downtilt angle) and $\Omega_{UT,\gamma}$ (UT slant angle)

angle). Give rotational motion of UT in terms of its bearing angle, downtilt angle and slant angle if UT rotation is modelled.

- e) Give speed and direction of motion of UT in the global coordinate system for virtual motion.
- f) Give system centre frequency/frequencies and bandwidth(s) for each of BS-UT links

If the bandwidth (denoted as B) is greater than c/D Hz, where c is the speed of light and D is the maximum antenna aperture in either azimuth or elevation, the whole bandwidth is split into K_B equal-sized frequency

bins, where $K_B \geq \lceil \frac{B}{c/D} \rceil$ is a per-implementation parameter taking into account the channel constancy as well

as other potential evaluation needs, and the bandwidth of each frequency bin is $\Delta B = \frac{B}{K_B}$. Within k -th

frequency bin, the channel power attenuation, phase rotation, Doppler are assumed constant, whose corresponding values are calculated based on the centre frequency of k -th frequency bin

$f_k = f_c - \frac{K_B - 2k + 1}{2} \Delta B$ for $1 \leq k \leq K_B$, where f_c is the centre frequency of the corresponding BS-UT link.

Step 3: Apply ray-tracing to each pair of link ends (i.e., end-to-end propagation between pair of Tx/Rx arrays).

- 2017) Perform geometric calculations in ray-tracing to identify propagation interaction types, including LoS, reflections, diffractions, penetrations and scattering (in case the digitized map contains random small objects), for each propagation path. In general, some maximum orders of different interaction types can be set.

The theoretical principles and procedures of geometric tracing calculations can be found in [6]~[10][12]. This description does not intend to mandate new concepts and/or procedures to the conventional ray-tracing algorithms; on the other hand, the implementation-based variations aiming to reduce computation complexity are allowed within limits of acceptable calibration tolerances.

The same geometric calculation is shared among all K_B frequency bins.

- b) Perform electric field calculations over propagation path, based on identified propagation interaction types (LoS, reflection, diffraction, penetration and scattering) and centre frequencies of frequency bins.

The details of electric field calculation can be found in [6]~[13].

The modelling algorithms in geometry and electric field calculations for different propagation interactions are summarized in the table below.

Table 8.4-1 Principles applied in ray-tracing

	Geometry calculation	Electric field calculation
LoS	Free space LoS	Friis equation [11]
Reflection	Snell's law with image-based method [7]	Fresnel equation [7]
Diffraction	Fermat's principle [12]	UTD [13]
Penetration	Snell's law for transmission through slab [8]	Fresnel equation [7]
Scattering (upon small objects)	Isotropic scattering [6]	RCS-based scattering coefficient [6]

Note: For reasons of simplicity and simulation speed, the maximum order of reflection on a path without diffraction is configurable from {1,2,3}; the maximum order of diffraction on a path without reflection is configurable from {1,2}; the path containing both reflection and diffraction has 1-order reflection and 1-order diffraction, besides any potential penetrations; and the maximum order of penetration on a path is configurable, with the recommended value equal to 5.

The outputs from Step 3 should at least contain following for each pair of link ends:

- the LoS/NloS flag to indicate whether a LoS propagation mechanism exists;
- the number of deterministic propagation paths L_{RT} (also referred as deterministic clusters in Step 8. To avoid the unnecessary computation complexity, these L_{RT} deterministic paths only include those paths whose powers are

higher than 25dB below the maximum deterministic path power, where the path power is denoted as $P_{l_{RT}}^{RT,real}$ and defined below);

- for each deterministic path (l_{RT} -th path sorted in ascending order of path delay):
 - the flag indicating whether the deterministic path is generated with scattering upon random small objects;
 - the normalized path delay $\tau_{l_{RT}}^{RT} = \tau_{l_{RT}} - \min_{l_{RT}}(\tau_{l_{RT}}')$ and the first arrival absolute delay $\min_{l_{RT}}(\tau_{l_{RT}}')$ (with $\tau_{l_{RT}}'$ to be the real absolute propagation delay of the path);
 - angles of arrival and departure [$\phi_{l_{RT},AOA}^{RT}, \theta_{l_{RT},ZOA}^{RT}, \phi_{l_{RT},AOD}^{RT}, \theta_{l_{RT},ZOD}^{RT}$];
 - the power $P_{l_{RT},k}^{RT,real}$ for k-th frequency bin, and the path power $P_{l_{RT}}^{RT,real} = \frac{1}{K_B} \sum_{k=1}^{K_B} P_{l_{RT},k}^{RT,real}$
 - the XPR $\kappa_{l_{RT}}^{RT}$ of the path, where $\kappa_{l_{RT}}^{RT} = \frac{1}{K_B} \sum_{k=1}^{K_B} \kappa_{l_{RT},k}^{RT}$ with $\kappa_{l_{RT},k}^{RT}$ being the XPR for k-th frequency bin.
 - to support for true motion, i.e. the case when a trajectory is specified for UT, a path ID is associated for each deterministic path. The same ID is associated for a path across a number of UT locations as far as 1) it has same interaction types in the same order and 2) its interactions occur in same walls or other surfaces.

The L_{RT} deterministic paths are sorted by normalized path delay ($\tau_{l_{RT}}^{RT}$) in ascending order. That is to say, $\tau_1^{RT} = 0$.

If $L_{RT}=0$ for a pair of link ends, the channel gain for this pair of link ends is assumed to be zero and the remaining steps are skipped with none of random cluster.

Step 4: Generate large scale parameters e.g. delay spread, angular spreads and Ricean K factor for random clusters.

The generation of large scale parameters takes into account cross correlation according to Table 7.5-6 and uses the procedure described in section 3.3.1 of [14] with the square root matrix $\sqrt{C_{M \times M}}(\mathbf{O})$ being generated using the Cholesky decomposition and the following order of the large scale parameter vector: $\mathbf{s}_M = [s_K, s_{DS}, s_{ASD}, s_{ASA}, s_{ZSD}, s_{ZSA}]^T$. Limit random RMS azimuth arrival and azimuth departure spread values to 104 degrees, i.e., $ASA = \min(ASA, 104^\circ)$, $ASD = \min(ASD, 104^\circ)$. Limit random RMS zenith arrival and zenith departure spread values to 52 degrees, i.e., $ZSA = \min(ZSA, 52^\circ)$, $ZSD = \min(ZSD, 52^\circ)$. For the parameter selection from Table 7.5-6, the LoS/NloS condition determined in Step 3 is applied. For the parameter selection from Table 7.5-6, the LoS/NloS condition determined in Step 3 is applied.

Step 5: Generate delays (denoted as $\{\tau^{RC}\}$) for random clusters.

Delays are drawn randomly according to the exponential delay distribution

$$\tau_n' = -\mu_\tau^{RC} \ln(X_n) \quad (8.4-1)$$

where $\mu_\tau^{RC} = \max\{\mu_\tau, \frac{1}{L_{RT}} \sum_{l_{RT}=1}^{L_{RT}} \tau_{l_{RT}}^{RT}\}$, $X_n \sim \text{uniform}(0,1)$, and cluster index $n = 0, \dots, L_{RC}'$ with L_{RC}' to be configurable. A recommended value for L_{RC}' is the number of clusters given in Table 7.5-6.

$\mu_\tau = r_\tau DS + \frac{L_{RT}}{L_{RC}' + 1} \left[r_\tau DS - \frac{1}{L_{RT}} \sum_{l_{RT}=1}^{L_{RT}} \tau_{l_{RT}}^{RT} \right]$, where r_τ is the delay distribution proportionality factor given in Table 7.5-6.

Normalise the delays by subtracting the minimum delay and sort the normalised delays to ascending order:

$$\tau_n = \text{sort}(\tau_n' - \min(\tau_n')) / C_\tau \quad (8.4-2)$$

where C_τ is the additional scaling of delays to compensate for the effect of LOS peak addition to the delay spread, and is depending on the heuristically determined Ricean K-factor [dB] as generated in Step 4:

$$C_\tau = \begin{cases} 0.7705 - 0.0433K + 0.0002K^2 + 0.000017K^3 & \text{LoS condition} \\ 1 & \text{NLoS condition} \end{cases} \quad (8.4-3)$$

For the delay used in cluster power generation in Step 6, the scaling factor C_τ is always 1.

The n -th random cluster is removed if $n=0$ or $|\tau_n - \tau_{l_{RT}}^{RT}| < \tau_{th}$ for any of $1 \leq l_{RT} \leq L_{RT}$, where τ_{th} is given by

$$\tau_{th} = \mu_\tau^{RC} \cdot \ln \left(\frac{1}{1 - p_0} \right), \text{ and } p_0 \text{ is the configurable probability for cluster inter-arrival interval to be}$$

less than τ_{th} . For example, set $p_0 = 0.2$ to obtain $\tau_{th} = 0.223 \mu_\tau^{RC}$.

Denote τ_n^{RC} for $1 \leq n \leq L_{RC}$ as the delays of the L_{RC} random clusters that remain after the cluster removal.

Step 6: Generate powers (denoted as $P_i^{RC,real}$ for $1 \leq i \leq L_{RC}$) for random clusters.

Cluster powers for the random clusters are calculated assuming a single slope exponential power delay profile. First, the virtual powers (denoted as $P_i^{RC,virtual}$ for $1 \leq i \leq L_{RC}$) of random clusters and virtual powers (denoted as $P_j^{RT,virtual}$ for $1 \leq j \leq L_{RT}$) of deterministic clusters are calculated as following.

Denote:

$$V_i^{RC} = \exp \left(-\tau_i^{RC} \frac{r_\tau - 1}{r_\tau DS} \right) \cdot 10^{\frac{-Z_{i,RC}}{10}} \quad (8.4-4)$$

$$V_j^{RT} = \exp \left(-\tau_j^{RT} \frac{r_\tau - 1}{r_\tau DS} \right) \cdot 10^{\frac{-Z_{j,RT}}{10}} \quad (8.4-5)$$

where $Z_{i,RC}$ and $Z_{j,RT}$ are the per cluster shadowing terms in [dB] and meet distribution of $N(0, \zeta^2)$. Then,

$$P_i^{RC,virtual} = \frac{1}{A+1} \frac{V_i^{RC}}{\sum_{i=1}^{L_{RC}} V_i^{RC} + \sum_{j=1}^{L_{RT}} V_j^{RT}} \quad (8.4-6)$$

$$P_j^{RT,virtual} = \frac{1}{A+1} \frac{V_j^{RT}}{\sum_{i=1}^{L_{RC}} V_i^{RC} + \sum_{j=1}^{L_{RT}} V_j^{RT}} + \frac{A}{A+1} \cdot \delta(j-1) \quad (8.4-7)$$

In the case of LoS condition, $A = K_R$ with K_R being the Ricean K-factor obtained in Step 4 and converted to linear scale; otherwise, $A = 0$. The real power (including effects of pathloss) per random cluster in k -th frequency bin is given by

$$P_{i,k}^{RC,real} = \frac{\sum_{j=1}^{L_{RT}} P_{j,k}^{RT,real}}{\sum_{j=1}^{L_{RT}} P_j^{RT,virtual}} \cdot P_i^{RC,virtual} \quad (8.4-8)$$

for $1 \leq i \leq L_{RC}$ and $1 \leq k \leq K_B$. Similar to path power of deterministic cluster, the path power of i -th random cluster is calculated as

$$P_i^{RC,real} = \frac{1}{K_B} \sum_{k=1}^{K_B} P_{i,k}^{RC,real} \quad (8.4-9)$$

Step 7: Generate arrival angles and departure angles for both azimuth and elevation, for each random cluster.

For azimuth angles of the n -th random cluster:

The composite PAS in azimuth of all random clusters is modelled as wrapped Gaussian (see Table 7.5-6). The AOA's are determined by applying the inverse Gaussian function with input parameters $P_n^{RC,real}$ and RMS angle spread ASA

$$\phi'_{n,AOA} = \frac{2(ASA/1.4) \sqrt{-\ln \left(P_n^{RC,real} / \max_{i,j} (P_i^{RC,real}, P_j^{RT,real}) \right)}}{C_\phi} \quad (8.4-10)$$

with constant C_ϕ defined as

$$C_\phi = \begin{cases} C_\phi^{NLOS} \cdot (1.1035 - 0.028K - 0.002K^2 + 0.0001K^3) & , \text{for LOS} \\ C_\phi^{NLOS} & , \text{for NLOS} \end{cases} \quad (8.4-11)$$

where C_ϕ^{NLOS} is defined as a scaling factor related to the total number of clusters and is given in Table 7.5-2.

In the LOS case, constant C_ϕ also depends on the Ricean K-factor K in [dB], as generated in Step 4.

Additional scaling of the angles is required to compensate for the effect of LOS peak addition to the angle spread.

Assign positive or negative sign to the angles by multiplying with a random variable X_n with uniform distribution to the discrete set of $\{1, -1\}$, and add component $Y_n \sim N(0, (ASA/7)^2)$ to introduce random variation

$$\phi_{n,AOA} = X_n \phi'_{n,AOA} + Y_n + \phi_{center,AOA} \quad (8.4-12)$$

where $\phi_{center,AOA}$ is calculated as

$$\phi_{center,AOA} = \arg \left(\sum_{l=1}^{L_{RT}} P_l^{RT,real} \cdot \exp(j\phi_{l,AOA}^{RT}) \right) \quad (8.4-13)$$

Note that $\phi_{l,AOA}^{RT}$ shall be given in radians here.

The generation of AOD ($\phi_{n,AOD}$) follows a procedure similar to AOA as described above.

For zenith angles of the n -th random cluster:

The generation of ZOA assumes that the composite PAS in the zenith dimension of all random clusters is Laplacian (see Table 7.5-6). The ZOAs are determined by applying the inverse Laplacian function with input parameters $P_n^{RC,real}$ and RMS angle spread ZSA

$$\theta'_{n,ZOA} = - \frac{ZSA \ln \left[P_n^{RC,real} / \max_{i,j} (P_i^{RC,real}, P_j^{RT,real}) \right]}{C_\theta} \quad (8.4-14)$$

with C_θ defined as

$$C_\theta = \begin{cases} C_\theta^{NLOS} \cdot (1.3086 + 0.0339K - 0.0077K^2 + 0.0002K^3) & , \text{ for LOS} \\ C_\theta^{NLOS} & , \text{ for NLOS} \end{cases} \quad (8.4-15)$$

where C_θ^{NLOS} is a scaling factor related to the total number of clusters and is given in Table 7.5-4.

In the LOS case, constant C_θ also depends on the Ricean K-factor K in [dB], as generated in Step 4. Additional scaling of the angles is required to compensate for the effect of LOS peak addition to the angle spread.

Assign positive or negative sign to the angles by multiplying with a random variable X_n with uniform distribution to the discrete set of $\{1, -1\}$, and add component $Y_n \sim N(0, (ZSA/7)^2)$ to introduce random variation

$$\theta_{n,ZOA} = X_n \theta'_{n,ZOA} + Y_n + \bar{\theta}_{ZOA} \quad (8.4-16)$$

where $\bar{\theta}_{ZOA} = 90^\circ$ if the UT is located indoors and $\bar{\theta}_{ZOA} = \theta_{center,ZOA}$ if the UT is located outdoors, where $\theta_{center,ZOA}$ is calculated as

$$\theta_{center,ZOA} = \arg \left[\sum_{l=1}^{L_{RT}} P_l^{RT,real} \cdot \exp(j\theta_{l,ZOA}^{RT}) \right] \quad (8.4-17)$$

Note that $\theta_{l,ZOA}^{RT}$ shall be given in radians here.

The generation of ZOD follows the same procedure as ZOA described above except equation (8.4-16) is replaced by

$$\theta_{n,ZOD} = X_n \theta'_{n,ZOD} + Y_n + \theta_{center,ZOD} + \mu_{offset,ZOD} \quad (8.4-18)$$

where variable X_n is with uniform distribution to the discrete set of $\{1, -1\}$, $Y_n \sim N(0, (ZSD/7)^2)$, $\mu_{offset,ZOD}$ is given in Table 7.5-7 to Table 7.5-10.

Step 8: Merge deterministic clusters and random clusters.

First, remove any deterministic or random cluster with less than -25 dB power compared to $\max\{P_j^{RT,real}, P_i^{RC,real}\}$ for all $1 \leq j \leq L_{RT}$ and $1 \leq i \leq L_{RC}$. Then, simply put the remaining deterministic clusters and random clusters into single set of clusters, and meanwhile maintain an attribute for each cluster to indicate whether the cluster is a deterministic cluster or a random cluster.

Step 9: Generate ray delays and ray angle offsets inside each cluster, where the cluster can be either random or deterministic.

Denote M as the number of rays per cluster, where $M=1$ if the cluster corresponds to $n=1$ in the LOS case, otherwise the value of M is given in Table 7.5-6.

When $K_B = 1$:

The relative delay of m -th ray within n -th cluster is given by $\tau'_{n,m} = 0$ for $m = 1, \dots, M$.

The azimuth angle of arrival (AoA) for the m -th ray in n -th cluster is given by

$$\phi_{n,m,AOA} = \phi_{n,AOA} + c_{ASA} \alpha_m \quad (8.4-19)$$

where c_{ASA} is the cluster-wise rms azimuth spread of arrival angles (cluster ASA) in Table 7.5-6, and offset angle α_m is given in Table 7.5-3. $\phi_{n,AOA}$ equals to the AOA angle output from Step 3 if n -th cluster is deterministic cluster, and equals to the AOA angle (8.4-12) in Step 7 if n -th cluster is random cluster.

The generation of AOD ($\phi_{n,m,AOD}$) follows a procedure similar to AOA as described above.

The zenith angle of arrival (ZoA) for the m -th ray in n -th cluster is given by

$$\theta_{n,m,ZOA} = \theta_{n,ZOA} + c_{ZSA} \alpha_m \quad (8.4-20)$$

where c_{ZSA} is the cluster-wise rms spread of ZOA (cluster ZOA) in Table 7.5-6, and offset angle α_m is given in Table 7.5-3. Assuming that $\theta_{n,m,ZOA}$ is wrapped within $[0, 360^\circ]$, if $\theta_{n,m,ZOA} \in [180^\circ, 360^\circ]$, then $\theta_{n,m,ZOA}$ is set to $(360^\circ - \theta_{n,m,ZOA})$. $\theta_{n,ZOA}$ equals to the ZOA angle output from Step 3 if n -th cluster is deterministic cluster, and equals to the ZOA angle (8.4-16) in Step 7 if n -th cluster is random cluster.

The zenith angle of departure (ZoD) for the m -th ray in n -th cluster is given by

$$\theta_{n,m,ZOD} = \theta_{n,ZOD} + (3/8)(10^{\mu_{lgZSD}}) \alpha_m \quad (8.4-21)$$

where μ_{lgZSD} is the mean of the ZSD log-normal distribution. $\theta_{n,ZOD}$ equals to the ZOD angle output from Step 3 if n -th cluster is deterministic cluster, and equals to the ZOD angle (8.4-18) in Step 7 if n -th cluster is random cluster.

When $K_B > 1$:

The relative delay of m -th ray within n -th cluster is given by $\tau_{n,m}^{\square} = \text{sort}(\tau_{n,m}^{\square} - \min_{1 \leq m \leq M} \tau_{n,m}^{\square})$ that are sorted in ascending order, where $\tau_{n,m}^{\square} \sim \text{unif}(0, 2c_{DS})$, with the cluster delay spread as given in Table 7.5-6. $\text{unif}(a, b)$ denotes the continuous uniform distribution on the interval $[a, b]$. Note that $\tau_{n,m}^{\square}$ shall be the independently generated.

The azimuth angles (AOA and AOD) and zenith angles (ZOA and ZOD) for the m -th ray in n -th cluster in each frequency bin is given by

$$\begin{aligned} \phi_{n,m,AOA} &= \phi_{n,AOA} + \phi_{n,m,AOA}^{\square} \\ \phi_{n,m,AOD} &= \phi_{n,AOD} + \phi_{n,m,AOD}^{\square} \\ \theta_{n,m,ZOA} &= \theta_{n,ZOA} + \theta_{n,m,ZOA}^{\square} \\ \theta_{n,m,ZOD} &= \theta_{n,ZOD} + \theta_{n,m,ZOD}^{\square} \end{aligned} \quad (8.4-22)$$

for $m = 1, \dots, M$, where $\phi_{n,\{AOA|AOD\}}$ and $\theta_{n,\{ZOA|ZOD\}}$ equal to the $\{AOA, AOD\}$ and $\{ZOA, ZOD\}$ angle outputs from Step 3 if n -th cluster is deterministic cluster, and equal to the $\{AOA, AOD\}$ and $\{ZOA, ZOD\}$ angle in Step 7 if n -th cluster is random cluster; and

$$\begin{aligned}
\phi_{n,m,AOA}^{\square} &\sim 2c_{ASA} \text{unif}(-1,1) \\
\phi_{n,m,AOD}^{\square} &\sim 2c_{ASD} \text{unif}(-1,1) \\
\theta_{n,m,ZOA}^{\square} &\sim 2c_{ZSA} \text{unif}(-1,1) \\
\theta_{n,m,ZOD}' &\sim 2c_{ZSD} \text{unif}(-1,1)
\end{aligned} \tag{8.4-23}$$

with the respective cluster angular spreads as given in Tables 7.5-6 ~ 7.5-10.

Assuming that $\theta_{n,m,ZOA}$ is wrapped within $[0,360^\circ]$, if $\theta_{n,m,ZOA} \in [180^\circ, 360^\circ]$, then $\theta_{n,m,ZOA}$ is set to $(360^\circ - \theta_{n,m,ZOA})$.

Step 10: Generate power of rays in each cluster, where coupling of rays within a cluster for both azimuth and elevation could be needed.

Given $P_{n,k}$ as the real power in k -th frequency bin for the n -th cluster (either deterministic or random) obtained from Step 8,

When $K_B = 1$:

Couple randomly AOD angles $\phi_{n,m,AOD}$ to AOA angles $\phi_{n,m,AOA}$ within a cluster n . Couple randomly ZOD angles $\theta_{n,m,ZOD}$ with ZOA angles $\theta_{n,m,ZOA}$ using the same procedure. Couple randomly AOD angles $\phi_{n,m,AOD}$ with ZOD angles $\theta_{n,m,ZOD}$ within a cluster n .

The power of m -th ray in n -th cluster and in k -th frequency bin is given by $P_{n,m,k} = P_{n,k} / M$ for $m = 1, \dots, M$.

When $K_B > 1$:

The power of m -th ray in n -th cluster and in k -th frequency bin is given by $P_{n,m,k} = P_{n,k} \cdot \frac{P_{n,m}^{\square}}{\sum_{m=1}^M P_{n,m}^{'}}$ for

$m = 1, \dots, M$, where

$$\begin{aligned}
P_{n,m}^{\square} = & \exp\left[-\frac{\tau_{n,m}^{\square}}{c_{DS}}\right] \exp\left[-\frac{\sqrt{2}|\phi_{n,m,AOA}^{\square}|}{c_{ASA}}\right] \exp\left[-\frac{\sqrt{2}|\phi_{n,m,AOD}^{\square}|}{c_{ASD}}\right] \\
& \cdot \exp\left[-\frac{\sqrt{2}|\theta_{n,m,ZOA}^{\square}|}{c_{ZSA}}\right] \exp\left[-\frac{\sqrt{2}|\theta_{n,m,ZOD}'|}{c_{ZSD}}\right]
\end{aligned} \tag{8.4-24}$$

and c_{DS} , c_{ASA} , c_{ASD} , and c_{ZSA} are respectively the intra-cluster delay spread and the corresponding intra-cluster angular spreads that are given in Table 7.5-6. The cluster zenith spread of departure is given by

$$c_{ZSD} = \frac{3}{8} 10^{\mu_{lgZSD}}, \tag{8.4-25}$$

with μ_{lgZSD} being defined in Tables 7.5-7, 7.5-8, 7.5-9, and 7.5-10.

Step 11: Generate XPRs

Generate the cross polarization power ratios (XPR) κ for each ray m of each cluster n . XPR is log-Normal distributed. Draw XPR values as

$$\kappa_{n,m} = 10^{X/10} \tag{8.4-26}$$

where $X \sim N(\mu, \sigma_{\text{XPR}}^2)$ is Gaussian distributed with σ_{XPR} given from Table 7.5-6. If n -th cluster is a deterministic cluster, $\mu = 10 \log_{10} \kappa_{l_{\text{RT}}}^{RT}$; otherwise, $\mu = \mu_{\text{XPR}}$ is given in Table 7.5-6.

Step 12: Draw initial random phases

Draw random initial phase $\{\Phi_{n,m}^{\theta\theta}, \Phi_{n,m}^{\theta\phi}, \Phi_{n,m}^{\phi\theta}, \Phi_{n,m}^{\phi\phi}\}$ for each ray m of each cluster n and for four different polarisation combinations $(\theta\theta, \theta\phi, \phi\theta, \phi\phi)$. The distribution for initial phases is uniform within $(-\pi, \pi)$.

In the LOS case, calculate an initial phase $\Phi_{\text{LOS}} = -2\pi d_{3D}/\lambda_0$ for both $\theta\theta$ and $\phi\phi$ polarisations, where d_{3D} is the 3D distance between transmitter and receiver and $\lambda_0 = c/f_c$ is the wavelength of the modelled propagation link.

Step 13: Generate channel coefficients for each cluster n and each receiver and transmitter element pair u, s .

In case of NLoS, the channel coefficients of ray m in cluster n for a link between Rx antenna u and Tx antenna s at time t in k -th frequency bin can be calculated as

$$H_{u,s,n,m,k}(t) = \begin{bmatrix} F_{rx,u,\theta}(\theta_{n,m,ZOA}, \phi_{n,m,AOA}) \\ F_{rx,u,\phi}(\theta_{n,m,ZOA}, \phi_{n,m,AOA}) \end{bmatrix}^T \begin{bmatrix} \exp(j\Phi_{n,m}^{\theta\theta}) & \sqrt{\kappa_{n,m}^{-1}} \exp(j\Phi_{n,m}^{\theta\phi}) \\ \sqrt{\kappa_{n,m}^{-1}} \exp(j\Phi_{n,m}^{\phi\theta}) & \exp(j\Phi_{n,m}^{\phi\phi}) \end{bmatrix} \begin{bmatrix} F_{tx,s,\theta}(\theta_{n,m,ZOD}, \phi_{n,m,AOD}) \\ F_{tx,s,\phi}(\theta_{n,m,ZOD}, \phi_{n,m,AOD}) \end{bmatrix} \cdot \exp\left[j2\pi \frac{f_k}{c} (\hat{r}_{rx,n,m}^T \cdot \bar{d}_{rx,u} + \hat{r}_{tx,n,m}^T \cdot \bar{d}_{tx,s})\right] \cdot \sqrt{P_{n,m,k}} \cdot 10^{\frac{-(OL_{n,m}(f_k) + BL_{n,m}(f_k, t))}{20}} \cdot \exp\left[j2\pi \frac{f_k}{c} \hat{r}_{rx,n,m}^T \cdot \bar{v}t\right] \quad (8.4-27)$$

where $F_{rx,u,\theta}$ and $F_{rx,u,\phi}$ are the receive antenna element u field patterns in the direction of the spherical basis vectors, $\hat{\theta}$ and $\hat{\phi}$ respectively, $F_{tx,s,\theta}$ and $F_{tx,s,\phi}$ are the transmit antenna element s field patterns in the direction of the spherical basis vectors, $\hat{\theta}$ and $\hat{\phi}$ respectively. The delay (TOA) for ray m in cluster n for a link between Rx antenna u and Tx antenna s is given by:

$$\tau_{u,s,n,m} = \tau_n + \tau'_{n,m} - \frac{1}{c} \hat{r}_{rx,n,m}^T \cdot \bar{d}_{rx,u} - \frac{1}{c} \hat{r}_{tx,n,m}^T \cdot \bar{d}_{tx,s} \quad (8.4-28)$$

For the m -th ray within n -th cluster, $\hat{r}_{rx,n,m}$ is the spherical unit vector with azimuth arrival angle $\phi_{n,m,AOA}$ and elevation arrival angle $\theta_{n,m,ZOA}$, given by

$$\hat{r}_{rx,n,m} = \begin{bmatrix} \sin \theta_{n,m,ZOA} \cos \phi_{n,m,AOA} \\ \sin \theta_{n,m,ZOA} \sin \phi_{n,m,AOA} \\ \cos \theta_{n,m,ZOA} \end{bmatrix} \quad (8.4-29)$$

$\hat{r}_{tx,n,m}$ is the spherical unit vector with azimuth departure angle $\phi_{n,m,AOD}$ and elevation departure angle $\theta_{n,m,ZOD}$, given by

$$\hat{r}_{tx,n,m} = \begin{bmatrix} \sin \theta_{n,m,ZOD} \cos \phi_{n,m,AOD} \\ \sin \theta_{n,m,ZOD} \sin \phi_{n,m,AOD} \\ \cos \theta_{n,m,ZOD} \end{bmatrix} \quad (8.4-30)$$

Also, $\bar{d}_{rx,u}$ is the location vector of receive antenna element u and $\bar{d}_{tx,s}$ is the location vector of transmit antenna element s , $\kappa_{n,m}$ is the cross polarisation power ratio in linear scale. If polarisation is not considered, the 2x2 polarisation matrix can be replaced by the scalar $\exp(j\Phi_{n,m})$ and only vertically polarised field patterns are applied.

The Doppler frequency component is calculated from the arrival angles (AOA, ZOA), and the UT velocity vector $\bar{\mathbf{v}}$ with speed v , travel azimuth angle ϕ_v , elevation angle θ_v and is given by

$$\bar{\mathbf{v}} = v \begin{bmatrix} \sin \theta_v \cos \phi_v & \sin \theta_v \sin \phi_v & \cos \theta_v \end{bmatrix}^T, \quad (8.4-31)$$

In case of LOS, the channel coefficient is calculated in the same way as in (8.4-27) except for $n=1$:

$$H_{u,s,n=1,k}(t) = \begin{bmatrix} F_{rx,u,\theta}(\theta_{LOS,ZOA}, \phi_{LOS,AOA}) \\ F_{rx,u,\phi}(\theta_{LOS,ZOA}, \phi_{LOS,AOA}) \end{bmatrix}^T \begin{bmatrix} \exp(j\Phi_{LOS}) & 0 \\ 0 & -\exp(j\Phi_{LOS}) \end{bmatrix} \begin{bmatrix} F_{tx,s,\theta}(\theta_{LOS,ZOD}, \phi_{LOS,AOD}) \\ F_{tx,s,\phi}(\theta_{LOS,ZOD}, \phi_{LOS,AOD}) \end{bmatrix} \\ \cdot \exp \left[j2\pi \frac{f_k}{c} (\hat{\mathbf{r}}_{rx,LOS}^T \cdot \bar{\mathbf{d}}_{rx,u} + \hat{\mathbf{r}}_{tx,LOS}^T \cdot \bar{\mathbf{d}}_{tx,s}) \right] \cdot \sqrt{P_{1,k}} \cdot 10^{\frac{-(OL_{n,m=1}(f_k) + BL_{n,m=1}(f_k,t))}{20}} \exp \left[j2\pi \frac{f_k}{c} \hat{\mathbf{r}}_{rx,LOS}^T \cdot \bar{\mathbf{v}} t \right] \quad (8.4-32)$$

where the corresponding delay (TOA) for cluster $n=1$ for a link between Rx antenna u and Tx antenna s is given by $\tau_{u,s,n=1} = \tau_n - \frac{1}{c} \hat{\mathbf{r}}_{rx,LOS}^T \cdot \bar{\mathbf{d}}_{rx,u} - \frac{1}{c} \hat{\mathbf{r}}_{tx,LOS}^T \cdot \bar{\mathbf{d}}_{tx,s}$.

In (8.4-27) and (8.4-32), the oxygen absorption loss, $OL_{n,m}(f)$, for each ray m in cluster n at carrier frequency f is modelled as

$$OL_{n,m}(f) = \alpha(f)/1000 \cdot c \cdot \left(\tau_n + \tau_{n,m} + \min_{l_{RT}}(\tau'_{l_{RT}}) \right) \text{ [dB]} \quad (8.4-33)$$

where:

- $\alpha(f)$ is the frequency dependent oxygen loss per distance (dB/km) characterized in section 7.6.1;
- c is speed of light (m/s); and
- τ_n is the delay (s) obtained from Step 3 for deterministic clusters and from Step 5 for random clusters. $\min_{l_{RT}}(\tau'_{l_{RT}})$ is from the output of Step 3.

In (8.4-27) and (8.4-32), blockage modelling is an add-on feature. If the blockage model is applied, the blockage loss, $BL_{n,m}(f,t)$ in unit of dB, for each ray m in cluster n at carrier frequency f and time t is modelled in the same way as given in section 7.6.4; otherwise $BL_{n,m}(f,t)=0$ dB for all f and t .

Annex A:

Calculation of angular spread

Based on the circular standard deviation in directional statistics, the following expression for the angular spread AS in radians is proposed

$$AS = \sqrt{-2 \log \frac{\sum_{n=1}^N \sum_{m=1}^M \exp(j\phi_{n,m}) P_{n,m}}{\sum_{n=1}^N \sum_{m=1}^M P_{n,m}}} \quad (A-1)$$

where $P_{n,m}$ is the power for the m th subpath of the n th path and $\phi_{n,m}$ is the subpaths angle (either AoA, AoD, EoA, EoD) given in radians.

Annex B: Change history

Change history							
Date	Meeting	Tdoc	CR	Rev	Cat	Subject/Comment	New version
2017-02	RAN1#88	R1-1703641				Skeleton TR based on TR 38.900 v14.2.0, adding new changes (from R1-1701231, R1-1701406, R1-1701410, R1-1701411, R1-1701412, R1-1701413, R1-1701414, R1-1701416, R1-1701417 and R1-1701425) to have a TR applicable for the frequency range 0.5 to 100 GHz	0.0.1
2017-02	RAN1#88	R1-1704145				Adding new agreements (from R1-1702701, R1-1703635, R1-1703873, R1-1703358, R1-1702703, R1-1703637, R1-1703354, R1-1703458, R1-1703647, R1-1701936) and reflecting comments from RAN1 e-mail discussions [88-17].	0.1.0
2017-02	RAN#75	RP-170394				Submitted to RAN for information	1.0.0